ΕΘΝΙΚΟ ΜΕΤΣΟΒΙΟ ΠΟΛΥΤΕΧΝΕΙΟ
Εργαστήριο Ατμοκινητήρων & Λεβήτων
Τομέας Θερμότητας της Σχολής Μηχανολόγων Μηχανικών

ΔΙΠΛΩΜΑΤΙΚΗ ΕΡΓΑΣΙΑ

«Energetic, exergetic and techno-economic comparison of thermal cooling technologies powered by waste heat»

Του Φοιτητή

Τζιρίτα Δημήτριου

Επιβλέπων

Καρέλλας Σωτήριος, Αναπληρωτής Καθηγητής,
Σχολή Μηχανολόγων Μηχανικών, ΕΜΠ

Αθήνα, Ιούλιος 2017

Ευχαριστίες

Αρχικά, θα ήθελα να ευχαριστήσω τον επιβλέποντα καθηγητή μου κύριο Σωτήριο Καρέλλα για την εμπιστοσύνη του και για την ευκαιρία που μου έδωσε να ασχοληθώ με ένα πολύ ενδιαφέρον θέμα, καθώς και για την καθοδήγησή του σε όλη τη διάρκεια της εκπόνησης της εργασίας. Επίσης, θα ήθελα να ευχαριστήσω τον Κωνσταντίνο Μπραϊμάκη, για τις χρήσιμες υποδείξεις και την βοήθειά του καθ' όλη τη διάρκεια της εργασίας. Τέλος, θα ήθελα να ευχαριστήσω την οικογένειά μου για τη στήριξη σε όλο το διάστημα εκπόνησης της εργασίας και γενικότερα σε όλη τη διάρκεια των σπουδών μου.

Abstract

The objective of this thesis is to compare four basic technologies for thermal cooling production powered by waste heat. The comparison is made from an energy, exergy and economic point of view. The four technologies compared are the combined Organic Rankine Cycle (ORC)-Vapor Compression Cycle (VCC) system, Ejector Compression Cycle (ECC) system, absorption chiller and adsorption chiller.

In the first chapter, a general description of each system is presented. More specifically, the principles of operation, the most usual working fluids, some usual configurations and the most common applications, as well as a literature review are presented. These justify the use of each system in that kind of application.

In the second chapter, the modeling process is explained. For the three chillers, the analytical modeling and the process of calculating the thermodynamic values is explained, along with the most basic assumptions, the variables and the required outputs for each case. Finally, for the adsorption chiller, the acquired data from manufacturers are presented and the process of calculating the rest of the results is explained.

In the third chapter, the results of the calculations are presented. First, the results for each chiller are presented and namely the variation of the Coefficient of Performance (COP), the cooling power and the exergetic efficiency of the chillers with the heat source inlet temperature. The results are given for three specific chilled water outlet temperatures. Then, a comparison among the chillers is made, to find out which chillers achieve the highest efficiency in each case and at which temperature value.

In chapter four, an economic analysis is done. By estimating the investment and operational costs for each chiller, a possible investment to substitute the electrical powered cooling is evaluated, using the Net Present Value (NPV), the Internal Rate of Return (IRR) and the Payback Period (PBP) measures.

Finally, in chapter five, the conclusions of this study are summarized, including some ideas for further study.

Περίληψη

Σκοπός αυτής της εργασίας είναι η μελέτη και σύγκριση τεσσάρων τεχνολογιών θερμικής ψύξης από απορριπτόμενη θερμότητα. Στην εργασία έγινε ενεργειακή, εξεργειακή και οικονομική ανάλυση και σύγκριση των κύκλων. Οι τέσσερις τεχνολογίες που εξετάστηκαν είναι: οργανικός κύκλος Rankine συνδυασμένος με έναν ψύκτη μηχανικής συμπίεσης ατμών (ORC-VCC), ψύκτης συμπίεσης ατμών με ακροφύσιο (ECC), ψύκτης απορρόφησης και ψύκτης προσρόφησης.

Στο πρώτο κεφάλαιο γίνεται μια γενική περιγραφή του κάθε εξεταζόμενου συστήματος. Αρχικά, παρουσιάζονται οι βασικές αρχές λειτουργίας του κάθε συστήματος, τα πιο συνηθισμένα εργαζόμενα μέσα, κάποιες παραλλαγές του κύκλου και οι πιο βασικές εφαρμογές του. Τέλος γίνεται μια βιβλιογραφική ανασκόπηση κάθε συστήματος.

Στο δεύτερο κεφάλαιο γίνεται η ανάλυση της μοντελοποίησης του συστήματος. Για τους τρείς πρώτους ψύκτες, η μοντελοποίηση και ο τρόπος υπολογισμού των θερμοδυναμικών ιδιοτήτων επεξηγείται αναλυτικά. Επίσης, οι βασικές παραδοχές, οι μεταβλητές και οι παράμετροι για την αξιολόγηση της απόδοσης αναφέρονται για κάθε περίπτωση. Για τον ψύκτη προσρόφησης, για τον οποίο δεν έγινε αναλυτική μοντελοποίηση, παρουσιάζονται τα δεδομένα που βρέθηκαν από κατασκευαστές και επεξηγείται ο τρόπος υπολογισμού των υπολοίπων μεγεθών.

Στο τρίτο κεφάλαιο παρουσιάζονται τα αποτελέσματα των υπολογισμών. Αυτά είναι ο συντελεστής απόδοσης (COP), η παραγόμενη ψυκτική ισχύς και ο εξεργειακός βαθμός απόδοσης, για τα οποία παρουσιάζεται η διακύμανσή με την θερμοκρασία εισόδου του ζεστού νερού στον κύκλο. Τα αποτελέσματα δίνονται για τρείς διαφορετικές θερμοκρασίες εξόδου του ψυχόμενου νερού. Στη συνέχεια, γίνεται η σύγκριση μεταξύ των ψυκτών, ώστε να φανεί ποιος κύκλος μπορεί να επιτύχει την υψηλότερη απόδοση σε κάθε περίπτωση και για ποια θερμοκρασία.

Στο τέταρτο κεφάλαιο, παρουσιάζεται η οικονομική ανάλυση των συστημάτων . Αρχικά, γίνεται μια εκτίμηση του κόστους επένδυσης και του κόστους συντήρησης και λειτουργίας κάθε συστήματος. Στη συνέχεια, μελετάται μια πιθανή επένδυση για κάθε σύστημα, η οποία αφορά στην υποκατάσταση της χρήσης συμβατικού ψύκτη συμπίεσης, με βάση την καθαρή παρούσα αξία, τον εσωτερικό συντελεστή απόδοσης και την περίοδο αποπληρωμής.

Τέλος, στο κεφάλαιο πέντε, αναφέρονται τα συμπεράσματα της εργασίας και προτείνονται ιδέες για περαιτέρω μελέτη πάνω στο συγκεκριμένο θέμα.

Nomenclature

A	Area, m^2
C_p	Specific heat capacity at constant pressure, kj/kg K
e	Specific exergy kj/kg
$\dot{E}$	Exergy flow, kW
h	Specific enthalpy, kj/kg
K	Investment cost, €
k	Interest rate
$\dot{m}$	Mass flow, kg/s
M	Mach number
N	Investment evaluation period, years
$\dot{P}$	Mechanical power kW
U	Heat exchanger's overall heat transfer coefficient, $W/m^2 K$
Q	Heat flux, kW
P	Pressure, (bar)
u	Velocity, m/s
w	Entrainment ratio
s	Specific entropy, kj/kg K
SIC	Specific investment cost €/kW
T	Temperature, K
t	Temperature, ℃
X	Concentration of lithium bromide
Greek letters	
γ	Specific heat ratio
ε	Effectiveness of heat exchanger
η	Efficiency
ρ	Density, kg/m^3
υ	Specific volume m^3/kg

Subscripts

0	reference state
I	evaporator I
c	cold
comp	compressor
cond	condenser
cw	chilled water
d	diffuser
evap	evaporator
ex	exergetic
g	gas
gen	generator
h	hot
he	heat exchanger
hw	hot water (heat source)
in	inlet
is	isentropic
max	maximum
mech	mechanical
min	minimum

mix	mixing
n	nozzle
out	outlet
tot	total
turb	Turbine
r	refrigerant
s	strong
sat	saturation
vc	vapor compression
w	weak

Abbreviations

COP	Coefficient of performance
ECC	Ejector compression cycle
GWP	Global warming potential
IRR	Internal return rate
LMTD	Log mean temperature difference
NCF	Net cash flow
NPV	Net present value
ODP	Ozone depletion potential
ORC	Organic Rankine cycle
PBP	Payback period
SIC	Specific investment cost
VCC	Vapor compression cycle

Contents

List of figures

List of tables

1. Introduction

One of the biggest problems that concern the humanity nowadays is the global warming. One of the most important factors that cause it is the greenhouse effect, which is caused by the large emissions of greenhouse gases. The greenhouse gas that is principally emitted is the carbon dioxide, which mainly comes from the combustion that takes place in the industry, the IC engines etc. The greenhouse gases emissions for electricity and heating accounted for 25 % of the total global emissions for the year 2014, while the industry's emissions for 21 % [1]. In order to constrain the progress of the greenhouse effect, the humanity must effectively reduce the emissions of carbon dioxide and the other greenhouse gases. To that direction, the Kyoto protocol aimed at reduction of the greenhouses gases' emissions of the industrialized countries by 5,2 % comparing with the emissions of 1990 [2].

In the same time, the problem of the non-renewability of fossil fuels is always becoming worse. The developing economies are in need of great sums of energy to feed their advancing industry, so they use fossil fuels with an always higher rate. In the same time, in the developed countries, even though renewable energy is used to an extent, fossil fuels remain the main source of energy. That makes the need of constraining the use of fossil fuels, wherever possible, demanding.

Both these demands can be addressed by the same solution. The consumption of fossil fuels should be reduced, thus reducing the carbon dioxide emissions. A possible and effective way of doing that is by utilizing the energy (usually heat) of processes that is wasted, in order to get useful products and save fossil fuels.

1.1 Industrial waste heat and cooling

1.1.1 Industrial waste heat

Industrial waste heat can be defined as the proportion of heat produced in an industrial process which escapes from the system without being practically used. In many industrial processes, the nature of the process demands that there will be waste heat, due to thermodynamic limitations, or because after the process is completed, a part of the generated heat is no longer useful [3]. For example 50-70 % of the fuel consumption is waste heat in a thermal power plant, while 50-60 % in an Internal Combustion Engine [4], due to their efficiency. Furthermore, in several industrial processes large amounts of waste heat are emitted. Examples of such industries are the cement industry (40 % of the available heat is wasted [5]), glass, steel, aluminium, food, paper, chemical and non-metallic minerals industry. These streams in many cases contain large amounts of exergy and are able to produce useful products [6].

Waste heat can be released as gases from combustion, flue gases from industrial processes, other heated products like cooling water or radiation [6] A proportion of waste heat, in form of losses, cannot be avoided. However, another big proportion of the waste heat can be utilized in order to produce a useful output, like electricity, cooling or heating. Waste heat recovery includes the process of capturing and reusing the waste heat. Some of the most

usual waste heat sources are furnaces, waste or cooling water or motors [6]. In some cases of waste heat sources, the source may be inappropriate for heat recovery because of technical or economical reasons (for example radiation released heat) [7]. Nevertheless, sources like gases or heated water can be ideal for waste heat recovery.

In the U.S., the industry consumes about one third of the total consumed energy and therefore is responsible for the respective greenhouse gases emissions. About 20-50 % of this energy is lost as waste heat [3]. Likewise, in China, the industry consumes about 70 % of the total energy. Of this energy, industrial waste heat accounts for 10–50% of the total fuel consumption [8]. The waste heat recovery potential is big all over the world. Europe has 1106-2708 PJ of industrial waste potential heat per year, while US have 1501-1583 PJ per year [9].

1.1.2 Cooling

Cooling is nowadays one of the most electricity-consuming purposes. Large amounts of cooling are required both in the industry and in residencies. Approximately 15% of the electricity production in the whole world is employed for refrigeration and air-conditioning processes [4]. In the EU, it is estimated that 7.2 Mtoe (million tonnes of oil equivalent) are used for cooling [10]. Cooling is produced mainly with vapor compression chillers, which consume electricity. Furthermore, many commercial chillers use refrigerants that have high Global Warming Potential (GWP) and some of them have high Ozone Depletion Potential ODP [4]. In the same time, systems for producing cooling by means of heat are known for years now, even though not all of them are widely used. These systems are powered by all kinds of heat, even low grade heat, and can produce cooling from sources that are free of charge and would otherwise be wasted, like waste heat or solar heat. Moreover, these methods are using environmental-friendly refrigerants, like water or hydrocarbons

So, for all the aforementioned reasons, the use of heat powered chillers seems like an ideal solution for industrial or even residential applications, in order to save money, as well as fossil fuels and carbon dioxide emissions.

1.2 Waste heat recovery to cooling technologies description

The concept of waste heat recovery to cooling can be implemented by several systems. All those systems are substituting the electricity-powered compressor of the vapor compression cycle (VCC) system with another component (or combination of components), which can result in the compression of the working fluid. All of them are powered by heat. The ORC-VCC system substitutes the electricity consumption by feeding the VCC cycle with mechanical power from an Organic Rankine cycle (ORC). The Ejector compression cycle (ECC)

system uses an ejector to achieve the compression of the fluid. The absorption and adsorption chillers are based on the phenomena of absorption and adsorption in order to accomplish the compression of the working fluid. These four systems are presented below.

1.2.1 ORC-VCC

The ORC-VCC system is the first examined option for waste heat recovery for cooling production. The system consists of two subsystems. The first system is the Organic Rankine Cycle (ORC). This is a configuration similar to the Rankine cycle, which can operate with lower temperature inputs and smaller amounts of energy than the water-steam Rankine cycle. ORC's function is same as the steam Rankine cycle. The only difference is that the organic fluids that are used require lower temperatures, as well as smaller amounts of heat, in order to evaporate and superheat. That makes them ideal for applications like low temperature waste heat recovery, where a steam Rankine cycle cannot operate. In general, ORC's are a configuration which has been extensively studied, both theoretically and experimentally and there a lot of information in the literature. ORC's have been implemented and used in several different applications (waste heat recovery, solar energy, etc.).

The other component of the system is the vapor compression chiller (VCC), which is the most common configuration used for refrigeration and cooling in almost every application (industry, buildings, automobiles etc.). In its original form, it is powered by electricity via a compressor and produces cooling. However, in the ORC-VCC system, the VCC is powered by the ORC cycle and as a result, no electric power is needed to produce cooling (except from the electricity to operate the system's pumps, controls, etc.). That makes this configuration capable of recovering waste heat and producing cooling. The two systems can be connected in several ways. In this thesis, the two systems are considered to be connected mechanically, as the turbine of the ORC powers the compressor of the VCC. Furthermore, the two systems have the same condenser, something that makes them have the same working fluid as well. Those two connections can be different, depending on the case.

1.2.1.1 Principles of operation

ORC

As mentioned before, the ORC system is identical with the steam Rankine cycle. However, it uses fluids which require lower temperatures, as well as smaller amounts of heat, in order to evaporate and superheat. A comparison among some of the organic fluids and water can be seen in Figure 1.

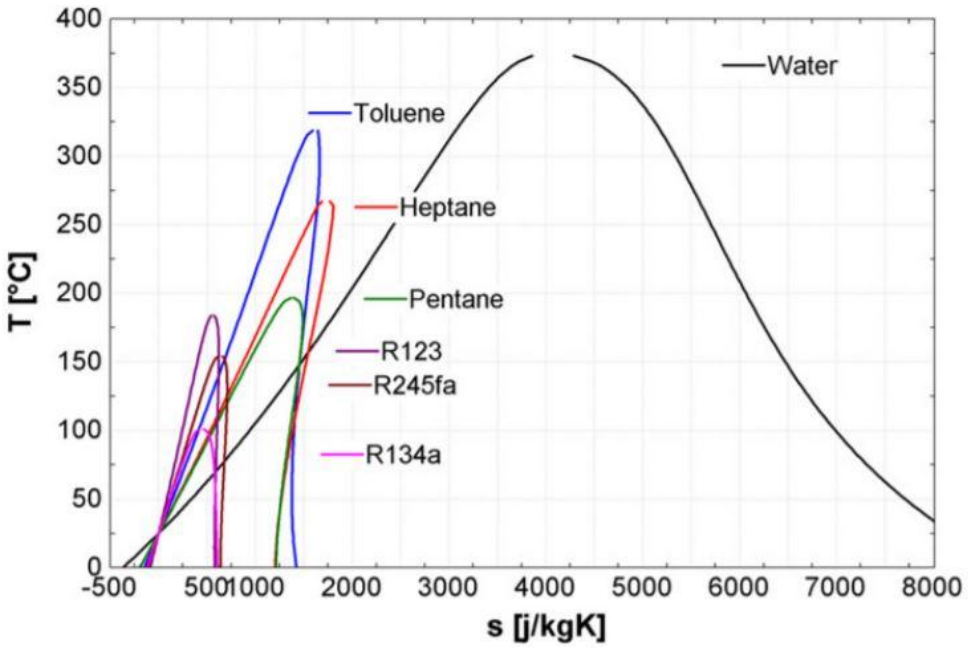

Figure 1 : Comparison among organic fluids and water [5]

The system has five components, the evaporator, the condenser, a pump, a turbine and a generator (Figure 2). The system operates under two pressure levels, the evaporator pressure and the condenser pressure. In the case of waste heat recovery, the heat recovery can be succeeded by using either one or two heat exchangers. In the first case, the source of waste heat (gas, water etc.) is directly feeding the evaporator of the ORC. In the second case, a heat exchanger transfers heat between the flue gas and the heat transfer fluid, which can be pressurized water or some other fluid. The second heat exchanger is the evaporator of the system and transfers heat from the pressurized water to the organic working fluid. In most cases, the working fluid exits the evaporator in superheated state, in order to ensure that no working fluid in liquid phase enters the turbine. After heating and evaporating, the fluid enters the turbine, where it expands by producing the cycle's power output, reaching the condenser's pressure. Then it passes through the condenser, from where it exits in saturated or subcooled liquid state. Finally, the working fluid is pumped to the high pressure of the system and sent to the evaporator inlet. In some cases, like in this study, the system has no electrical consumption, as the turbine is considered to power the pump, via a mechanical connection. The useful gross mechanical work of the turbine is feeding the generator to produce electricity. However, that may vary in some cases where mechanical work and not electricity is needed, like in the case of ORC-VCC.

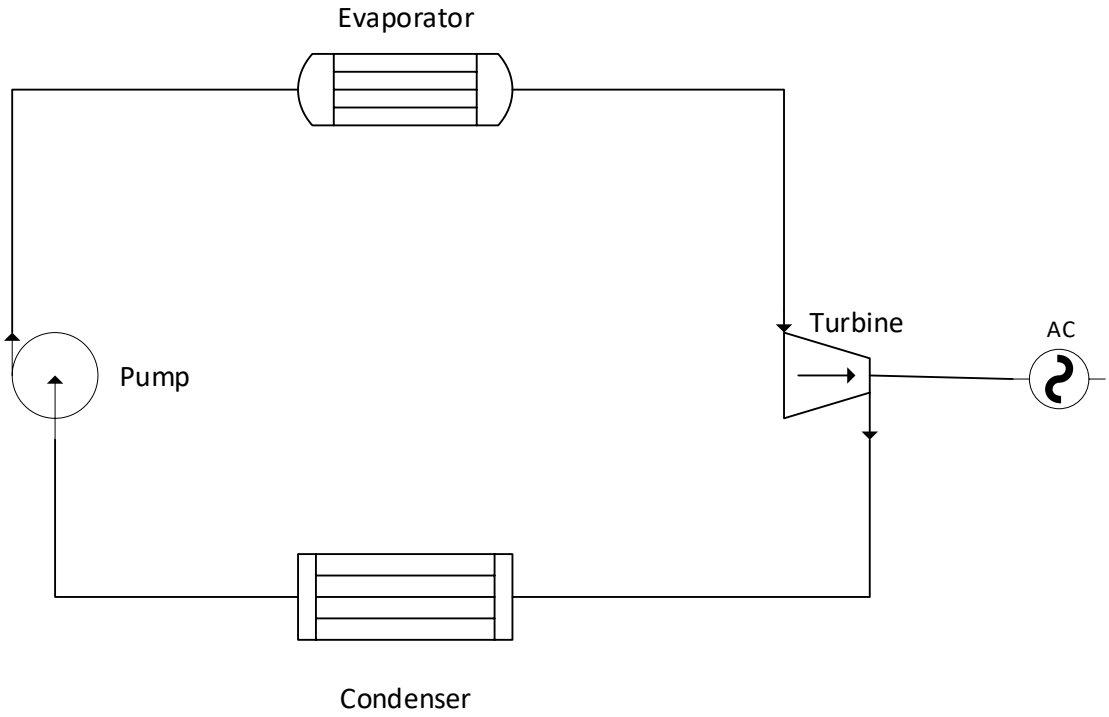

Figure 2: Simple ORC configuration

VCC

The common refrigeration cycle has four components; the condenser, the evaporator, a compressor and a throttling valve (Figure 3). It operates under two pressure levels, the evaporator pressure and the condenser pressure. The cooling work is produced in the evaporator, where the working fluid enters usually as binary mixture and by absorbing the heat off the cooled fluid, evaporates and leaves the evaporator as saturated or superheated vapor. Superheating ensures that no liquid phase will enter the compressor, as that can be detrimental for it. This process is taking place under the evaporator pressure. Then, the fluid is compressed to the high pressure of the system (condenser pressure). By flowing through the compressor, the fluid is cooled and condensed and exits in saturated or subcooled liquid state. Subcooling offers higher cooling capacity, as will be explained later. Finally, the fluid is throttled through the valve to the system's low pressure.

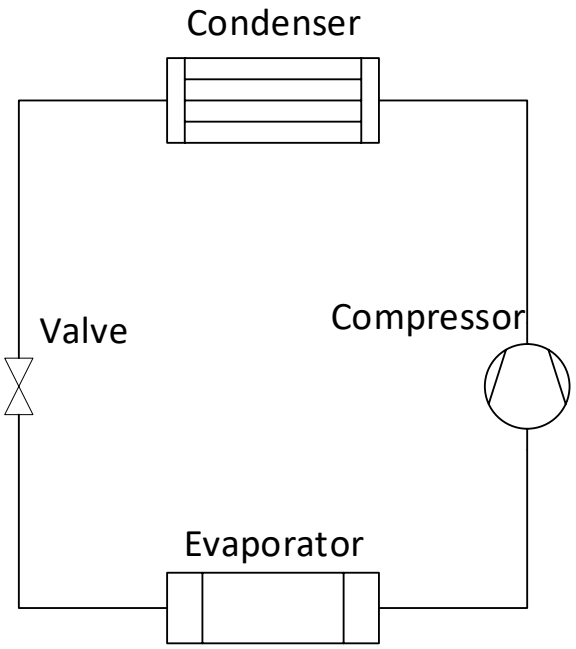

Figure 3 : Simple VCC configuration

1.2.1.2 Working fluids

Both these systems operate with organic fluids. There is a big variety of fluids that can be used in such systems. Especially in the VCC cycles, which are common practice for many years, many fluids have been commercially tested and used. However, the Kyoto Protocol [2] and the Montreal Protocol [11] have caused regulations in the use of certain working fluids. The former aims to restrict fluids with high GWP and the latter those with high ODP. In the case of VCC, traditionally and extensively used fluids like R22 where phased out due to their high ODP and GWP [12]. Even other fluids like R134a, which substituted R22 are now gradually phased out. In the case of ORC, as a relatively new technology, no standard fluids exist. So, fluids with low GWP and ODP are very interesting choices for these cycles. Intensive research is conducted on the issue of finding the most suitable fluids for each cycle, which are both environmentally sound and can result in cycles with high efficiency.

There is a variety of organic fluids that can operate in such a system. More specifically, other than their environmental soundness, there is a great variety of critical pressures and temperatures which can fulfill each cycle's requirements. For example, the properties of the heat source of the ORC can determine which fluid is more effective for the cycle. That means that especially for the ORC, there are no ideal working fluids and the best solution depends on the case. The basic desirable properties that a fluid must have for these systems are listed below [13]:

Working fluid properties

- The fluid must not be harmful for the environment (low ODP, low GWP)
- The fluid must be safe for operating in places where people are working (non-toxic, non-corrosive, non flammable)
- It is preferable that the fluid is available and at low cost

- The latent heat of the fluid should be high, in order to absorb an amount of heat with the least flow rate (smaller size of installation and less pump work needed)
- It must be chemically stable
- The fluid should operate in relatively low pressures, because as the pressure level increases, so does the complexity and the cost of the application
- The freezing point must be lower than the temperature needed in each application (for the VCC)
- Low viscosity for lower friction losses
- High conductivity for higher heat transfer coefficient in the heat exchangers

1.2.1.3 Configurations

Both these systems can have several configurations in order to increase their efficiency. In order to increase the cycle's efficiency, in many cases the working fluids of the ORC are operating in supercritical cycle. In this kind of cycle, the fluid heating is taking place in a pressure above its critical pressure and the condensation below the critical pressure [14]. Other configurations can include components like recuperator, reheater or economizer, which can improve the efficiency of the system [15]. Moreover, the ORC-VCC connection can be different. The ORC can feed a generator to produce electricity and the electricity is fed to the VCC's compressor. In that case, cogeneration of electricity and cooling is possible and in times when no cooling is needed, the ORC can be totally isolated and produce only electricity. Another possibility is the use of different working fluid in each cycle. That can allow combinations of fluids which can lead to higher efficiency.

1.2.1.4 Applications

Generally, this system has not been implemented widely, but has been investigated theoretically and experimentally. Many researchers propose that this system can compete with other similar cooling systems for the utilization of low grade heat. However, since both subsystems are widely used, this system can be used in several occasions. Since both systems can operate in a wide range of temperatures (heat source and chilled water) and capacities (mechanical power and cooling capacity), the implementation of this system can be done for small cooling capacity units (domestic applications), for bigger capacities in the industry or for air-conditioning applications. Even an application for bus air conditioning has been proposed [16].Furthermore, it can be used for electricity and power cogeneration, a configuration that provides flexibility to the cooling load produced. Finally, this system can be used in cases of trigeneration [17].

1.2.1.5 Literature review

The combined ORC-VCC system has been studied by several researchers for use in the field of waste heat recovery. Wang et al. [18] proposed and tested a system which combined an ORC with a VCC in order to recover low grade waste heat (200 °C). The turbine of the ORC powered the compressor directly to avoid losses. R245fa was used in the ORC, while R134a was used in the VCC. The system reached a capacity of 4.4 kW, even though its nominal capacity was set to 5kW, and resulted in a COP value of 0.5. Molés et al. [19] studied a combined ORC and VCC system with different working fluid in each component, activated by

low temperature heat sources. The system could work either for cooling or for electricity production. They found that the total COP of the system ranged from 0.3 to 1.1. Also, they estimated that for a 100kW cooling capacity and a COP of 0.84, with 4000 hours of cooling demand per year and 4000 hours of electricity production, such an investment would be very beneficial. Li et al. [15] studied the use of hydrocarbons in ORC-VCC cooling systems. More specifically, the use of four hydrocarbons R290 (propane), R600 (butane), R600a (isobutane) and R1270 (propene) was studied for boiler temperatures from 60-90 ℃, as well as the change on the performance that each parameter had (temperatures, efficiencies) .They estimated that with a boiler exit temperature of 90 ℃, R600, which had the higher COP among the fluids, reached a COP value of 0.470. Finally, they proposed that with the addition of some devices like recuperator, reheater and economizer, the system's performance will improve and the system will be able to compete with other technologies in the field of cooling production from low grade heat. Nasir and Kim [20] found that among other fluids for an ORC-VCC system for air conditioning with different working fluids in each component, the best combination of fluids was R134a ORC- Isobutane VCC. The system operated with an input of 100 ℃ and 1 atm. For this combination, they optimized the system based on some of the system's parameters and resulted in a maximum COP value of 0.281. Wang et al. [21] studied the operation of the ORC-VCC cycle and several configurations of it. The basic cycle, which included a recuperator, with a boiler temperature of 190 ℃ and a cooling capacity of 5.3kW achieved a COP value of 0.54. With the addition of subcooling the COP reached 0.63, while with the addition of subcooling and cooling recuperation the COP reached 0.66. All systems operated with R245fa as the working fluid. Finally, the use of a third recuperator or the use of different fluid in each component (dual fluid system) was proposed as configurations with potential of reaching an even higher COP. Cola et al.[22] studied and compared the use of an ORC-VCC, TEG (thermo-electric generator)-VCC and absorption cycle for waste heat recovery in waste heat temperatures ranging between 100-200 ℃. The ORC-VCC system operated with R134a in the VCC and R141b in the ORC. The COP was found increasing as the heat source temperature increased, reaching approximately 1 for 35 ℃ condensing temperature and 200 ℃ generator temperature. Same thing happened for the TEG-VCC generator, with slightly higher values. The absorption chiller operated with lithium-bromide/water mixture, with 90 ℃ maximum heater temperature. The latter limitation stabilized the chiller's COP to a value of 0.74. Finally, it is mentioned that even though the absorption chiller has higher COP in smaller generator temperatures, as the generator temperature rises, the ORC-VCC system has a better efficiency. Aneke et al.[23] compared the use of an absorption ammonia/water chiller and a vapor compression cycle powered by an orc, both recovering waste heat from the food industry. They found that by utilizing 1224.93 kW of waste heat at 164 ℃, the ORC-VCR system produced 703.68 kW of cooling, with its COP being 0.57. The aforementioned studies show that the ORC-VCC system can be an effective way of waste heat recovery, comparing to other similar technologies. Moreover, it is suggested by many studies that with improvements like the addition of a recuperator or the use of different fluid in the ORC and in the VCC can yield in higher efficiency. Finally, in many cases, it is shown the production of both electricity and cooling can be a profitable investment.

1.2.2 ECC

The ejector compression cycle is the second technology that was evaluated in this thesis. It is a system that can recover waste heat and directly produce cooling, without having to produce mechanical power or electricity first. This system has many similarities to the VCC system, as many of its components are the same with the VCC. However, its greatest difference is that it doesn't use a compressor for the fluid compression, but instead another configuration that has the same effect. The ECC comprises of an ejector, a generator and a pump which substitute the compressor. The generator is fed with the heat that powers the cycle. That means that this system is powered by heat and doesn't need electricity to operate. This heat can come either from combustion or from other kinds of heat like solar or waste heat. The system is relatively simple and considered reliable. Moreover, its acquisition cost is low, as well as the running cost. Finally, the system can operate with environmental-friendly fluids [24]. The ejector compression system has been investigated extensively and is considered an interesting choice when it comes to waste heat recovery. However, its COP is generally lower than that of other similar systems and that is the main reason why ECC is not commercially implemented.

1.2.2.1 Principles of operation

The system is composed of three heat exchangers, the generator, the condenser and the evaporator, an ejector, a throttling valve and a pump (Figure 4). It operates among three pressures, the generator, condenser and evaporator pressure, which are determined by the respective temperatures. As mentioned before, the system has a generator where the working fluid is heated by the heat transfer fluid. The heat transfer occurs under the generator pressure. In waste heat recovery applications, when the waste heat source is gases, another heat exchanger may be present, which transfers the heat from the gases to a heat transfer fluid, as mentioned before. The stream that exits the generator enters the ejector. So does the stream that comes from the evaporator. The ejector consists of three parts. In the first part, there is the nozzle and the suction chamber. The second part has constant area and in there, the mixing of the streams is happening. The last part is a diffuser. The high pressure stream first enters a nozzle, where its pressure decreases as it accelerates and expands. As it exits the nozzle, it has acquired supersonic speed, resulting in a very low pressure, slightly lower than the evaporation pressure. The stream from the evaporator enters the ejector due to the pressure difference. The two streams are gradually mixing, as they flow through constant area part of the ejector. The mixed stream, which has low pressure, has supersonic velocity. At the end of the constant area of the ejector, a compression shock occurs which lowers the fluid's velocity and increases its pressure. After that, the fluid's pressure is constantly increasing, as it flows through the diffuser, until it reaches the condenser pressure. So, in that way, the stream coming from the evaporator is compressed to the condenser pressure. The fluid exits the condenser in saturated or subcooled liquid state and is distributed to the two other exchangers. A part of the fluid flows through the throttling valve, in order to decrease its pressure to the evaporator pressure and reaches the evaporator. The other part is pumped to generator pressure and reaches the generator. The pump is the only basic part of the system that consumes electricity. However, its consumption is significantly lower than the compressor's.

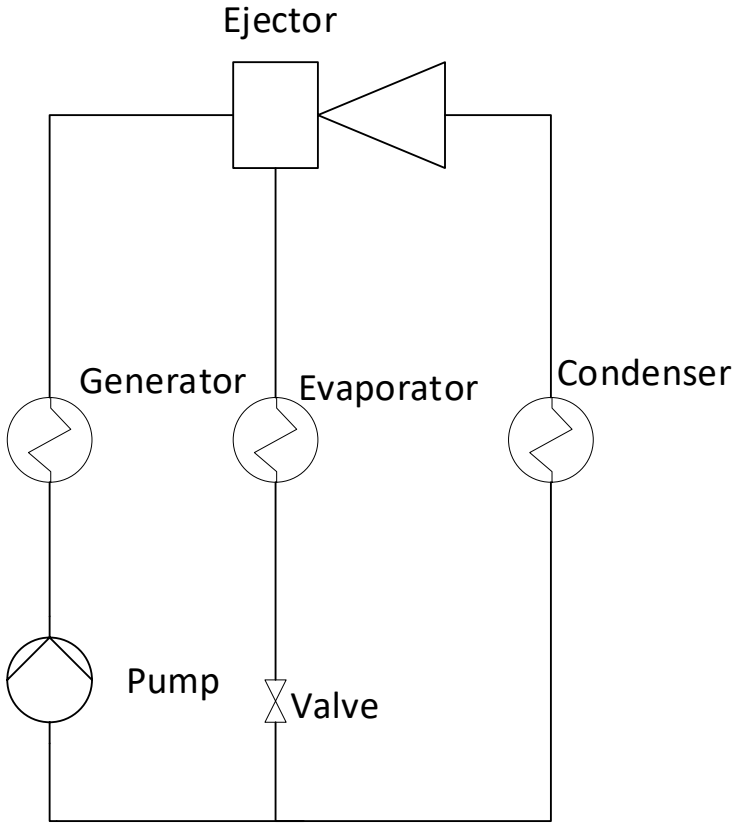

Figure 4 : ECC simple configuration

1.2.2.2 Working fluids

The working fluids of the ECC are mainly the same as those of the ORC-VCC system. In order to comply with the environmental laws, such a system must operate with low GWP and ODP fluids. The properties of the fluid that are desired in such a system are the same with these mentioned for the ORC-VCC fluids.

1.2.2.3 Configurations

The ECC system's principal problem is the fact that its COP is lower than that of other similar systems, a fact that restrains its use in practical applications. However, there are some combinations that include the ejector compression cycle, which can achieve higher efficiency. The most important of them are [25]:

- The combined power and ejector, which combines an ORC with an ejector for producing electricity and cooling
- The combined vapor and ejector compression, where the two systems can interact in several ways (for example the ECC is fed by the VCC's condenser [26])
- The combined adsorption and ejector refrigeration, where the ECC helps overcoming the intermittent operation of the adsorption chiller
- The combined absorption and ejector refrigeration, where the system is designed to achieve the enhancement of the COP from three different perspectives, i.e. the absorption process or the evaporation process or the concentration process

1.2.2.4 Applications

The ECC system can be used in cases with low grade heat, such as waste, geothermal or solar heat. The waste heat recovery can be implemented either in the industry for cooling or in smaller applications for air conditioning. Moreover, the ECC system has been proposed for use in automobile air conditioning, recovering waste heat from exhaust gases. There are also applications of cooling using solar heat [27]. Finally, the ECC system can be used in trigeneration.

1.2.2.5 Literature review

In the literature, there are several theoritical or experimental investigations of the use of ejector compression cycle for the utilization of low grade heat (waste heat).Milazzo et al.[28] built a prototype of ejector chiller for industrial use. The ejector operated with 100 ℃ generator temperature and 5 ℃, conditions similar to waste heat recovery. The system's COP reached 0.26. Thongtip et al. [29] developed and tested a steam jet ejector with 3 kW cooling capacity for the production of chilled water. The ejector achieved a COP value of 0.45 when operating under a generator temperature of 100 ℃ and an evaporator temperature of 17 ℃. Yapıcı and Yetişen [30] designed and constructed an ejector refrigeration system which operated with hot water and used R11 as refrigerant. For generator temperatures from 90-102 ℃ and evaporator temperatures from 0-16℃, a maximum COP of 0.25 was found. They suggested that in order to achieve higher efficiency, higher generator temperatures should be used. Saleh [31] studied the performance of an ejector refrigeration cycle for low grade thermal energy source operation and compared the use of several working fluids. The result was that for generator temperature of 90 ℃ and evaporator temperature of 10 ℃, R245ca displayed the best performance, achieving a COP value of 0.74. Alexis and Katsanis [32] studied an ejector refrigeration unit operating with methanol and powered by medium temperature thermal source. For generator, condenser and evaporator temperatures ranging from 117.7 to 132.5 ℃, from 42 to 50 ℃, from -10 to -5 ℃ respectively, they found the COP value ranging from 0.139 to 0.467. Meyer et al. [33] tested a steam jet ejector for waste heat or solar heat applications. For a generation temperature of 95 ℃ and an evaporator temperature of 10 ℃, the system's COP was 0.253. Furthermore, some applications in order to recover waste heat from IC engines have been proposed. For example, Sadeghi et al. [34] studied and optimized an ejector refrigeration system which was powered by the waste heat of the exhaust gases of an IC engine. For the optimized case, the refrigerator system produced 6.03 kW of cooling, with generator, condenser and evaporator temperature being 94.54 ℃, 33.44℃ and 0.03 ℃ respectively, resulting in a COP value of 0.14. A similar study was presented by Zegenhagen and Ziegler [35], resulting in a COP between 0.07 and 0.26, with R134a as working fluid.

Due to the fact that the ejector compression cycle has low efficiency, some hybrid systems have been proposed too, in order to combine the ejector chiller with another system and achieve a better performance or more than one product. Zhu and Jiang [26] developed a system which combined the vapor compression cycle with an ejector compression cycle for improved efficiency. The ejector cycle was fed by the waste heat of the vapor compression cycle condenser. With that system, the efficiency of the vapor compression cycle was

improved by 9.1 % with R22 as working fluid. In that case, the COP of the ejector was 0.73, while the generator output temperature was 85.54 ℃. Moreover, there have been some studies proposing a combined power and ejector refrigeration cycle [36, 37].

1.2.3 Absorption chiller

Absorption chiller is the third system which was examined. The basic advantage of this system, comparing to VCC is that it uses any kind of heat as input. The insertion of heat can be done either by combustion or by utilizing other sources of heat of lower temperatures like solar heat, geothermal heat or waste heat, like this thesis investigates. An absorption chiller can be powered by water temperatures, ranging from even as low as 90 ℃ to 130 ℃ [38]. So, instead of using electricity, which is a more expensive and fine form of energy, absorption chillers can use heat, which in cases like waste heat recovery, would otherwise be dumped to the environment. Furthermore, absorption chillers have no rotating or big parts, something that makes them more reliable than the common chillers[39]. However, the efficiency of absorption chillers is by far lower than that of common chillers, with their COP ranging from 0.7 to 0.8 for single stage chillers and 1.1 to 1.2 for more complex configurations (multistage) [38], while the COP of common VCCs can reach 4 or 5 in commercial chillers. Usual one stage absorption chillers can reach a chilled water outlet temperature somewhere between 4 and 15 ℃. The latter restriction is due to the freezing point of water [38].

1.2.3.1 Principles of operation

The operation of the absorption chiller is similar to that of the common vapor compression chiller. The main difference is that the absorption chiller, instead of using a compressor which consumes electricity, utilizes the absorption and desorption phenomena in order to compress the working fluid. These phenomena only require the extraction and insertion of heat respectively and are carried out in the absorber and desorber. Other than that, absorption chillers use a condenser, an evaporator and valves, like the vapor compression chillers (Figure 5). Finally, a difference between the two cycles is the fact that the vapor compression chiller works among two temperatures (condenser and evaporator temperature), while the absorption chiller works among three temperatures (condenser, evaporator and generator temperature).

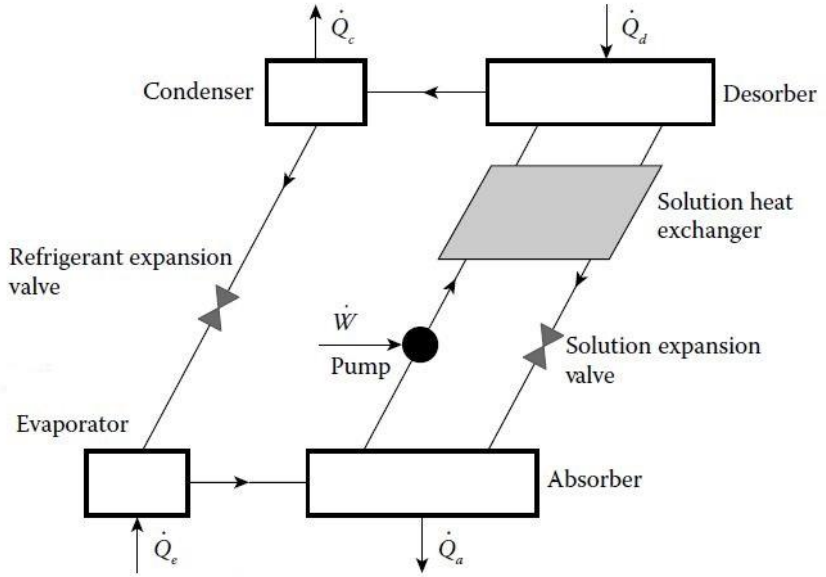

Figure 5 : Absorption chiller [40]

The chiller's function is based on the fact that due to the desorption and absorption phenomena, the steam that comes from the evaporator can be absorbed by the mixture and by performing some processes of the mixture, the steam is desorbed by the mixture in saturated or superheated state. [40] With the assumption of zero pressure losses in the heat exchangers and the tubes, the system works among two pressures which are determined by the condenser and evaporator temperature. The four heat exchangers of the system, namely the condenser, the evaporator, the generator (desorber) and the absorber are operating in two different vessels. [41] The evaporator and the absorber are in the same vessel and work under the evaporation pressure, while the condenser and the desorber are in the other vessel and work under the condensation pressure. Moreover, the system operates among three values of concentration of the working fluid. In the part of the system where the condenser and evaporator are, the working fluid is pure refrigerant (it may contain a small amount of absorber in the case of water/ammonia mixture). The stream that exits the generator and enters the absorber has a high concentration of the absorber and the concentration is called strong [38].Finally, the stream that flows from the absorber to the generator has a lower concentration of absorber and is thus called weak concentration[38]. The two basic processes that the system is based on are explained below.

Desorption (Generator)

Desorption is the process when steam is produced by a mixture, which was previously in liquid or solid state. This term is different from evaporation, because in desorption only one of the mixture components evaporates, while in evaporation the whole mixture evaporates [40]. That is due to the difference in evaporation temperature between the mixture

components, which is a requirement for sound function of the chiller. In relation with that, a problem that the water/ammonia mixture has is that that evaporating temperature difference is not high enough and as a result, in the desorption process, the produced steam consist of a small proportion of water, something that impedes the system's efficient function. The weak mixture is inserted in the generator, where desorption takes place and results in the refrigerant vapor, in saturated or superheated state, and strong mixture. Because desorption is an endothermic process, heat is inserted, usually by pressurized water. Moreover, the exiting streams are in higher temperature than the inserted one.

Absorption (Absorber)

Absorption is the process which results in a liquid or solid mixture from a component that was in vapor state and a component that was in liquid or solid state. It differs from condensation because in condensation all the components where in vapor state before turning into liquid [40]. The absorption takes place in the absorber, where the steam from the evaporator, in saturated or superheated state, and the strong solution enter the absorber, while the mixture in weak solution leaves the absorber. Absorption is an exothermic process so the absorber must be cooled.

Other than these processes and these two heat exchangers, absorption chillers use condenser and evaporator heat exchangers with the refrigerant undergoing the same processes as in the VCC. The refrigerant exiting from the generator enters the condenser, exits in saturated liquid state and then is throttled in the low pressure of the system by flowing through the valve. Finally, it enters the evaporator, where it evaporates by cooling the water in the outer circuit of the heat exchanger and exits it in vapor state.

1.2.3.2 Working fluids

There are a lot of mixtures which could be used in such a system[41]. However, in absorption chiller's commercial applications two mixtures are mainly used. These mixtures are water /lithium-bromide and ammonia/water. The mixture consists of two components, the refrigerant, which is the fluid that flows into the condenser and the evaporator, and the absorbent. In the first case, water is the refrigerant, while in the second case, ammonia is the refrigerant and water is the absorbent.

There are some basic properties that the working fluid must have in order to be used in an absorption chiller [40],[41]:

- The refrigerant must be more volatile than the absorbent, so that in the desorption phase only refrigerant vapor leaves the generator
- The mixture must be soluble in all conditions (temperatures, pressures) it may work
- The mixture shouldn't be corrosive, harmful for the environment (low ODP, low GWP) or dangerous for people working near. It shall be chemically stable
- The refrigerant must have high latent heat in order to use less quantity per unit of cooling capacity

- No solid phase must occur during the operation of the chiller, because that leads to crystallization (mainly in lithium bromide-water chillers) and impedes the sound operation of the chiller
- It is better for the system not to work under extremely low or high pressures, because in both cases the chiller's cost is higher

Neither of the two mixtures which are usually used in absorption chillers satisfies all of the above mentioned properties.

The lithium bromide-water mixture satisfies most of them. However, it works in very low pressures (1-20 kPa), due to the fact that water is the refrigerant. For example, for a condenser temperature of 40 ℃, the operating pressure is only 0.0738 bar. That introduces problems related with the design of such a cycle (for example that the cycle must be totally secluded from the environment). Moreover, this mixture faces the problem of crystallization. That phenomenon occurs when, due to high absorbent concentrations and low temperatures, a fraction of the absorbent turns into solid, clings to the tubes and restricts the flow of the liquid mixture [40]. That phenomenon will be explained later. This mixture can be corrosive to metals like carbon steel and copper [40]. Finally, lithium bromide-water absorption chillers cannot work for chilled water temperatures under 0 ℃ (usually as low as 3-4 ℃), since they use water as refrigerant.

Ammonia-water mixture also satisfies most of the mentioned properties. However, the evaporation temperature difference between absorbent and refrigerant is not high enough. As a result, the steam that exits the generator has a small fraction of water. That fraction of water, if it reaches the evaporator, can reduce the system's performance. So, a rectifier is used in order to reduce it. Moreover, contrary to lithium bromide-water, ammonia water operates under high pressures, which can reach 15 bar. Ammonia is also toxic and corrosive to copper and copper alloy [41].

The basic difference between the two mixtures is that ammonia-water can be used in low temperature applications, as its freezing point is -77.73 ℃, while lithium bromide-water mixture is restricted to temperatures over 0 ℃. However, the latter's COP is usually higher[38].

1.2.3.3 Configurations

There are a lot of different configurations of the absorption cycle, which originate from the single effect configuration, in order to increase the chiller's COP, or better utilize the temperature of the feeding water. There are called multi-stage absorption chillers. The difference is that they have some of the heat exchangers more than one time, operating at different pressures. A specific case of multi-stage chillers are the multi-effect chillers. These chillers use the driving heat more than one time. They most usual are the double-effect and the triple-effect. In the double effect cycle, there are three operating pressures and two generators and two condensers are used. The heat from the high pressure condenser powers the low pressure generator, thus producing more refrigerant and more cooling. With this configuration, more cooling comes from the same amount of incoming heat, thus increasing the COP of the system. However, this configuration is powered by higher water temperatures than the single effect. The triple effect has a similar working principle [39].

In this thesis, the waste heat recovery using an absorption chiller is investigated. With the use of an intermediate heat exchanger, the flue gases from a process are heating pressurized water and then the water feeds the absorption chiller. Heat recovery come from cooling water that comes from industrial processes, which can directly power the absorption chiller.

1.2.3.4 Applications

Absorption chillers are used in several applications related to cooling. Since the chiller can be powered either by fuel combustion or by other source of heat, its applications have a big variety. They can be used in building air conditioning or industrial cooling, since their range of cooling capacity is big. There are also some applications of district cooling. They can be used in many cases of waste heat recovery, in order to produce cooling which is needed for an industrial process (for example in gas turbines) [40]. Moreover, they can be used in trigeneration systems [42]. Solar applications of absorption chillers are also common, since absorption chillers can utilize heat sources in the temperatures of the solar heat [43], [44].

1.2.3.5 Literature review

The absorption chiller has been extensively studied, both theoretically and experimentally. There are a lot of studies regarding its use in waste heat recovery for cooling production. Mortazavi et al [45] used waste heat from a gas turbine in an LNG plant to power a double effect water/lithium-bromide absorption chiller, which provided cooling in several processes of the LNG plant. They found that this could reduce the compressor power and the gas turbine fuel consumption by 21.3 %. Rodgers et al [46] investigated the use of several configurations of absorption cycles in the propane cooling cycle, in order either to sub cool propane or to precool the condenser's cooling water. They found that sub cooling propane after the condenser by approximately 21 ℃ relative to the base cycle enhanced the propane cycle COP and total cooling capacity by 13% and 23%, respectively, while precooling the cooling water enhanced the propane cycle COP and total cooling capacity by 63% and 22%. Popli et al [47] studied the use of exhaust waste heat of a gas turbine to power absorption chiller for reducing the inlet temperature of the gas turbine compressor, instead of evaporative media coolers or electrical vapor compression coolers. They found that three single effect lithium-bromide/water absorption chillers could recover 17 MW from the exhaust and produce 12.3 MW of cooling. Kalinowski et al [48] investigated the replacement of the propane vapor compression chiller by an ammonia/water absorption chiller. They found that a single effect cycle can recover 5.2 MW of waste heat from a power generating gas turbine and save 1.9 MW of electricity. Aneke et al.[23], as mentioned before, compared the use of an absorption ammonia/water chiller and a vapor compression cycle powered by an orc, both recovering waste heat from the food industry. They found that by utilizing 1224.93 kW of waste heat at 164 ℃, the absorption chiller produced 671.68 kW of cooling, with its COP being 0.55. Popli et al.[42] conducted a techno-economic analysis on a trigeneration system using lithium-bromide/water double effect absorption chillers. The result was that a recovery of 37.1 MW of waste heat could be recovered from three chillers providing 45 MW of cooling at 5 ℃. Hedström [49] studied the waste heat recovery from the chemical industry using orc and absorption chiller (both lithium-bromide/water and

ammonia/water). For the absorption chillers, the result was that they can recover up to 35 MW of heat. The lithium-bromide/water chiller reached 23.3 MW of cooling, while the ammonia/water chiller only 10.6 MW. The above mentioned works show that the absorption chillers can be implemented in industrial applications reaching high cooling capacities. As it was expected, in cases where very low temperature cooling is needed, the ammonia/water chiller is the only alternative when it comes to absorption cooling. However, when temperatures greater than 0 ℃ are needed, the lithium-bromide/water chiller reaches higher COP and cooling capacity, so its use is preferred.

1.2.4 Adsorption chiller

The adsorption chiller is the last thermal cooling system that was investigated. Adsorption chillers are based on the phenomenon of adsorption. Attention on these chillers begun to be intense in the 70s. Adsorption chillers can operate with a variety of adsorbents and working fluids and the adsorption can be either physical or chemical. Comparing to absorption chillers, such a chiller can operate in a bigger range of heat source temperatures from 50 ℃ to 400 ℃, depending on the adsorbate-adsorbent combination and without using the solution pump or any rectification equipment, like in the absorption chiller configurations. Adsorption chillers use no moving or rotating parts, something that makes them reliable and requires less maintenance costs [4]. Moreover, the working pairs of adsorption chillers don't confront problems like crystallization or corrosion. Finally, adsorption systems are considered more suitable for applications where intense vibration is expected, like mobile applications because the adsorbent is in solid and not liquid [50].However, their biggest drawbacks are the relatively low COP, as well as their big size, comparing with other similar technologies. These drawbacks are impeding their wide commercialization. [51].

Adsorption chillers have been commercially implemented by several companies and in several cooling capacities. However, there are not as widely spread as absorption chillers and their capacities are limited in relatively low values.

1.2.4.1 Principles of operation

The adsorption chiller operation is based on the phenomenon of adsorption, which takes place in the adsorbent bed. The operation and the components of the system are similar to vapor compression chiller, with the difference being that the compression of the refrigerant is achieved by using the adsorbent bed instead of the compressor (Figure 6). Much like the absorption chiller, in the adsorption chiller two phenomena take place in order to achieve the compression of the refrigerant. These are called adsorption and desorption and are pretty much opposite to each other. The basic difference between absorption-desorption and adsorption-desorption processes is that in absorption, a liquid substance is used, while a solid substance is used in adsorption. The solid adsorbent is placed on a bed called adsorption bed, where the adsorption and desorption process take place. The two basic phenomena that occur during that cycle are described below.

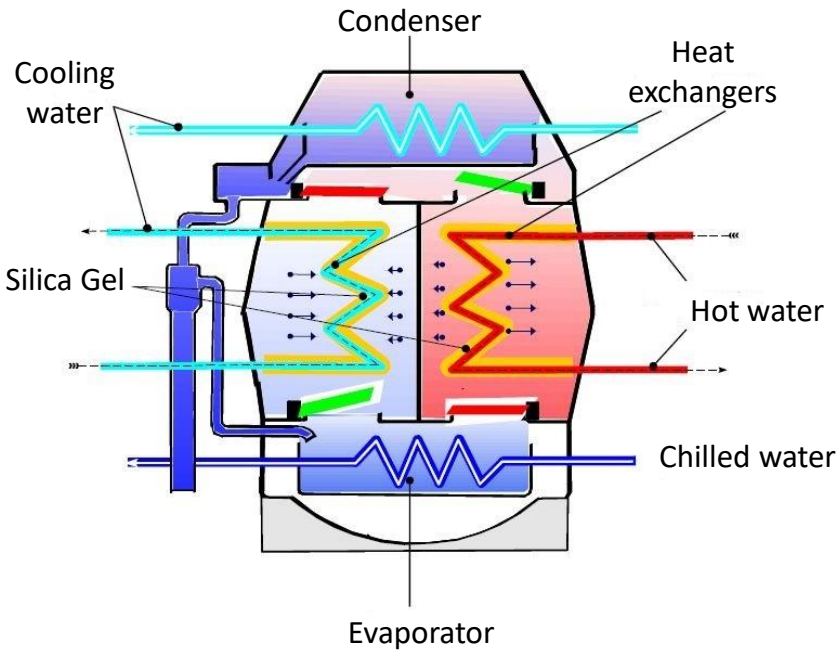

Figure 6 : Adsorption chiller scheme [52]

Adsorption (Adsorption Bed)

Adsorption can be defined as the adhesion of molecules of a gas or a liquid to a surface of a substance called adsorbent. That creates a film of adsorbate (the adsorbed substance) on the adsorbent's surface, with an exothermic process. There are two kinds of adsorption. The first kind is the physical adsorption, which is driven by the van der Waals force among the molecules and takes place on the surface of the adsorbent. It is a process similar to condensation and the adsorption heat is similar to condensation heat for a specific refrigerant. The second kind is the chemical adsorption, in which a chemical reaction takes place and the new molecules are formed. These new molecules are then decomposed during the desorption process. The reason that chemical adsorption is considered is because the adsorption and desorption heat are higher than in physical adsorption [51].

Desorption (Adsorption Bed)

Desorption is the opposite process of adsorption. When the adsorber is heated and has reached a certain temperature and pressure, it starts desorbing the fluid it had previously adsorbed, in vapor state. That procedure continues up to a specific concentration of adsorbate in the adsorbent, which can't be further reduced. Desorption is an endothermic process and that is why a supply of heat is needed.

Cycle description

The phases of the cycle and the processes of the working pair can be demonstrated in a p-T diagram (Figure 7). In general, the cycle operates between two pressures, the evaporator

and the condenser pressure, determined by the respective temperatures. Furthermore, the cycle has three characteristic concentrations of working fluid (adsorbate). The higher (100 %) corresponds to the pure refrigerant which flows through the evaporator and the condenser. The medium corresponds to the concentration of fluid in the end of the adsorption phase, when the maximum quantity of working fluid is adsorbed. Finally, the lowest concentration corresponds to the minimum quantity of refrigerant which doesn't leave the adsorption bed after the desorption phase.

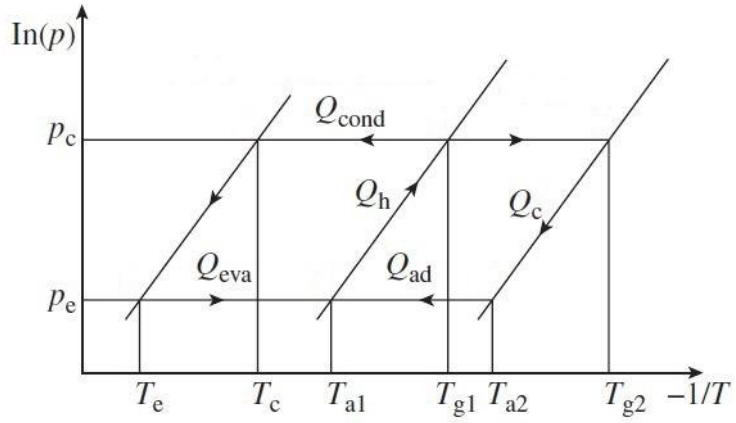

Figure 7 : p-T diagram for adsorption refrigeration cycle [51]

The cycle consists of four phases [53] (Figure 8):

1) Heating of adsorbent and pressure raise

That phase can be considered as the corresponding to compression of the refrigerant phase of the VCC. The adsorbent bed has already adsorbed the refrigerant, reaching the maximum concentration of refrigerant in the bed, and is heated from the heat source of the system. As the heating takes place, the temperature and pressure of the adsorbent bed is raised and starting from the evaporator pressure, it reaches the condenser pressure.

2) Desorption and condensation

In that phase the condensation of the refrigerant takes place. After reaching the condenser pressure, the adsorber starts desorbing the refrigerant and it is connected with the condenser. So, during the desorption process, refrigerant in the condenser pressure and vapor state flows from the bed and condenses in the condenser, exiting in saturated liquid state. As process continues, the bed's temperature increases and the concentration of adsorbed refrigerant reduces. The process ends when the minimum quantity of refrigerant is left in the bed. In the same time, the bed's temperature has reached its highest value as well.

3) Cooling of adsorbent and pressure reduction

During this phase, the bed starts to be cooled and its pressure gradually decreases, until it reaches the evaporator pressure, while its temperature falls as well. The concentration of the adsorbed refrigerant remains at its minimum value. Moreover, during this stage, the adsorbent bed is disconnected from the condenser. That stage is corresponding to the throttling of the refrigerant stage of the VCC.

4) Adsorption and evaporation

The final stage starts when the adsorbent bed pressure has reached the evaporator pressure and it is connected with the evaporator. The bed cooling continues and in the same time, the refrigerant flows through the evaporator, producing the cooling. Then, it is adsorbed by the adsorber. This stage continues until all the refrigerant has passed through the evaporator and has been adsorbed.

The cycle, as described before, is intermittent, which means that the cooling production is not continuous, as the evaporator doesn't operate constantly. However, with the addition of a second bed, the production of cooling can be continuous [53]. In that configuration, when the first adsorber is in the desorption phase, the other is in the adsorption phase and vice versa.

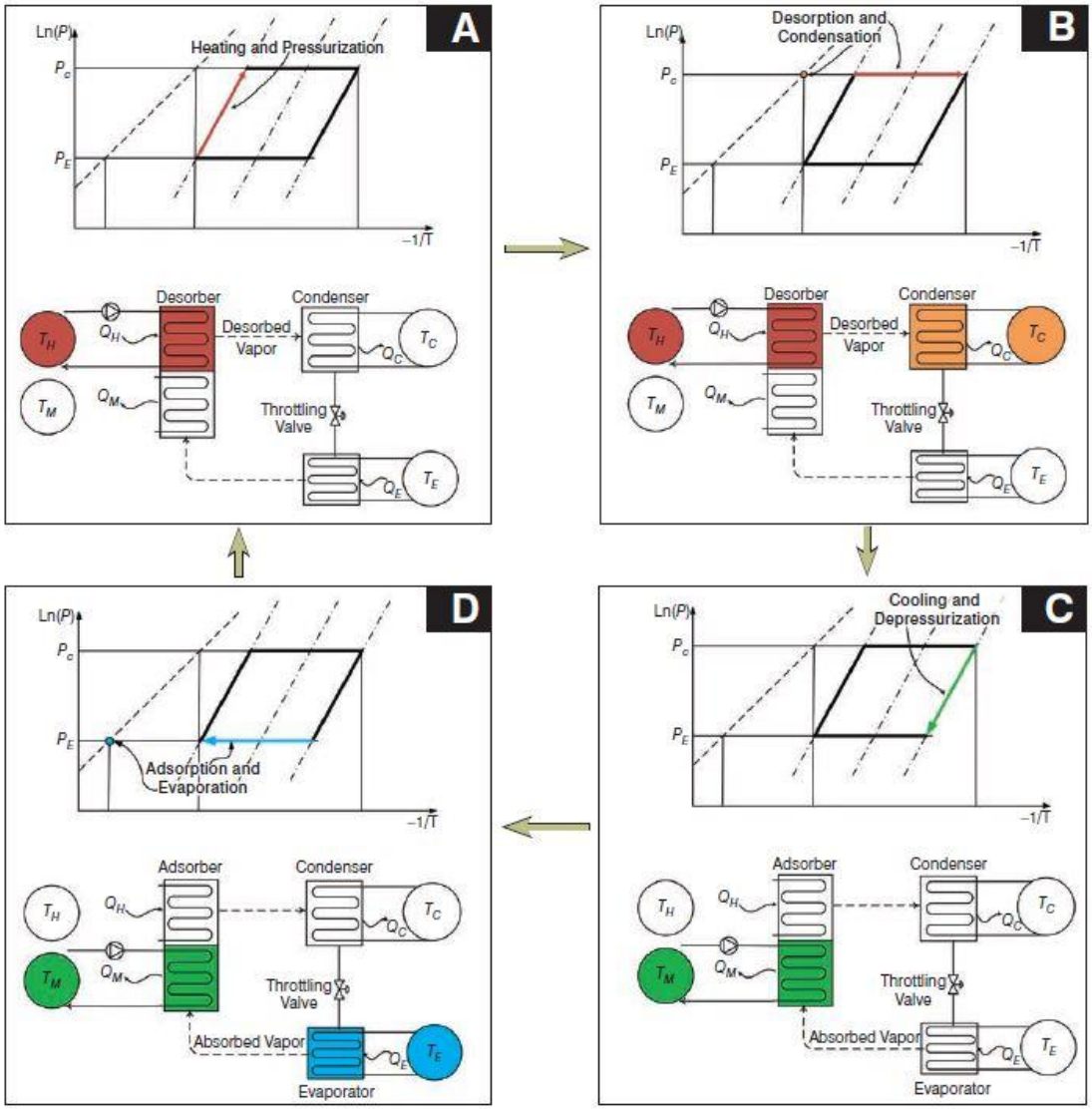

Figure 8 : Description of the phases of the adsorption chiller operation [54]

1.2.4.2 Working pairs

The working fluid and adsorbent which can be used in adsorption cycles are a lot. However, some specific combinations have dominated and are widely used, both in studies and in commercial applications. The working pairs are divided into two categories, the physical and the chemical pairs. For the first category, as long as the adsorbents are concerned, activated carbon, silica gel and zeolite are the most used physical adsorbents. The refrigerant of the adsorption chiller should have the following properties (much like the refrigerant in previous chillers)[50]:

- High latent heat
- Thermal stability
- Not being harmful for the environment
- Not being flammable
- Operating under pressures not far from the environmental pressure

Of course, like in all the other cases of refrigerant selection, none of the candidates could satisfy all these requirements. In the adsorption chillers case, the most used refrigerants are ammonia, water and methanol.

The most commonly used combinations are listed in Table 1 together with their properties and operational range [50],[55]:

Table 1: Physical adsorption pairs

	Silica gel-Water	Zeolite-Water	Activated Carbon-Methanol	Activated Carbon-Ammonia
Temperature Range	50 °C<T<120 °C	Above 200 °C	Up to 120 °C	Even above 200 °C
Adsorption Heat(kj/kg)	2500	3300-4200	1800-2000	2000-2700
Pressure	<1bar	<1bar	<1bar	>1 bar

In connection to this table, the following facts must be mentioned:

- The adsorption heat accounts for the largest part of the heat consumption of the chiller, so lower adsorption heat means lower heat consumption
- In the cases that the heat source temperature cannot be more than 120 °C, the adsorbent either loses it capability of adsorption (silica gel) or it is decomposed (activated carbon)
- The pressures below 1 bar occur due to the presence of water and methanol. The combination of activated carbon and ammonia can be an alternative, as it works in pressures higher than 1 bar. However, in that case, the problem of ammonia's toxicity occurs
- The presence of water makes it impossible to cool below zero

From the above mentioned properties of each working pair, it is obvious that the zeolite-water and activated carbon-ammonia pairs are used in high heat source temperatures, where the others pairs cannot operate. On the other hand, the silica gel- water and activated carbon- methanol pairs are ideal for low heat source temperatures, even up to 50 °C. The latter's ability makes adsorption chillers the only technology that can effectively recover waste heat from such low heat source temperatures.

As long as the chemical adsorption is concerned, usually used pairs are metal hydride-hydrogen and metal chloride-ammonia [55].

1.2.4.3 Configurations

In order to improve the efficiency of the adsorption cycle, some configurations have been proposed and tested. Some of them are [4], [51]:

- Heat recovery: This configuration is used when the chiller has at least two adsorber beds. When the cooling of the adsorber that was before in the desorption phase is about to begin, the heat from this adsorber is transferred to the other adsorber,

which is about to be heated, via a thermal fluid. That reduces the heat input and increases the COP, even by 25 % [56].

- Mass recovery: In that case when the adsorption and desorption processes are over the two beds are connected and more fluid is desorbed and adsorbed from the respective beds, due to the pressure difference, until the two beds reach the same pressure. That increases the adsorption quantity and thus the cooling effect. For a mass recovery adsorption cycle, the refrigeration capacity is enhanced, while the effect on the COP is not certain [53]. It is suggested that especially for high condensing and low evaporator and generator temperatures, mass recovery is beeneficial. Usually, this technique is combined with heat recovery. That the combination can improve the COP by even 10 % (comparing with the heat recovery adsorption cycle) [56].
- Thermal wave cycle: This cycle includes connection between the two beds and exploiting the heat by the exothermic reaction of adsorption in order to reduce the heat input to the desorber. That would increase the performance of th system. Up to 80 % of the adsorption heat can be recovered in such a cycle [51].
- Forced convective wave cycle: In this configuration, the refrigerant transfers the heat itself in a thermal wave cycle, instead of heating the bed directly. In that way, no heat exchanger mass is absorbing heat which is wasted.

Other than these configuration, there have been several other configurations in the literature, including cascading cycles, multi-bed and multi-stage cycles. In multi-stage cycles, the desorption of a bed is coupled with the adsorption of another, in order to reduce the temperature requirements of the heat source. Cascading cycles use more than one pair of beds. There is the high temperature pair, which is directly fed from the heat source and the low temperature pair, which is heated by the refrigerant that flows into it and by the adsorption and sensible heat of the high temperature beds. It should be mentioned that for the cascading cycles,usually the working pair is different in each pair of beds.

1.2.4.4 Applications

The adsorption chillers are a technology not so widely used comparing to absorption chillers. However, there are several applications where adsorption chillers are used, especially in lower cooling capacity ranges, as will be seen from the literature review. Adsorption chillers can be used in waste heat recovery applications, however up to a certain cooling capacity, as can be observed from the several studies and basically from the manufactured adsorption chillers' capacities. Such applications are in the food, beverage processing or chemical industry [57],[52]. In such cases, they can be used for ice-making, chilled water production or air-conditioning. An ideal use is in automobile waste heat recovery for air-conditioning [50], as mentioned before. Solar applications are also a possibility, since the heat temperatures are in the range of operation of adsorption chillers([43], [44]). Finally, adsorption chillers can also be used in trigeneration[58],[51].

1.2.4.5 Literature review

As a rule, the applications of adsorption chillers in the field of low grade heat and especially of waste heat are mainly on low cooling capacities, contrary to absorption chillers, which operate in all cooling capacities. Saha et al. [59] designed and tested a two-stage silica gel-

water adsorption chiller to exploit temperatures from 40 to 75 ℃. For a heat source temperature of 55 ℃, the COP of the chiller was 0.36. Khan et al. [60] studied the performance of a solar/waste heat driven multi-bed adsorption chiller with mass recovery. The chiller operates with temperatures between 60 and 90 ℃ and chilled water temperature of 7 ℃. It was reported that the mass recovery raised the COP of the system comparing to the system without mass recovery only for temperatures lower than 65 ℃. Saha et al. [61] studied a waste heat driven, dual mode adsorption chiller capable of operating with heat source temperatures between 40 and 95 ℃. For operation with temperatures from 40-60 ℃, a three stage adsorption chiller was used, capable of reaching a maximum COP of approximately 0.2 between 50 and 55 ℃. The other mode was a single stage multi-bed (6 bed) chiller, reaching its maximum COP value between 80 and 85 ℃. Liu et al. [62] tested an adsorption chiller capable of operating with heat source temperature from 70-95 ℃. The chiller operated with a maximum COP of 0.33 and cooling power of 6.37 kW at 10 ℃ evaporator temperature. It was also reported that through the heat recovery, a COP increase of 34.4 % can be achieved, while mass recovery could increase the COP by 18.3 % and the cooling power by 13.7 %. Myat et al. [63] tested a zeolite adsorption cooling system driven by low grade waste heat source. The heat source temperature can range from 55 to 80 ℃ for a chilled water temperature if 12 ℃. The maximum COP value is 0.48 for heat source temperature of 65 ℃. A common field where adsorption chillers are used is the small scale CCHP. Grisel et al.[64] developed and tested a silica gel-water adsorption chiller powered by low grade waste heat for trigeneration. The chiller had a cooling power of 3.6 kW and achieved a COP value of 0.62 . Kong et al. [65] investigated the use of an adsorption chiller in a natural gas and LPG-fired micro-CCHP. The rated electricity power was 12 kW and by recovering the heat from the engine jacket cooling water and the exhaust gases, the adsorption chiller can produce 9 kW of cooling, with a COP of 0.3 and 13 ℃ evaporation temperature. 28 kW heat can be produced as well. Chorowski and Pyrka [66] modeled a three bed adsorption chiller of 90 kW cooling capacity. The chiller achieved a maximum COP value of 0.642 for hot water temperature of 60 ℃ and a maximum cooling capacity value of 90.5 kW for hot water temperature of 64 ℃. Finally, Wang and Oliveira [67] mention that there have been several CCHP applications of adsorption chillers, such as in hospitals or universities. Another application of interest is the waste heat recovery from engines for air conditioning of vehicles. Bigger vehicles are better for such an application, because of the big size of adsorption chillers[67]. This application was reviewed by Hamdy et al. [68]. Their review divided the applications into two categories: the exhaust gas waste heat powered and the engine coolant heat powered. For the first category, the COP ranged from 0.21 to 0.6, for temperatures ranging from 115 to 550 ℃. For temperature values of 200 ℃ and greater, the used pair was zeolite-water, while for lower temperatures activated carbon-methanol and silica gel-water was used. The highest COP was achieved for the Silica gel – Water chiller. For the second category, the COP values ranged from 0.1 to 0.66 for temperatures ranging from 70 to 200 ℃. In this case, many different working pairs were used. Finally, another intresting application is the waste heat recovery for ice production. This application was reviewed by Sah et al. [69], where the applications' temperatures ranged from -13 to -21 ℃, while the COP ranged from 0.16 to 0.4.The used pairs was activated carbon-methanol and activated carbon-ammonia. Finally, it should be mentioned

that even though there are few industrial applications of waste heat in the literature, there is potential of using adsorption chillers in power or chemical plants or industries [4].

1.2.4.6 Commercial adsorption chillers

Commercially produced adsorption chillers are mentioned by Wang and Oliveira [67]. According to them, Nishiyodo Kuchouki, Co. Ltd. was the first company to develop adsorption chillers. The chillers operated with hot water of temperature 50-90 ℃ for chilled water temperature of 3 ℃. The maximum COP value of the chiller is 0.7 for water temperature of 90 ℃. Another company involved in adsorption chiller development is Mycom, which can operate with hot water at 75 ℃ and chilled water at 9 ℃, with a COP value of 0.6. Those chillers' capacity ranges from 20 to 100 RT. Other manufacturers are [70]:

- ECO-MAX: Silica gel-water chillers from 3 to 330 RT and zeolite-water chillers from 250 to 450 [57]
- Meyekawa: Zeolite-water chillers from 20 to 100 RT
- Union: Silica gel-water chillers from 10 to 125 RT
- Sortech: 13-104 kW zeolite water chillers [71]
- InvenSor : 10-105 kW zeolite water chillers [72]

1.3 Purpose of the thesis

As mentioned before, waste heat recovery can be very beneficial for the environment, as well as an interesting option for industries to reduce the costs related with the consumption of energy. In the sector of cooling production, waste heat recovery can be implemented and substitute the electricity powered cooling, saving electricity and thus money and carbon dioxide emissions. The above facts make it interesting to investigate the efficiency that such technologies can achieve and whether such an investment would be profitable.

This thesis is trying to investigate waste heat recovery for the purpose of cooling production. As it is known from the literature, there are several configurations which can perform that. This thesis investigates and compares four of these technologies and more specifically combined ORC-VCC cooling, ECC cooling, absorption cooling and adsorption cooling. Other possible technologies were not included in the study.

The purpose of the thesis is to calculate the COP, cooling power and exergetic efficiency of each system under different heat source temperatures and find out which technology can achieve the highest efficiency. Furthermore, the investment of such systems is evaluated, in

order to find whether it would be profitable to implement them and substitute the electrical powered vapor compression chillers.

The calculation of the efficiency of the ORC-VCC, ECC and Absorption Chiller was performed by modeling these systems. The models were implemented in Matlab and the efficiency of each system was calculated in a range of heat source temperatures, in order to depict the change in the COP, cooling power and exergetic efficiency with the heat source temperature. For the adsorption chiller, such diagrams were acquired by several manufacturers, in a form which enabled the comparison among the four systems. Finally, in order to evaluate a possible investment of such a system for substitution of a common vapor compression chiller, the investment and operation cost of each system were estimated and an economic analysis was conducted by calculating the most basic investment performance measures, namely the net present value (NPV), internal rate of return (IRR) and payback period (PBP). These are calculated for a case study and the incomes of the investment are estimated as the money saved from not using electricity.

2. Modeling of the cooling systems

In this chapter, the modeling of the operation of the four systems is explained. For the three systems (ORC-VCC, ECC, Absorption chiller) a detailed explanation of the working fluids, assumptions, variables and objective of the modeling are explained, followed by a description of the calculation of the thermodynamic properties in each point of the system. Moreover, the modeling of the heat exchangers and the assumptions used in the modeling of the heat source are presented. Finally, for the adsorption chiller, the data which were found from manufacturers are presented.

2.1 Heat exchangers

The heat exchangers are very important components of all the investigated systems. With these the systems perform the basic operations, like transferring the heat from the heat source, cooling the water and cooling the working fluid. Three basic methods to model the heat exchangers are presented here. The implementation of these models to each heat exchanger of each system will be explained in the respective paragraph.

An important relationship that connects the temperature differences in the heat exchanger with the heat that is transferred is equation 2.1. It connects the heat exchanger's overall heat transfer coefficient U with the exchanger's area A and the logarithmic mean temperature difference ΔTLM.

$$Q = U * A * LMTD \qquad 2.1$$

The logarithmic mean temperature difference is defined as:

$$LMTD = \frac{(T_{h,in} - T_{c,out}) - (T_{h,out} - T_{c,in})}{\ln(\frac{T_{h,in} - T_{c,out}}{T_{h,out} - T_{c,in}})} \quad 2.2$$

This equation allows designing of the heat exchanger or deriving some qualitative conclusions about the heat exchanger.

Another important factor related to the heat exchangers is the pinch point. The pinch point is the minimum temperature difference between the two streams that exchange heat. For the design of the heat exchanger, the pinch point has an important effect. Low pinch point accounts for low Log Mean Temperature Difference (LMTD), something that leads to higher area for the exchanger. On the other hand, smaller pinch point values provide higher heat exchange efficiency [14].

Finally, a last approach to the modeling of heat exchangers is through the effectiveness of the heat exchanger. In general, the effectiveness of a heat exchanger can be defined as the ratio of the exchanged heat divided by the maximum amount of heat that could be exchanged. That can is displayed in the following equation:

$$\varepsilon = \frac{\dot{m}C_{p_h}(T_{h,in} - T_{h,out})}{\dot{m}C_{p_{min}}(T_{h,in} - T_{c,in})} \quad 2.3$$

In cases where the minimum $\dot{m}C_p$ is known and constant, the equation can be used to calculate the temperatures of the streams of the heat exchanger.

2.2 Modeling of the heat source

The heat source of the system is considered to be the flue gases from an industrial process. The gases exit the process with a temperature of 200 ℃ and with a flow rate of 907 $\frac{\mathrm{Nm}^3}{\mathrm{min}}$. The gases are supposed to leave the system with a temperature of 120 ℃. As no information on the composition of the flue gases is given, they were modeled as air.

All systems employ two heat exchangers to perform the heat recovery. The first heat exchanger operates with the flue gases on one side, as the hot fluid, and pressurized water on the other side. The pressure of the water is considered 2 bar greater than the vaporization pressure of water in the outlet water temperature of the heat exchanger. In that way, it is secured that the water is in liquid phase.

In general, the heat transfer in such cycles can be done directly between the flue gases and the working fluid as well. However, the use of an intermediate heat exchanger is commonly

applied, since it gives the advantage of better controllability and stability of the system, as the possible rapid variations in the heat source are controlled by the intermediate fluid. Furthermore, some fluids may face problems of deterioration if the temperatures of the gases are higher than a specific value, something that may occur in transient situations [5].

For the first two cases, a pinch point value for the first heat exchanger was determined. The investigation was done by calculating the cycle's performance for several temperatures of the pressurized water. Since both temperatures of the flue gases, as well as its mass rate, are known, by defining the water's outlet temperature, the inlet temperature and the mass rate of the water are calculated, with respect to the determined pinch point and the energy balance between the two streams. In that way, all the properties of the hot water were known.

In the third case, the temperature difference of the pressurized water was determined. Again, the investigation was done by calculating the cycle's performance for several temperatures of the pressurized water. In this case however, only the mass flow of the water was unknown and was calculated by the energy balance between the two streams. In that way, all the properties of the heating water were known. The pinch point of the first heat exchanger is calculated in this case, instead of being defined.

Finally, it must be mentioned that the heat input to the cycle is constant in each cycle, as the temperatures and the mass flow of the gas is known.

2.3 Modeling of the ORC-VCC

2.3.1 Working fluids

An important choice that has to be done considering the cycle is the working fluid. The working fluid has a great effect on the cycle's efficiency. As mentioned before, there is no specific fluid which is considered ideal for all the applications of the ORC. Every application has its own heat source and its own cycle working conditions, which determine which fluid is the most appropriate. In this thesis, there has been a selection of several fluids for testing. The choice was based on two factors. The first factor is the fluid's environmental soundness. That means that only fluids with zero or extremely low GWP and ODP are tested. The other direction is the critical temperature of each fluid. The chosen fluids had a variety of critical temperatures, in order to find the fluid which best fits with the cycle's working conditions. The examined fluids are shown in Table 2.

Table 2: Tested working fluids

	Tcrit(°C)	Pcrit (bar)	GWP	ODP	Safety Group
R1234ze	110	36	6	0	A2L
Isobutane	135	36	3	0	A3
Butane	152	38	4	0	A3
Isopentane	187	33	4	0	A3
Isohexane	225	30	-	-	-

These working fluids have similar critical pressures but their critical temperature is ranging from 110 to 225 ℃. A first result that is wanted is to find the critical temperature for which the system will achieve the highest performance. Furthermore, it is obvious that all fluids have zero ODP and an extremely low GWP, something that makes them perfectly comply with the legislation about working fluids. According to the working fluid safety classification of ASHRAE, each fluid belongs to a safety group, with a letter and a number. The letter corresponds to the toxicity of the refrigerant, while the number for the flammability. Letter A stands for low toxicity, so these working fluids are not toxic. However, number 1 stands for low flammability, so these fluids are all flammable, especially the hydrocarbons. This problem does not exclude these refrigerants, as long as they don't auto-ignite and there is no ignition source around [12].

The working fluids used in the VCC are the same with those in the ORC, as the two systems have the same condenser. However, it must be mentioned that the difference of the several fluids on the COP of the VCC is not expected to be that large. In fact, as mentioned by Bayrakçi and Özgür [73], who compared the use of several hydrocarbons in a vapor compression refrigeration system, the difference in the COP is small.

2.3.2 Assumptions

For the modeling of the system, the ORC's evaporator is referred to as "evaporator I", while the VCC's evaporator is referred to as "evaporator".

2.3.2.1 Assumptions for the ORC

The modeling of the cycle was based on certain assumptions, which regarded the operation of several components of the cycle. First, the isentropic efficiencies of the turbine and the pump were determined. The values that were considered are common values from the literature.

Since the flow rate of the organic fluid is estimated at about 0.4 $\frac{\mathrm{m}^3}{\mathrm{s}}$, the type of pump that should be used is centrifugal [74].

The expander type of the ORC was considered to be a radial turbine because that type is suitable for the power range of the specific ORC [12]. Furthermore, in [12], it is mentioned that the maximum isentropic efficiency for a radial turbine is 85 %. Finally, it is mentioned that this type of expander cannot work in the two phase region.

As long as the isentropic efficiency of the pump, expander and compressor of the system are concerned, values that were considered are common values from the literature. From

several studies ([75], [15], [16]), the turbine isentropic efficiency ranges from 0.7 to 0.9, the pump efficiency from 0.75 to 0.9 and compressor efficiency from 0.65 to 0.8. All these three efficiencies were considered to be 0.8, as was considered in three relative studies [76],[19], [20].

Also, a mechanical efficiency was considered to express the losses in the transfer of mechanical work among the turbine and the other system components. From the literature [16], this efficiency was found to range from 0.95 to 1. Here, it was considered 0.98. Another assumption was that the condenser temperature was 40 ℃. This is a normal condenser temperature which remained steady for the investigation that followed. However, higher or lower temperatures could be considered as well. In connection with that, a pinch point of 10 K was considered for the condenser and cooling water inlet temperature of 20 ℃.

Another assumption was about the superheating of the working fluid in the exit of the evaporator I. In the case of turbines, the presence of liquid phase in the working fluid is unwanted, as it can damage the turbine. That depends on the fluid and more specifically, on whether the fluid is dry or wet. As it appears on Figure 9 the fluids can be classified according to the slope of their saturated vapor curve. The importance of that classification is that the slope of the saturated vapor curve determines whether there is a possibility that the fluid enters the two-phase region during the expansion. In order to find the needed superheating, the maximum entropy value and the corresponding pressure in the saturated vapor curve can be found. In case that the refrigerant is wet, it can be seen from Figure 9 that during the expansion the fluid will probably enter the two phase region. On the other hand, in case the fluid is dry and its maximum working pressure is lower than the pressure at which the maximum entropy appears, there is no possibility of entering the two-phase region during the expansion. That means that for the cases of wet fluid or dry fluid with maximum working pressure higher than the pressure which corresponds to the maximum entropy, a superheat must be given so that the fluid comes to the maximum entropy point. For the other case of dry fluid, no superheat is needed. It has been stated by several studies that superheating for dry fluids is not needed [74],and that the excess superheating is wasted and only adds to the condenser cooling load [12].However, is some cases, a small superheating degree is given. In this case, a minimum superheat of 2 K was given in all cases and when needed (wet fluids), more superheat was considered.

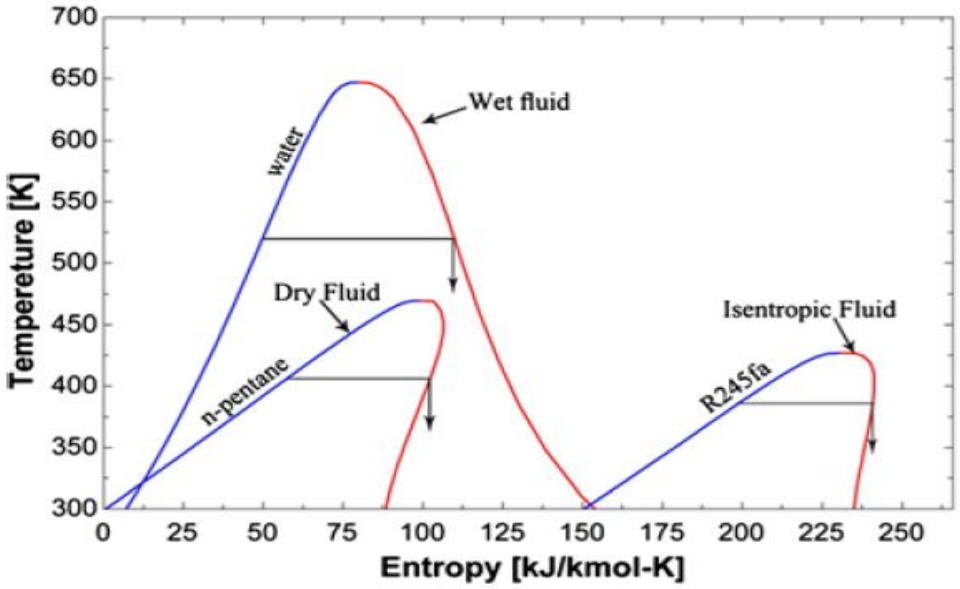

Figure 9: Dry,wet and isentropic fluids

In this case, the pinch point of the flue gases-water heat exchanger was considered to be 20 K. Usually, in the condenser outlet, subcooling is applied, in order to ensure that the stream exits in liquid state. Since the stream afterwards enters the pump, the possibility of cavitation must be avoided. A subcooling of 5 K was considered. In the other heat exchanger (evaporator I), different restrictions were imposed, as will be explained later. The assumptions for the ORC are presented in Table 3.

Table 3: ORC cycle assumptions

Efficiencies	
η_{pump}	0,8
η_{turb}	0,8
η_{mech}	0,98
Condenser	
Temperature(°C)	40
Pinch point (K)	10
Cooling water inlet temperature (°C)	15
Subcooling (K)	5
Flue gases-water heat exchanger	
Pinch point (K)	20
Evaporator I	
Superheating degree (K)	2

2.3.2.2 Assumptions for the VCC

For the VCC the isentropic efficiency of the compressor was an important assumption, which was based on values from the literature, as mentioned in paragraph 2.3.2.1. Furthermore, the throttling in the valve is considered isenthalpic.

In the VCC system, an important parameter is the superheating and subcooling of the working fluid. As the working fluid exits the evaporator, it is theoretically in saturated vapor state. However, as it enters the compressor afterwards, it must be ensured that no liquid phase occurs, as that will damage the compressor. In order to ensure that, the vapor is superheated up to a certain point. There are two kinds of superheat. There is the superheat that happens inside the evaporator and as a result, increases the cooling effect of the cycle. This can be called the useful superheating. There is also the unhelpful superheating, which occurs in the pipes, as the stream flows towards the compressor. The useful superheating can be from 5 to 10 K [77]. In this case, 5 K of superheating was considered, all of it useful.

On the other hand, subcooling the fluid in the condenser outlet has a beneficial effect on the cooling capacity. Since the throttling process is isenthalpic, the more cooled the fluid is when exiting the condenser, the more cooling capacity it can offer. However, the subcooling is given by the condenser, so extreme subcooling is not a viable option. As in the previous case, subcooling may occur in the pipes. In that case, that is beneficial for the cycle performance [77]. However, in this case, a subcooling of 5 K, which occurs exclusively in the condenser, was considered.

For the condenser, a pinch point of 10 K was considered like in the ORC case, since the two systems share the same condenser.

The final assumptions that should be mentioned are those that have to do with the chilled water that is produced by the VCC. In refrigeration, two concepts that are related to the chilled water are introduced. These are the range and the approach. Range stands for the temperature difference between the inlet and the outlet stream of water. Approach stands for the temperature difference between the chilled water outlet temperature and the evaporator temperature. These two concepts are very important for the system, as they determine the evaporator temperature and the water mass flow that can be handled by the chiller.

$$Range = T_{cw,in} - T_{cw,out} \quad (2.4)$$

$$Approach = T_{cw,out} - T_{evap} \quad (2.5)$$

These parameters took values which are usual for a refrigeration system. The approach was considered 5 K. The chosen value is used in commercial refrigeration systems [78]. Furthermore, this value defines the pinch point of the evaporator, so the lower it is, the bigger the area of the evaporator must be and the higher the cost will be. So, lower values, which would allow higher evaporator temperatures and thus higher efficiency of the cycle,

were eliminated. The range was considered 5 K as well. This is a value used by some manufacturers for different types of chillers ([79],[52]), while others use similar temperature differences ([57],[80]).

The assumptions for the VCC system are listed in Table 4.

Table 4: Assumptions for the VCC

Efficiencies	
η_{comp}	0,8
Condenser	
Temperature(℃)	40
Pinch point (K)	10
Cooling water inlet temperature (℃)	15
Subcooling degree (K)	5
Evaporator	
Superheating degree (K)	5
Range	5
Approach	5

Finally, it must be mentioned that zero pressure losses through the heat exchangers and the pipes are considered. Likewise, no heat loses are considered in the heat exchangers.

2.3.3 Variables

Except from the assumptions connected with the ORC and VCC, there are some variables which obtain specific values during the cycle calculations, in order to find the value, at which the cycle demonstrates the better performance. These variables are the hot water temperature, the evaporator I temperature and the chilled water outlet temperature (Table 5). The evaporator I pressure ranges from the pressure that corresponds to temperature of 50 ℃ to 30 bar. The latter value is defined as the maximum allowed pressure of the system. The hot water temperature ranges from 110-180 ℃, in order to maintain the pinch point of the flue gases-water heat exchanger to 20 K. For each temperature of the hot water, an internal optimization is performed, in order to find the maximum COP and exergetic efficiency and the evaporator I pressure and temperature at which these occur. Finally, the calculations are done for three chilled water outlet temperatures (4,7,10 ℃). That temperature practically defines the evaporator temperature, since:

$$T_{evap} = T_{cw,out} - Approach \quad (2.6)$$

Those three temperatures correspond to some common temperatures for industrial cooling, given the fact that since water is chilled, temperatures below 2-3 ℃ are not preferred because of the freezing of water.

Table 5: Variables

Variable	Range
Hot water inlet temp (℃)	110-180
Evaporator I pressure (bar)	Psat(T=50 ℃)-30 bar
Chilled water outlet temperature (℃)	4,7,10

Another important factor in the calculation of the system is the screening out of the evaporator I temperatures, for which the heat transfer is not possible. Since the temperatures of both streams in evaporator I of the system are known, the pinch point of the heat exchanger can be calculated. However, since there is no check on these temperatures, the temperatures of the working fluid may be higher than these of the water, or very close to them. In order to eliminate such cases, there is a check of the pinch point of evaporator I and in case it is negative or lower than 5, the heat transfer is considered impossible. Negative pinch point implies impossible heat transfer, while extremely small pinch point implies big heat exchanger area and thus high cost. The pinch point of evaporator I is considered a variable, since its value changes during the calculations.

2.3.4 Objective

The objective of the modeling of the ORC-VCC system is to calculate the maximum cooling power that can be produced by the cycle, as well as the maximum exergetic efficiency. The outputs of the cycle calculations are presented in Table 6. In order to do that, the mechanical work from the turbine of the ORC must be calculated first. Then, with that value as input to the VCC, the cooling power of the VCC must be calculated. Finally, the COP of the system and the exergetic efficiency can be calculated.

Table 6: Outputs of the cycle calculations

Porc (kW)
Qevap (kW)
COP
η_{ex}

To sum up, the process with which the efficiency of the system is calculated is described in the following flow chart (Figure 10), which summarizes the most basic steps of the process.

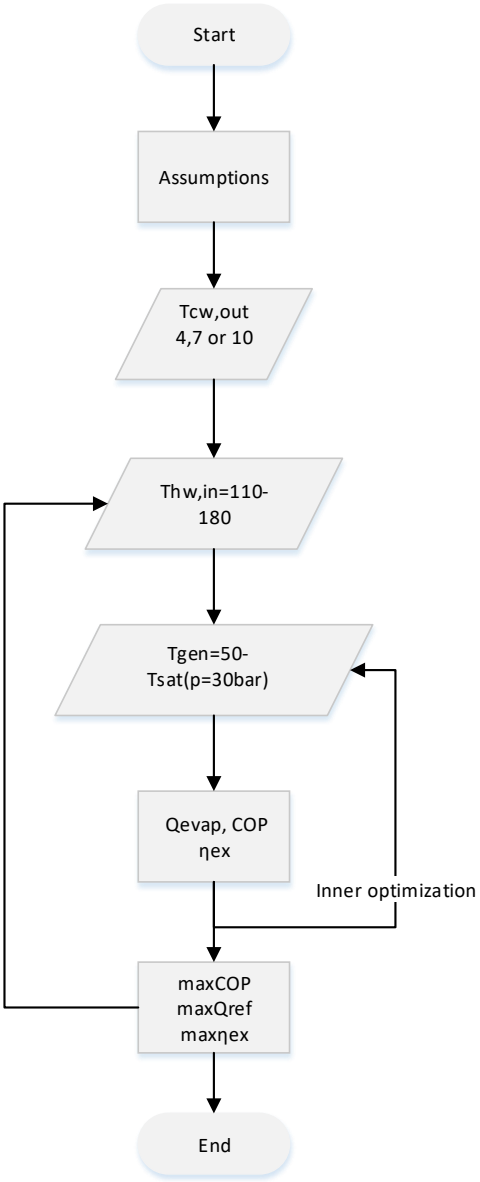

Figure 10 : Flow chart of the process of calculating the efficiency of the ORC-VCC

2.3.5 Calculation of thermodynamic properties and efficiency

Given the aforementioned assumptions, the calculation of the thermodynamic properties in each point of the ORC-VCC is possible. The description will be done with respect to Figure 11.

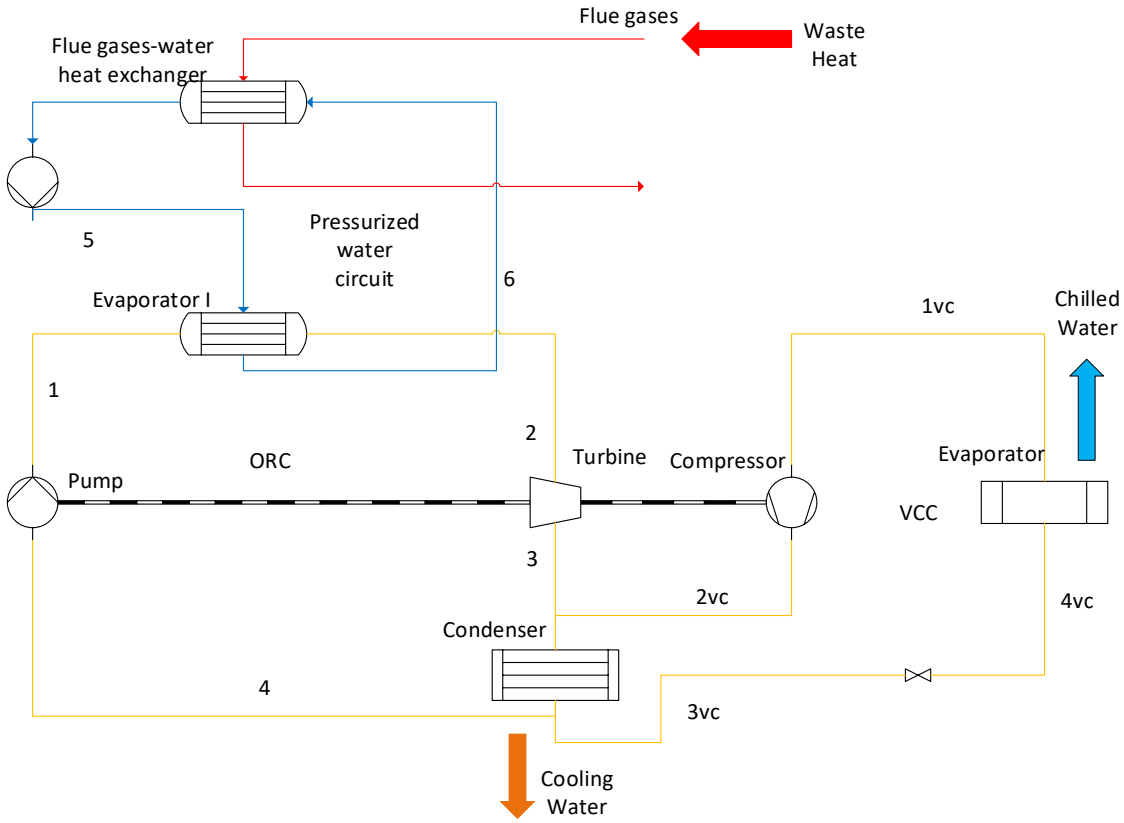

Figure 11: ORC-VCC system

In every point, the properties that are needed in order to calculate the system's efficiency are: Pressure, temperature, enthalpy and entropy. In order to calculate all the properties' values, two of these need to be known.

The compression of the pump is not isentropic, so given the isentropic efficiency, the enthalpy of point 1 equals:

$$h_1 = h_4 + \frac{h_{1,is} - h_4}{\eta_{pump}} \qquad 2.7$$

The enthalpy of the point 1_{is} equals:

$$h_{1,is} = h(P = P_{evap\ ,I}, s = s_4) \qquad 2.8$$

Since the pressure equals the evaporator I temperature, the point is fully defined.

As long as point 2 is concerned, the pressure equals the evaporator I pressure and the temperature is known, given that the needed superheat has been calculated, depending on

whether the fluid is dry or wet, as well as on the evaporator I pressure. So, the temperature equals the saturation temperature plus the superheat. All the properties from that point can be calculated based on these.

Given that one stream of the evaporator I (water) is totally defined and the temperatures of the other stream are defined as well, only the mass flow of the working fluid can be calculated, from the energy balance as:

$$\dot{m}_{orc} = \frac{\dot{m}_{hw}(h_{hw,in} - h_{hw,out})}{h_2 - h_1} \quad 2.9$$

For point 3, with the efficiency of the turbine, the enthalpy of point 3 can be calculated as:

$$h_3 = h_2 - (h_2 - h_{3,is})\eta_{turb} \quad 2.10$$

The enthalpy of the point 3_{is} equals:

$$h_{3,is} = h(P = P_{cond}, s = s_2) \quad 2.11$$

Since the pressure equals the condenser temperature, the point is fully defined.

Finally, point 4 is determined, since the pressure equals the condenser pressure and the temperature has a known subcooling degree.

Now, as all points are fully defined, the most important energy balances can give the efficiency of the system.

The produced power from the turbine equals

$$\dot{P}_{mec\,h} = \dot{m}_{orc}(h_2 - h_3)\eta_{mec\,h} \quad 2.12$$

However, a proportion of that power is consumed by the pump:

$$\dot{P}_{pump} = \dot{m}_{orc}\frac{(h_1 - h_4)}{\eta_{mec\,h}} \quad 2.13$$

So, the gross power that can be transferred to the VCC compressor is:

$$\dot{P}_{gross} = (\dot{P}_{mec\,h} - \dot{P}_{pump})\eta_{mec\,h} \quad 2.14$$

The power of the evaporator I and the condenser is:

$$\dot{Q}_{evap\ ,I} = \dot{m}_{orc}(h_2 - h_1) \quad 2.15$$

Finally, the efficiency of the ORC cycle is:

$$\eta_{orc} = \frac{\dot{P}_{gross}}{\dot{Q}_{evap\ ,I}} \quad 2.16$$

The ORC cycle is fully calculated. Its connection with the VCC cycle is the turbine gross power, which is transmitted to the VCC cycle and powers the compressor. It must be mentioned again that the whole amount of power is considered to power the VCC cycle, as no electricity is produced.

Point 1 of the VCC has pressure equal with that of the evaporator and its temperature has a known superheating. Thus, the point is defined.

Point 2 comes after the compression of the fluid. Its enthalpy equals:

$$h_{2,vc} = h_{1,vc} + \frac{h_{2,vc,is} - h_{1,vc}}{\eta_{comp}} \quad 2.17$$

The enthalpy of the point $2_{vc,\mathrm{is}}$ equals:

$$h_{2,vc,is} = h(P = P_{evap}\ , s = s_{1,vc}) \quad 2.18$$

The pressure of point 2 equals the condenser pressure. So it is fully defined.

Point 3 has the condenser pressure as well and its temperature has a known subcooling degree. Thus it is fully defined.

Finally, point 4 comes from the throttling of the working fluid, which is considered isenthalpic. That means that its enthalpy is equal to h_2 and its pressure is equal to the evaporator pressure. Thus, it is fully defined.

The working fluid mass flow that the compressor is capable of compressing can be calculated as:

$$\dot{m}_{vcc} = \frac{\dot{P}_{gross}}{h_{2,vc} - h_{1,vc}} \quad 2.19$$

Finally, it must be mentioned that the streams of the two subsystems mix before the condenser, enter it together and exit with the same subcooling degree, and then split. This process is considered to happen without pressure losses.

With the above calculations, it is possible to calculate the cooling power of the evaporator, which is the product of the cycle, as well as the power of the condenser which comes from the VCC.

The power of the evaporator equals:

$$\dot{Q}_{evap} = \dot{m}_{vcc}\,(h_{1,vc} - h_{4,vc}) \quad 2.20$$

The COP of the VCC equals:

$$COP, vc = \frac{\dot{Q}_{evap}}{\dot{P}_{gross}} \quad 2.21$$

For the whole system, the COP can be calculated.

$$COP = \frac{\dot{Q}_{evap}}{\dot{Q}_{evap\ ,I}} \quad 2.22$$

Finally, for the condenser, adiabatic mixing of the streams has been considered, before they enter the condenser. The properties of this point can be calculated as:

$$\dot{m}_{cond\ ,in} = \dot{m}_{orc} + \dot{m}_{vcc} \quad 2.23$$

$$\dot{m}_{cond\ ,in}\, h_{cond\ ,in} = \dot{m}_{orc}\, h_3 + \dot{m}_{vcc}\, h_{2,vc} \quad 2.24$$

So, the condenser power is equal to

$$\dot{Q}_{cond} = (\dot{m}_{orc} + \dot{m}_{vcc})\big(h_{cond\ ,in} - h_4\big) \quad 2.25$$

Exergy calculations

An exergy analysis was performed for the system, in order to determine the exergy inlets and outlets, as well as the exergy destruction that takes place in each component of the cycle.

To begin with, the inlet and outlet streams of the cycle are those of the water, which serves as heating, cooling or chilled water.

The specific exergy of a fluid equals to:

$$e = (h - h_0) - T_0(s - s_0) \quad 2.26$$

The quantities h_0, s_0, T_0 are calculated in the reference state, whose temperature and pressure are 15 ℃ and 1.013 bar respectively.

The exergy rate of a stream is equal to:

$$\dot{E} = \dot{m}\big((h - h_0) - T_0(s - s_0)\big) = \dot{m}e \qquad 2.27$$

So, for each water flow that enters or leaves the chiller, the exergy rate can be calculated using the above equation. Same thing goes for the exergy of the points of the cycle.

After these calculations, the exergy destruction in each component can be calculated. The exergy destruction is the difference between the exergy inlets and outlets. The destruction in each component equals to:

Flue gases-water heat exchanger

$$\dot{E}_{d,he} = \dot{m}_g\big(e_{g,in} - e_{g,out}\big) + \dot{m}_{hw}\left(e_{hw,in,he} - e_{hw,out,he}\right) \qquad 2.28$$

Evaporator I

$$\dot{E}_{d,eI} = \dot{m}_{hw}\big(e_{hw,in,I} - e_{hw,out,I}\big) + \dot{m}_{orc}\left(e_1 - e_2\right) \qquad 2.29$$

Evaporator

$$\dot{E}_{d,e} = \dot{m}_{cw}\big(e_{cw,in} - e_{cw,out}\big) + \dot{m}_{vcc}\big(e_{4,vc} - e_{1,vc}\big) \qquad 2.30$$

Condenser

$$\dot{E}_{d,cond} = \dot{m}_{cool,w}\big(e_{cool,w,in} - e_{cool,w,out}\big) + (\dot{m}_{vcc} + \dot{m}_{orc})\big(e_{cond,in} - e_4\big) \qquad 2.31$$

Turbine

$$\dot{E}_{d,turb} = \dot{m}_{orc}\left(e_2 - e_3\right) - \dot{P}_{mech} \qquad 2.32$$

Pump

$$\dot{E}_{d,pump} = \dot{m}_{orc}\left(e_4 - e_1\right) + \dot{P}_{pump} \qquad 2.33$$

Compressor

$$\dot{E}_{d,comp} = \dot{m}_{vcc}\big(e_{1,vc} - e_{2,vc}\big) + \frac{\dot{P}_{gross}}{\eta_{mech}} \qquad 2.34$$

Valve

$$\dot{E}_{d,v} = \dot{m}_{vcc}\left(e_{3,vc} - e_{4,vc}\right) \quad 2.35$$

Mixing

Another exergy destruction point is the mixing of the two streams of fluids before the condenser, which is equal to:

$$\dot{E}_{d,mix} = \dot{m}_{vcc}\, e_{2,vc} + \dot{m}_{orc}\, e_3 - (\dot{m}_{vcc} + \dot{m}_{orc}) e_{cond\,,in} \quad 2.36$$

The total exergy destruction is equal to:

$$\dot{E}_{dtot} = \dot{E}_{d,he} + \dot{E}_{d,eI} + \dot{E}_{d,e} + \dot{E}_{d,cond} + \dot{E}_{d,turb} + \dot{E}_{d,pump} + \dot{E}_{d,comp} + \dot{E}_{d,v} \quad 2.37$$

Finally, it must be mentioned that the total exergy destruction can be calculated from the following equation:

$$\sum \dot{E}_{in} = \sum \dot{E}_{out} + \dot{E}_{dtot} \quad 2.38$$

For the calculation of the exergetic efficiency of the cycle, the exergy of the incoming stream of gas and the exergy of the exiting stream of chilled water were used.

The exergetic efficiency equals:

$$n_{ex} = \frac{\dot{E}_{cw\,,out}}{\dot{E}_{g,in}} \quad 2.39$$

The results from the exergetic analysis are displayed in chapter 3, for each case of chilled water outlet temperature.

The above-mentioned calculations are implemented by an algorithm (Figure 10), which works in Matlab.

2.4 Modeling of the ECC

The ECC is a configuration similar to the previous mentioned ORC-VCC, as it consists of an evaporator and the condenser, like the VCC, and of the generator, like the ORC. So, to an extent, the modeling is the same as in the previous case. However, the biggest difference of the two systems is the ejector, which is employed in the ECC system and operates differently.

2.4.1 Working fluids

The working fluids which were tested were the same as in the ORC-VCC case (2.3.1). There have been several studies regarding the choice of the working fluid in an ejector compression cycle. For example Chen et al.[81] studied the performance of several working

fluids in an ECC. For condenser temperature of 35 ℃ and evaporator temperature of 10 ℃, they found that R600 (butane) reached the higher COP value of 0.38, while R600a (isobutane) reached a value of 0.35. Furthermore, Besagni et al.[82] proposed that each refrigerant has a range of temperatures where it achieves high performance. For example, R134a and R152a were suitable for low temperatures (70-100 ℃), R600 for medium temperatures (100-130 ℃) and R601 (pentane) for high temperatures (130-180 ℃).

2.4.2 Modeling of the ejector

As mentioned before, the ejector is a device which consists of three different parts (Figure 12). The first part contains the nozzle, where the primary stream flows, and the suction chamber, where the secondary stream flows. Primary and secondary are the streams that come from the generator and the evaporator respectively. After that, there is the mixing section, which has constant area and the mixing of the two streams is taking place. Finally, the mixed stream flows through the diffuser to recover pressure, in order to exit with pressure equal to that of the condenser. In those three parts, three efficiencies must be defined, in order to account for the losses in the respective parts of the ejector. These are the nozzle, mixing and diffuser efficiency. As mentioned by ([83]), the selection of these efficiencies has a great impact on the system's efficiency. Finally, it is mentioned by some researchers that these efficiencies vary depending on the working conditions, geometry or the working fluid ([83],[82]). Moreover, equations to correlate the efficiencies with the working conditions have been proposed as well ([83]). However, these values were considered constant for the different fluids which were tested.

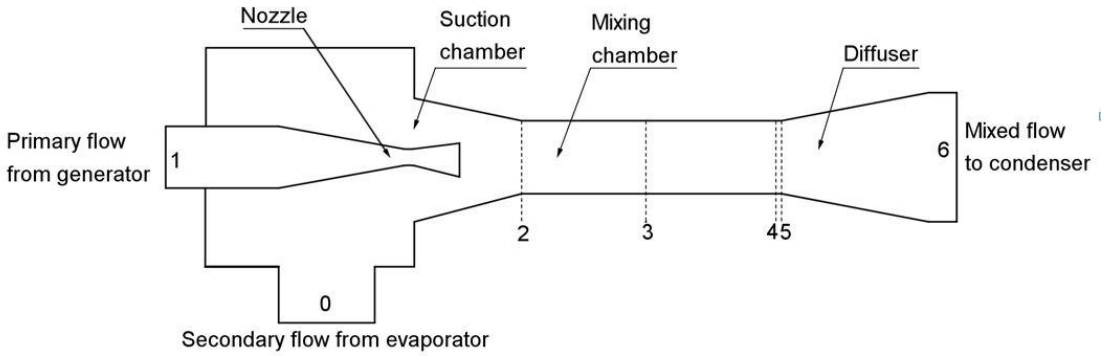

Figure 12 : Ejector

2.4.2.1 Assumptions for the ejector

The basic assumptions for the ejector modeling are [84],[24]:

- The flow inside the ejector is steady state
- The losses during the compression, mixing and expansion of the fluid are modeled by the efficiency of the respective component

- No heat losses occur in the ejector (adiabatic ejector)
- The velocities of the fluid streams entering the ejector and exiting it are considered negligible.
- Specific heat ratio γ is constant and equal to 1.3 [85]
- The compression shock occurs at the end of the constant area of the ejector
- Ideal gas behavior
- The mixing occurs under constant pressure

About the last assumption, it must be noted that there have been two models describing the mixing of the two fluids. One is considering that the mixing occurs under constant pressure. The other considers mixing under constant volume. The constant pressure model is used by most researchers [84].

The nozzle, mixing and diffuser efficiencies were chosen based on literature values [24],[81],[84],[86]. As long as the mixing efficiency is concerned, the three first studies, which used the same definition of the mixing efficiency as that used here, proposed values of 0.85, 0.9 and 0.95 respectively. The value 0.9 was chosen for this study. The remark about the mixing efficiency was made because the mixing efficiency is not defined in the same way in all the studies, unlike the nozzle and diffuser efficiencies. The nozzle efficiency ranges from 0.9 to 0.95 and the diffuser efficiency from 0.85-0.95. The nozzle efficiency was considered to be 0.95 and the diffuser efficiency was set to 0.9.

An important assumption that has to be made is about the superheating degree of the stream that enters the ejector (point 1). That stream must obtain a superheating degree, due to the fact that the formation of droplets impedes the operation of the ejector. As mentioned by several researchers ([87],[81]) the gas dynamic process will be affected and so will the performance as well. The degree of superheat varies depending on the specific fluid used[81]. That is due to the form of each fluid's saturation curve and the distinction between dry, wet and isentropic fluids. So, a process of identifying the category to which each fluid belongs is necessary, and then the needed superheating can result from a process identical to that described in paragraph 2.3.2.1, where the process of calculating the superheating degree for the turbine inlet stream was described. Similar to that case, a minimum superheating degree of 2 K is considered in this model as well, which can become higher is needed. There is also a superheating degree in the evaporator outlet. That is something not as necessary as the superheating of the primary fluid. For example, Khalil et al. [86] used no superheat in the secondary flow. However, in this case, a superheating degree of 5 K is considered, given that it can make the cooling capacity higher. In connection with superheat value Khalil et al. [86] found out that the superheating degree practically didn't have an effect on the COP, but had an effect on the entrainment ratio (w increased with increase of the superheat). The assumed values for the ejector modeling are demonstrated in Table 7.

Table 7: Assumptions for the ejector modeling

γ	1,3
Generator Superheating (K)	5
Evaporator Superheating (K)	5
η_n (%)	95
η_{mix} (%)	90
η_d (%)	90

2.4.2.2 Ejector inner properties calculation

The description is done based on Figure 12.

An important parameter of the ejector is the entrainment ratio w, which is defined as:

$$w = \frac{\dot{m}_{evap}}{\dot{m}_{gen}} \quad 2.40$$

Before the stream enters the nozzle, it has an enthalpy value which will be referred to as h_1. The nozzle efficiency is defined as:

$$\eta_n = \frac{h_1 - h_2}{h_1 - h_{2,is}} \quad 2.41$$

After flowing through the nozzle, the fluid's pressure is reduced, reaching a value slightly lower than the evaporation pressure. This pressure will be referred to as $\mathrm{P}_{\mathrm{low}}$.

In point 2, the two streams start the mixing, which is considered complete at the end of the mixing chamber of the nozzle. The primary fluid has just exited the nozzle, while the secondary fluid is flowing from the suction chamber.

The enthalpy at the point $2_{is,gen}$ is defined as:

$$h_{2,is,gen} = h(P = P_{low}, s = s_{gen,out}) \quad 2.42$$

So, given the nozzle efficiency, the enthalpy at point 2 can be calculated from 2.41

Energy balance for the primary fluid stream (inlet to outlet of the nozzle):

With the assumption of zero speed before the entrance in to the ejector, the speed of the primary stream is given by the equation:

$$u_{2,gen} = \sqrt{2 * \eta_{nozzle} * (h_1 - h_{2,is,gen})} \quad 2.43$$

Finally, the Mach number in point 2 is given by the equation:

$$M_{gen\,,2} = \sqrt{\frac{2 * \eta_{nozzle}}{\gamma - 1}\left[\left(\frac{P_{gen}}{P_{low}}\right)^{\frac{\gamma-1}{\gamma}} - 1\right]} \qquad 2.44$$

Point 2 (considering the secondary stream)

This process is considered isentropic, due to the fact that the velocity of the secondary fluid at point 2 is extremely low and only small losses occur. With that assumption, the velocity is:

$$u_{2,evap} = \sqrt{2 * \left(h_0 - h_{2,evap}\right)} \qquad 2.45$$

The enthalpy at point 2_{evap} is given, considering the process isentropic:

$$h_{2,evap} = h(P = P_{low}, s = s_{evap\,,out}) \qquad 2.46$$

Finally, the Mach number of the secondary stream at point 2 is given by the equation:

$$M_{evap\,,2} = \sqrt{\frac{2}{\gamma - 1}\left[\left(\frac{P_{evap}}{P_{low}}\right)^{\frac{\gamma-1}{\gamma}} - 1\right]} \qquad 2.47$$

After the total mixing of the two streams, conservation equations can be used to calculate the mass flow and the velocity in each point. The conservation of mass can be expressed as:

$$\dot{m}_{gen} + \dot{m}_{evap} = \dot{m}_{tot} = \dot{m}_{cond} \qquad 2.48$$

As mentioned before, a compression shock occurs which lowers the fluid's velocity and increases its pressure. The point before the shock occurs is named 4, and the point after that 5. The conservation of momentum enables the calculation of the velocity in that point:

$$P_{in} A_{in} + \dot{m}_{gen} u_{2,gen} + \dot{m}_{evap} u_{2,evap} = P_{out} A_{out} + (\dot{m}_{gen} + \dot{m}_{evap}) u_4{}' \qquad 2.49$$

Given that the mixing process is considered to occur under constant pressure and that the mixing section is considered to have constant area, the terms PA can be deleted from equation 2.49. Moreover, this equation is valid considering that the mixing process is ideal. The velocity which would occur for ideal mixing is represented as $u_4{}'$. With the definition of mixing efficiency (Equation 2.50), the calculation of the real velocity u_4 is possible.

$$\eta_{mix} = \frac{u_4}{u_4'} \tag{2.50}$$

Using equation 2.40, the momentum conservation equation can be transformed to:

$$u_4' = \frac{u_{2,gen} + w u_{2,evap}}{1+w} \tag{2.51}$$

Using the mixing efficiency, the real velocity can be expressed as:

$$u_4 = \frac{u_{2,gen} + w u_{2,evap}}{1+w} \sqrt{\eta_{mix}} \tag{2.52}$$

From the energy conservation equation between the inlet of the ejector and point 4 results in equation 2.53 :

$$h_4 = \frac{h_1 + w h_0}{1+w} - \frac{{u_4}^2}{2} \tag{2.53}$$

For every point, the critical values can be defined, as the values of the several variables which occur in the point where there is sonic velocity (M=1). The Mach number with the sound speed at the sonic velocity can be defined as M^*.

For point 4, that can be written as:

$${M_4}^* = \frac{({M_{gen,2}}^* + w {M_{evap,2}}^* * \sqrt{\frac{T_{evap}}{T_{gen}}})}{\sqrt{(1+w) * (1 + w\frac{T_{evap}}{T_{gen}})}} \sqrt{\eta_{mixing}} \tag{2.54}$$

Furthermore, equation 2.55 gives the connection between M and M^*

$$M^* = \sqrt{\frac{M^2(\gamma+1)}{M^2(\gamma-1)+2}} \tag{2.55}$$

So ${\mathrm{M}_4}^*$ is calculated first and then M_4.

Point 5 is defined as the point just after the compression shock. That means that the compression shock is taking place between points 4 and 5. According to the equations that describe the compression shock, the Mach number and the pressure of point 5 can be given by the equations:

$$M_5 = \sqrt{\frac{{M_4}^2 + \frac{2}{\gamma - 1}}{\frac{2\gamma {M_4}^2}{\gamma - 1} - 1}} \quad 2.56$$

$$\frac{P_5}{P_4} = \frac{1 + \gamma {M_4}^2}{1 + \gamma {M_5}^2} \quad 2.57$$

The efficiency of the diffuser is defined as:

$$n_d = \frac{h_{6,is} - h_4}{h_6 - h_4} \quad 2.58$$

The enthalpy of point 6_{is} is equal to:

$$h_{6is} = h(s = s_4, P = P_c) \quad 2.59$$

According to the energy balance between point 4 and the outlet of the ejector (or inlet of condenser) and given that the velocity of the stream in the outlet of the ejector is considered zero, the enthalpy of the stream at the outlet of the ejector is equal to:

$$h_6 = h_4 + \frac{{u_4}^2}{2} \quad 2.60$$

Finally, the ejector outlet pressure (also condenser pressure) is given by the equation:

$$\frac{P_{cond\ ,new}}{P_5} = [\frac{\gamma - 1}{2} {M_5}^2 + 1]^{\frac{\gamma}{\gamma - 1}} \quad 2.61$$

Since the pressure that is calculated by the equation 2.61 is the condenser pressure, the process that has been described must result in that pressure. That means that an iteration must be done, until the pressure value converges to the defined condenser pressure.

Finally, using the equations 2.43,2.45,2.58,2.60 , equation 2.52 can be transformed to the following equation 2.62, which calculates the mass ratio. However, the mass ratio is already assumed. That means that an iteration must be done, until the value of the mass ratio converges.

$$w = \frac{\sqrt{2 * n_n * (h_1 - h_{2,is,gen})} - \sqrt{\frac{2(h_{6,is} - h_4)}{n_d n_{mix}}}}{\sqrt{\frac{2(h_{6,is} - h_4)}{n_d n_{mix}}} - \sqrt{2 * (h_0 - h_{2,evap})}} \quad 2.62$$

With those two iterations, the calculation of the values of the several variables of the ejector is completed. The most important result from that process, which is necessary for the calculation of the efficiency of the system, is the mass ratio that corresponds to the given assumptions (efficiencies, pressures). Other than that, the calculation for the other parts of the system can be done.

To sum up, two iterations are needed in order to fully calculate the properties of the flow inside the ejector. There are two iterative processes needed, the inner and the outer. The outer process starts by assuming a value for P_{low} and continues until the exit pressure of the ejector is the same with the defined condenser temperature. The inner iteration calculates the mass ratio for each assumed mixing pressure, by first assuming a value for the mass ratio and then renewing it by equation 2.62.

A diagram of the process is given below (Figure 13):

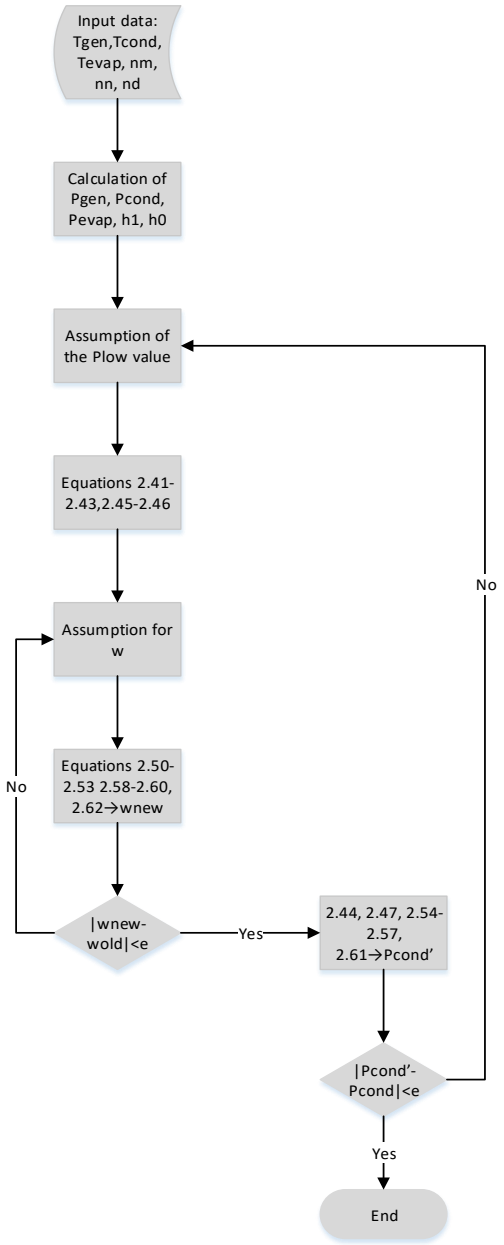

Figure 13 : Ejector's properties calculation process

This method of calculation was chosen over other methods. In general, there have been many studies on the ECC system. Moreover, there are many different approaches to the process of calculation of the properties of the flow inside the ejector. For example Yu et al.[84] proposed a process, in which the mixing pressure is considered same with the evaporation pressure, since the difference is small. However, the study calculates the mass ratio with an iterative process similar to that presented here. On the other hand, El-Dessouky et al.[85] proposes a process where either the mass ratio is defined and the mixing pressure is calculated or the areas of the ejector are defined and the mass ratio is calculated. The latter process, by defining the areas, indirectly defines the mixing pressure. The method followed here was mainly based on the model of Chen et al.[24] and other similar models (Saleh [31], Rashidi [88]), which calculate both parameters (mixing pressure and mass ratio) in the same time, without defining one of this parameters directly or indirectly. Finally, it must be mentioned that a calculation of the ejector's dimensions can be easily implemented, even though that is not within the purpose of this thesis.

The rest of the system was modeled in a similar way to the ORC-VCC cycle.

2.4.3 Assumptions

The rest of the assumptions that have to do with the ECC system are similar to those done on the ORC-VCC system. The pump was considered to have an isentropic efficiency of 0.8. Furthermore, since the pump is powered by a motor in this case, a motor efficiency was considered for the pump, to account for the losses during the conversion from electricity to mechanical work [14]. The assumptions are displayed in Table 8.

Table 8: Assumptions for the ECC cycle

Pump	
Isentropic efficiency	0,8
Motor efficiency	0.85
Condenser	
Temperature (°C)	40
Pinch point (K)	10
Cooling water inlet temperature (°C)	15
Subcooling degree (K)	5
Evaporator	
Superheating degree (K)	5
Range	5
Approach	5

2.4.4 Variables

The variables chosen in this system, as well as the range of their values, are exactly the same with that of the ORC-VCC system, since a comparison between these two is the purpose. So, this paragraph is same with paragraph 2.3.3.

2.4.5 Objective

The objective of the modeling of the ECC system is to calculate the maximum cooling power that can be produced by the cycle. The outputs of the cycle calculations are presented in Table 9. The cooling power, the COP of the system and the exergetic efficiency can be calculated, with the process that is shown in Figure 10.

Table 9: Outputs of the ECC cycle calculations

Qevap (kW)
COP
ηex

2.4.6 Calculation of thermodynamic properties and efficiency

The description of the system will be done with respect to Figure 14.

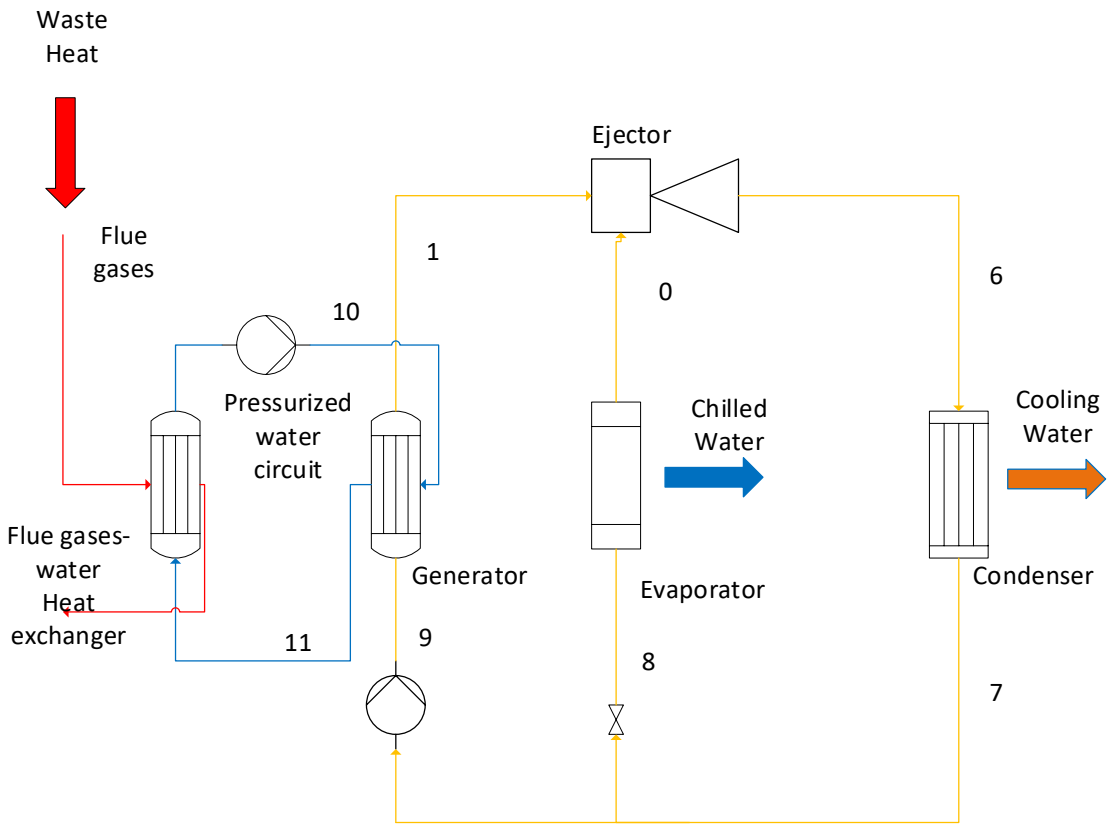

Figure 14: ECC system configuration

Since the inlet to the condenser is known, the outlet (point 7) is determined since its pressure is equal to the condenser pressure and the temperature is has a defined subcooling value. Enthalpy at point 8 (inlet to the evaporator) is equal with h_7 and its pressure is equal to the evaporator pressure. Likewise, at point 9, the pressure is equal to the generator pressure and the enthalpy is given by the definition of the isentropic efficiency of the pump:

$$h_9 = h_7 + \frac{h_{9,is} - h_7}{\eta_{pump}} \qquad 2.63$$

Enthalpy at point 9_{is} is given by the equation:

$$h_{9,is} = h(P = P_{gen}, s = s_7) \qquad 2.64$$

Point 0 (exit from evaporator) is considered to have a superheating degree of 5 K, so its temperature and pressure are known.

Finally, point 1 has a known pressure and a known superheating degree, so it is fully defined.

The working fluid mass flow can be calculated by the energy balance in the generator. Since both temperatures of the two streams and the mass flow of the hot water are known in the generator, the mass flow of the fluid can be given by equation:

$$\dot{m}_{fluid} = \frac{\dot{m}_{hw}(h_{hw,in} - h_{hw,out})}{h_1 - h_9} \quad 2.65$$

With the above calculations, it is possible to calculate the input power, cooling power of the evaporator, which is the product of the cycle, as well as the power of the condenser which comes from the ECC.

The power of the generator equals:

$$\dot{Q}_{gen} = \dot{m}_{fluid}\,(h_1 - h_9) \quad 2.66$$

The power of the evaporator equals:

$$\dot{Q}_{evap} = \dot{m}_{fluid}\,(h_{1'} - h_8) \quad 2.67$$

The power of the condenser equals:

$$\dot{Q}_{cond} = \dot{m}_{fluid}\,(h_6 - h_7) \quad 2.68$$

Finally, the electrical demand for the pump operation is:

$$\dot{P}_{pump} = \frac{\dot{m}_{fluid}\,(h_9 - h_7)}{\eta_{motor}} \quad 2.69$$

The COP of the whole system is equal to:

$$COP = \frac{\dot{Q}_{evap}}{\dot{Q}_{gen}} \quad 2.70$$

After these calculations, the exergy destruction in each component can be calculated. The exergy destruction is the difference between the exergy inlets and outlets. The destruction in each component is equal to:

Flue gases-water heat exchanger

$$\dot{E}_{d,he} = \dot{m}_g\left(e_{g,in} - e_{g,out}\right) + \dot{m}_{hw}(e_{hw,in,he} - e_{hw,out,he}) \quad 2.71$$

Generator

$$\dot{E}_{d,gen} = \dot{m}_{hw}\left(e_{hw,in,gen} - e_{hw,out,gen}\right) + \dot{m}_{gen}\left(e_9 - e_1\right) \quad 2.72$$

Ejector

$$\dot{E}_{d,ejector} = \dot{m}_{gen}\, e_1 + \dot{m}_{evap}\, e_0 - \dot{m}_{tot}\, e_6 \quad 2.73$$

Evaporator

$$\dot{E}_{d,e} = \dot{m}_{cw}\left(e_{cw,in} - e_{cw,out}\right) + \dot{m}_{evap}\left(e_8 - e_0\right) \quad 2.74$$

Condenser

$$\dot{E}_{d,cond} = \dot{m}_{cool,w}\left(e_{cool,w,in} - e_{cool,w,out}\right) + \dot{m}_{cond}\left(e_6 - e_7\right) \quad 2.75$$

Pump

$$\dot{E}_{d,pump} = \dot{m}_{gen}\left(e_7 - e_9\right) + \dot{P}_{pump} \quad 2.76$$

Valve

$$\dot{E}_{d,v} = \dot{m}_{evap}\left(e_7 - e_8\right) \quad 2.77$$

The total exergy destruction is equal to:

$$\dot{E}_{dtot} = \dot{E}_{d,he} + \dot{E}_{d,gen} + \dot{E}_{d,e} + \dot{E}_{d,cond} + \dot{E}_{ejector} + \dot{E}_{d,pump} + \dot{E}_{d,v} \quad 2.78$$

Finally, it must be mentioned that the total exergy destruction can be calculated from the following equation:

$$\sum \dot{E}_{in} = \sum \dot{E}_{out} + \dot{E}_{dtot} \quad 2.79$$

In 2.79, the exergy inlets include the pump power, which in this case is an inlet to the system.

Exergetic efficiency

The exergetic efficiency in this case is calculated by the following equation:

$$n_{ex} = \frac{\dot{E}_{cw,out}}{\dot{E}_{g,in} + \dot{P}_{pump}} \quad 2.80$$

The above-mentioned calculations are implemented by an algorithm, which works in Matlab. The algorithm is also depicted in Figure 10 (similar to ORC-VCC).

2.5 Modeling of the absorption chiller

The absorption chiller is a different system, comparing with the previous systems. That is due to the fact that its operation is based on a phenomenon, which occurs between the refrigerant and the absorbent. So, the chiller's model requires a proper modeling of the phenomenon and the calculation of the properties of the working fluid, which is a mixture.

2.5.1 Working fluid

As mentioned in paragraph 1.2.3, the chosen mixture was lithium-bromide/water. Since the water temperatures that are tested in this thesis are above 0 ℃, the lithium-bromide/water mixture can operate up to a chilled water outlet temperature and produce the cooling effect. In the same time, absorption chillers with lithium-bromide/water mixture have greater efficiency than the water/ammonia chillers [38]. So, the lithium-bromide/water mixture was chosen to be examined, since in any case it would come out better than water/ammonia. However, if the study was about cooling under 0 ℃, water/ammonia would be the only choice, since water as refrigerant cannot operate under 0 ℃. However, the lithium-bromide/water chiller, with the specific modeling, could reach 6 ℃ of chilled water outlet temperature. Since the calculation of the mixture properties is necessary, some things about it must be mentioned first and then the calculation process will be demonstrated.

2.5.1.1 Properties of the lithium-bromide/water mixture

The thermodynamic properties of the mixture can be derived from two diagrams. These are the Dühring diagram, which a pressure-temperature diagram and the enthalpy-concentration diagram. The thermo-physical properties of the mixture, as well as the two diagrams are given by ASHRAE [39].

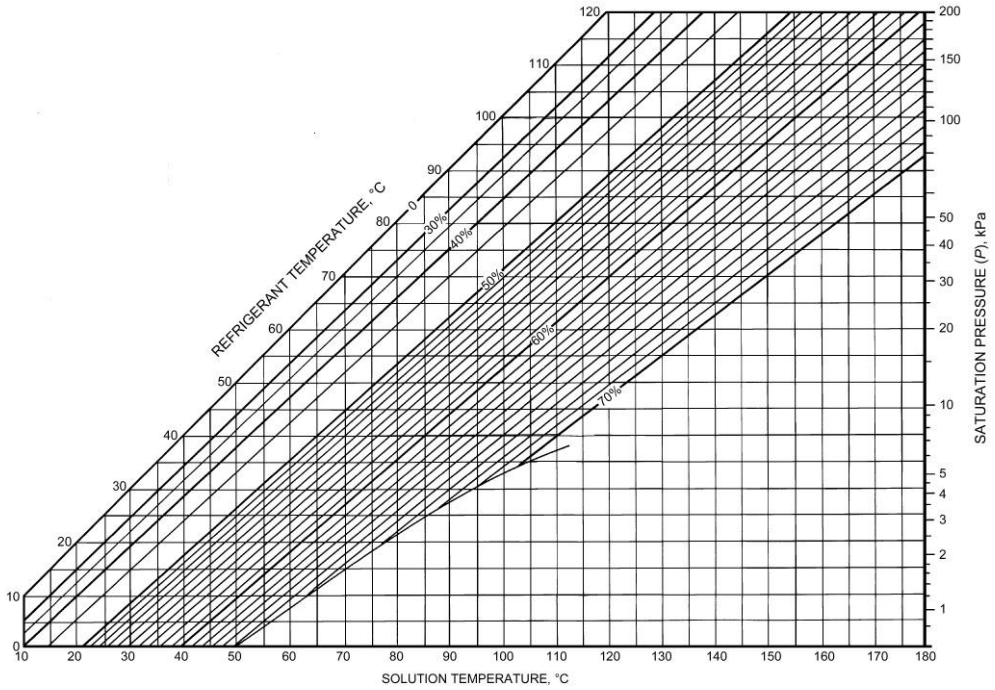

Figure 15 : Dühring diagram [39]

The Dühring diagram (Figure 15) connects the solution temperature with the refrigerant temperature (or the saturation pressure, since these two are directly connected), with the concentration of the mixture as a parameter. The maximum concentration depicted is that of 70 %, since higher concentrations result in problems in the operation of the absorption chiller. Moreover, the crystallization line is visible, which sets the limit for sound operation of the mixture in the chiller. This diagram has an analytical description, which is given by ASHRAE. However, for all the variables of the diagram, there specific limits within which their values range.

The variables that appear on the following equations are:

Table 10: Variables for the description of the Dühring diagram

Mixture temperature (℃)	t
Refrigerant temperature (℃)	t’
Mixture concentration	X
Refrigerant temperature (K)	T’
Saturation pressure (kPa)	P

The basic equations are:

$$t = \sum_{0}^{3} B_n X^n + t' \sum_{0}^{3} A_n X^n \qquad 2.81$$

$$t' = \frac{(t - \sum_0^3 B_n X^n)}{\sum_0^3 A_n X^n} \quad 2.82$$

$$logP = C + \frac{D}{T'} + \frac{D}{T'^2} \quad 2.83$$

$$T' = \frac{-2E}{D + [D^2 - 4E(C - logP)]^{0.5}} \quad 2.84$$

The constants that appear have the following values (Table 11):

Table 11: Constants of equations 2.81-2.84

$A_0 = -2.00755$	$B_0 = 124.937$	$C = 7.05$
$A_1 = 0.16976$	$B_1 = -7.71649$	$D = -1596.49$
$A_2 = -3.133362 * 10^{-3}$	$B_2 = 0.152286$	$E = -104095.5$
$A_3 = 1.97668 * 10^{-5}$	$B_3 = -7.95090 * 10^{-4}$	

Finally, the variables range within the following limits:

Table 12 : Range for each variable of equations 2.81-2.84

$-15 < t' < 110$ ℃
$5 < t < 175$ ℃
$45 < x < 70$ %

The second diagram that allows the calculation of thermodynamic properties of the Lithium-Bromide/Water mixture is the enthalpy-concentration diagram (Figure 16) provided by ASHRAE as well [39].

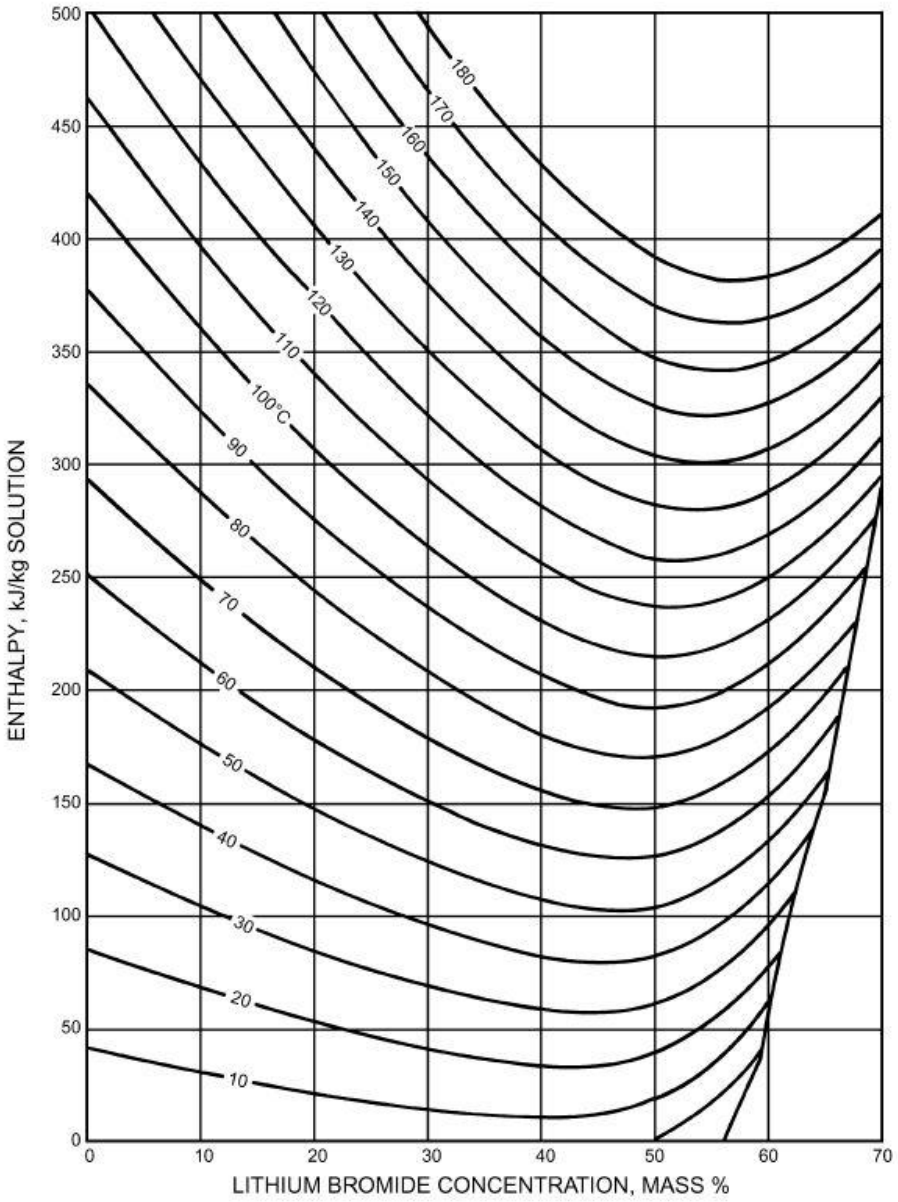

Figure 16 : Enthalpy-concentration diagram [39]

This diagram refers only to saturated points.

The analytical description of the diagram is given below.

The variables that appear on the following equations are:

Table 13 : Variables for the description of the h-X diagram

Enthalpy of mixture ($\frac{\text{kJ}}{\text{kg}}$)	h
Mixture temperature (°C)	t
Mixture concentration	X

The equation for the description of the diagram is:

$$h = \sum_{0}^{4} A_n X^n + t \sum_{0}^{4} B_n X^n + t^2 \sum_{0}^{4} C_n X^n \qquad 2.85$$

The constants that appear have the following values (Table 14)

Table 14 Constants of the equation 2.85

$A_0 = -2024.33$	$B_0 = 18.2829$	$C_0 = -3.7008214 * 10^{-2}$
$A_1 = 163.309$	$B_1 = -1.1691757$	$C_1 = 2.8877666 * 10^{-3}$
$A_2 = -4.88161$	$B_2 = 3.248041 * 10^{-2}$	$C_2 = -8.1313015 * 10^{-5}$
$A_3 = 6.302948 * 10^{-2}$	$B_3 = -4.034184 * 10^{-4}$	$C_3 = 9.9116628 * 10^{-7}$
$A_4 = -2.913705 * 10^{-4}$	$B_4 = 1.8520569 * 10^{-6}$	$C_4 = -4.4441207 * 10^{-9}$

Finally, the variables range within the following limits:

Table 15 : Range for each variable of Equation 2.85

$15 < t < 165$ ℃
$45 < x < 70$ %

With the above mentioned process, the two diagrams can be inserted into an algorithm and provide the properties of the mixture.

Finally, it must be mentioned that the density of the mixture is calculated by the relationships given in [89].

In that point, some important properties of the mixture must be mentioned, in order to explain the modeling of the system that took place.

Crystallization

An important issue in the operation of Lithium-Bromide/Water absorption chillers is the crystallization. In general, the Lithium-Bromide/Water mixture has some limits in its concentration of Lithium-Bromide. That means that for high concentrations in salt, the salt cannot be dissolved in the water and starts precipitating. That may lead to the solid lithium-bromide clinging in the pipes and impeding the flow of the mixture, or even, in extreme

cases, stop the flow of the mixture. As can be seen from Figure 17, as the concentration rises, the possibility of the formation of solid Lithium-Bromide is higher, especially when the temperatures are low. That means that as long as the absorption chiller is concerned, the points with high concentration and relatively low temperatures are those with the greatest possibility of crystallization. Moreover, as can be seen from Figure 155, there is the line of crystallization in the diagram, which defines the limit of safety operation for the chiller. So, as will be mentioned later, there must be a checking in the properties of the point which is closer to crystallization.

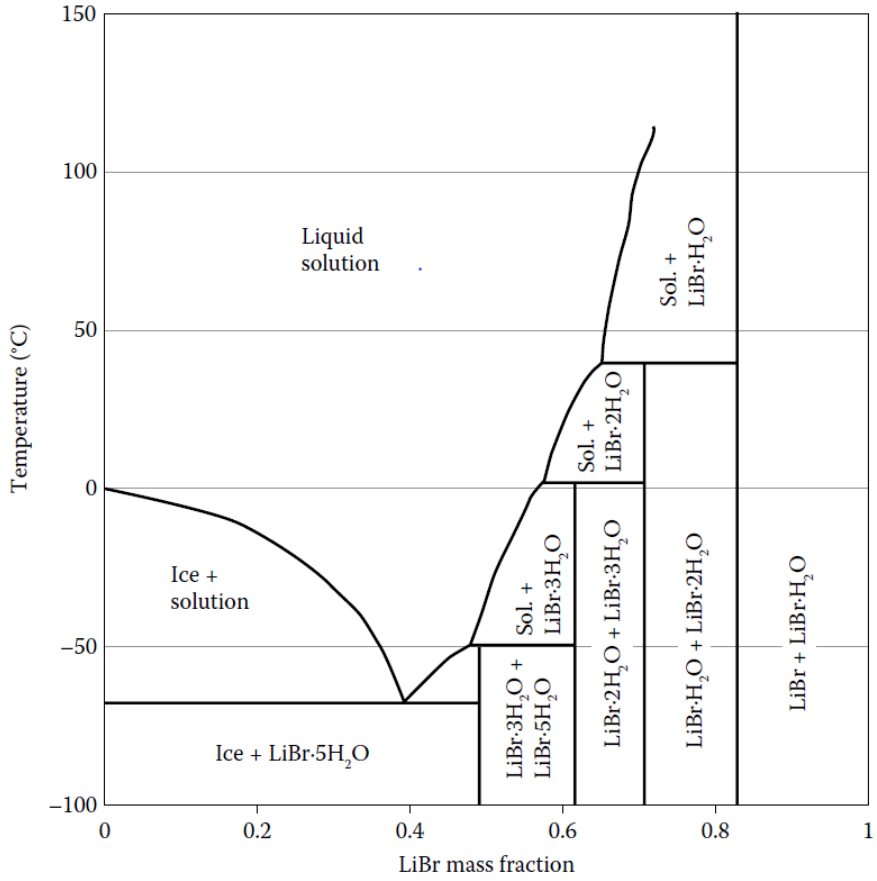

Figure 17: Phase diagram of Lithium-Bromide/Water mixture [40]

In general, the problems related with crystallization are not detrimental for the chiller. To solve them, the pipes are heated, in order to reduce their viscosity and then water is circulated to clean the pipes. However, this process of cleaning is time-consuming and costly [40].

Corrosion

Another problem of the absorption chillers is corrosion. Especially for the Lithium-Bromide/Water mixture, the presence of oxygen makes the mixture corrosive to metals like carbon steel and copper, which are the most likely to be used in absorption chillers, because of the working temperatures. Of course, the better insulated a system is, the less oxygen can

be present inside it. However, in the life of a chiller, there is corrosion of the materials, for which anti-corrosion substances are used [40].

2.5.2 Assumptions

The modeling of the system was based on several assumptions. In the literature, there have been many studies on absorption chillers, which are based on different assumptions. Moreover, the system's modeling is divided into the internal and the external model. The internal model evaluates the properties and describes the processes of the mixture in the chiller. The external model connects the inner model with heat source and with the cooling and the chilled water. This thesis was based on the following assumptions:

Internal model

- Zero pressure losses in the heat exchangers or the pipes
- Zero thermal losses in the heat exchangers
- Isentropic operation of the pump (will be explained later)
- Isenthalpic throttling in the valve
- The outlet of the generator is superheated vapor with temperature equal to $t(P = P_{high}, x = x_{weak})$
- The vapor at the outlet of the generator has zero Lithium-Bromide concentration
- The outlet from condenser and evaporator are saturated
- The absorber temperature is same with the condenser temperature
- Heat exchanger effectiveness equals 0.6

About the last assumption, from the literature, the values of effectiveness range from 0.5 to 0.7. Since the design properties of the heat exchanger (U,A) are not known, a typical value of 0.6 was chosen. It is also reported that the efficiency of the cycle depends on the effectiveness and more specifically, it rises as the effectiveness rise.

The assumption of isentropic pump will be analyzed further below:

For a fluid, the enthalpy can be expressed as:

$$dh = C_p\,dT + [\upsilon - T\left(\frac{\partial \upsilon}{\partial T}\right)_P]dP \qquad 2.86$$

Moreover, if the fluid is incompressible, equation 2.86 can become:

$$dh = C_p\,dT + \upsilon dP \qquad 2.87$$

The entropy of a fluid can be expressed as:

$$ds = C_p\,\frac{dT}{T} + \left(\frac{\partial \upsilon}{\partial T}\right)_P dP \qquad 2.88$$

From equation 2.88, it can be derived that an isentropic process of an incompressible fluid is also isothermal. So equation 2.87 can be transformed into

$$dh = vdP \quad 2.89$$

That means that for an isentropic process in the pump, the following equation can be obtained:

$$\Delta h = \frac{\Delta P}{n_{pump}\ \rho} \quad 2.90$$

The efficiency of the pump has been added (practically motor efficiency), to account for the electromechanical losses of it, with a value of 0.85 [40].

Heat exchanger

The heat exchanger of the system helps reducing the needed inlet heat to the system. The heat exchanger model of effectiveness was used for that heat exchanger (Paragraph 2.1). Equation 2.3 can be transformed into:

$$\varepsilon = \frac{(T_{h,in} - T_{h,out})}{(T_{h,in} - T_{c,min})} \quad 2.91$$

That transformation is done because in that case, the hot stream has the minimum mass flow rate and specific heat product [40].

From the properties of the mixture, the efficiency of the absorption chiller can be calculated with the generator temperature as parameter, as it is explained in 2.5.5.

External model

The first assumption has to do with the temperature of the generator in relation with the hot water inlet temperature. The generator temperature is assumed to be 10 K lower than the hot water inlet temperature. This assumption can be based on the following fact:

According to Herold et al. [40], when modeling the heat exchange in the generator, the temperatures of point 4 and point 7 are considered, while the temperature effect of point 3 (subcooled state inlet) is neglected. The LMTD of the heat exchanger is expressed as:

$$LMTD = \frac{(T_{11} - T_4) - (T_{12} - T_7)}{\ln(\frac{T_{11} - T_4}{T_{12} - T_7})} \quad 2.92$$

Furthermore, it is mentioned that the pinch point frequently occurs in either the inlet or the outlet of the heat exchanger. A normal value for the pinch point is 10 K. So, by assuming that the pinch point occurs between the temperatures of point 4 (generator temperature) and

the heat source inlet temperature, the previously mentioned assumption can be justified. However, in order to accept this assumption, it must be ensured that the temperature difference between the other two points (point 7 and heat source outlet temperature) is not lower than 10 K. So, a check in this temperature difference is added to the cycle model.

Finally, an assumption that the heat source temperature difference is 7 K is made. Those are values typical for such cases [90],[91],[92] .

Moreover, assumptions about the heat transfer in the condenser and evaporator are made, similar to those made for the other systems. The pinch point, cooling water inlet temperature and pressure and the subcooling degree of the working fluid are assumed and the water outlet and mass flow are calculated. For the evaporator, the superheating of the working fluid, the approach and the range are set and the chilled water mass flow is calculated.

The total assumptions appear in Table 16:

Table 16 : Assumptions for the absorption chiller modeling

Evaporator	
Range (K)	5
Approach (K)	5
Superheating (K)	5
Condenser	
Pinch Point (K)	10
Cooling water inlet temperature (°C)	20
Subcooling (K)	5
Generator	
Generator Temperature (°C)	$T_{hw,in} - 10$
Hot water outlet temperature (°C)	$T_{hw,in} - 7$
Pump	
Pump efficiency (motor efficiency)	0.85
Heat exchanger	
Heat exchanger effectiveness	0.6

2.5.3 Variables

The variables in this case are similar with those in the other cases, but not the same. The outlet temperature of the chilled water took several values that could be achieved by the chiller. More specifically, those were in the range 6-10 °C. Given the approach, the evaporator temperature is determined. The lower limit is set due to the fact that since the approach is set at 5 K, temperatures lower than 6 result in evaporator temperatures lower than 1 °C, something that can't be achieved. This is an expected restriction for an absorption chiller (1.2.3). The upper limit is not binding, as higher temperatures can be achieved.

Because of the temperature working range of absorption chiller, the pinch point of 30 °C cannot be implemented here, as the working temperatures are lower than in the other systems. So, as long as the heat exchanger between the gas and the water is concerned, there was just a check that the pinch point is greater than 5 K, in order to ensure that the

heat transfer is possible. In the second heat exchanger, the generator, the previous method of optimizing the generator pressure is not followed here. In the absorption chiller, there is a direct connection between the hot water inlet and outlet temperature and the generator temperature. That means that for a specific value of hot water inlet temperature, the generator temperature can obtain only one value. So, a number of different hot water temperatures were used, in order to find the highest COP and exergetic efficiency values.. Two additional checks are needed in the case of the temperatures which are calculated from the model. First, it must be ensured that the lower temperature difference occurs between the heat source inlet and the generator temperature. Thus, it must be secured that the temperature difference between the hot water outlet and the considered generator inlet temperature is greater than 10 K. The other check has to do with the temperature difference between the generator inlet and outlet temperature. That check corresponds to the demand that the weak concentration is lower than the strong concentration. That is an obvious demand, which however may not be succeeded in some cases and that leads to a generator outlet temperature lower than the inlet temperature. With those three checks, both the normal operation and the assumptions demands are secured.

Table 17: Variables

Variable	Range
Hot water inlet temperature (°C)	95-120
Chilled water outlet temperature (°C)	4,7,10

2.5.4 Objective

The objective of the study is to find out the variation of the COP, cooling power and exergetic efficiency of the absorption chiller, in a specific range of permitted hot water inlet temperatures. The variation is calculated for five achievable chilled water outlet temperatures. The outputs from the calculation of the cycle's efficiency for each chilled water outlet temperature are:

Table 18 : Outputs of the cycle calculations

Qevap (kW)
COP
ηex

2.5.5 Calculation thermodynamic properties and efficiency

The description of the calculation of the thermodynamic properties of each point of the cycle is presented below. The calculations are based on the two diagrams that describe the properties of the mixture, as well as to the calculation of water's properties. There are also some more assumptions concerning the points where the working fluid is the mixture, which help finding the properties of the points which are not saturated. The description of the calculations will be done based on Figure 18.

To begin with, points 1 and 4 are in saturated liquid state, while point 7 is in superheated vapor state, as its temperature (given in the assumptions) is higher than the saturated temperature corresponding to the condenser pressure. Points 8 and 10 have a specified subcooling and superheating degree, as they are the outlet of the condenser and evaporator respectively. Point 9 is in the two-phase region. Point 3 is in subcooled liquid state. However, it can be assumed that it is in saturated state, in order to use the h-x diagram and calculate its properties [43]. Same thing can be assumed for points 5 [43]and 6, since they are outlets from the system's components [44].

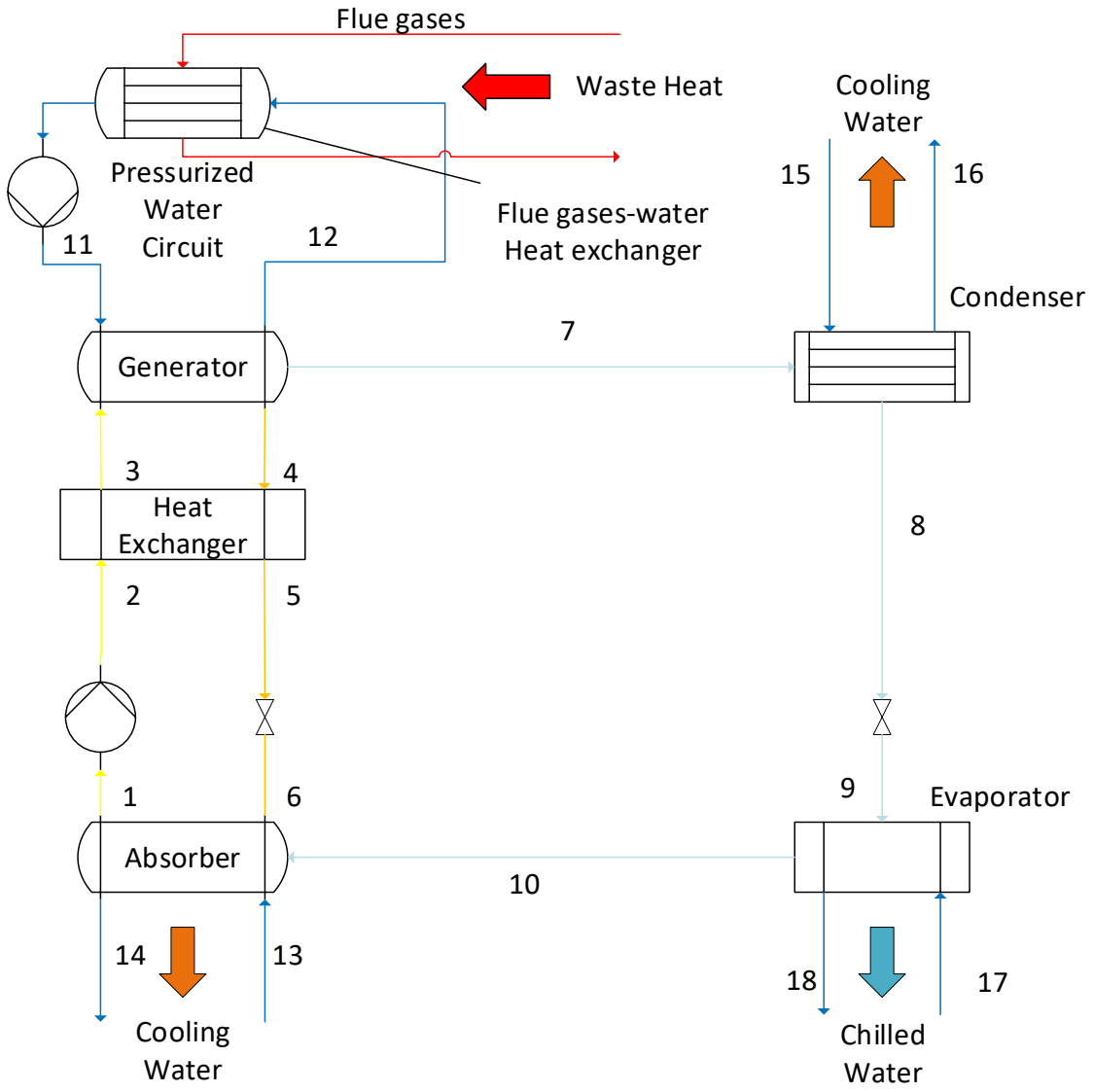

Figure 18 : Absorption chiller model

Point 1

This point represents the mixture's outlet from the absorber. The mixture has the low concentration of Lithium-Bromide. Its temperature is considered same with the absorber temperature and its pressure equal with the low pressure of the system. From those two properties, the concentration at this point can be determined for the Dühring diagram. This concentration is the weak concentration of the system (X_{weak}). A check is made on this concentration, on whether the concentration exceeds the maximum concentration (70 %), something that is however unlikely to happen.

Point 4

This point represents the mixture's outlet from the generator. The mixture has the high concentration of the system. Its temperature is the same with the generator temperature

and its pressure equal with the high pressure of the system. From those two properties, the concentration at this point can be determined from the Dühring diagram. This concentration is the strong concentration of the system (X_{strong}). A check is made on this concentration, on whether the concentration exceeds the maximum concentration (70 %), something that is possible. Another check is made between the strong and weak concentration, in case the latter is higher, something that is impossible to happen, but may occur during the calculations. Since the strong concentration is determined by the generator temperature and the generator temperature is determined by the hot water inlet temperature, those two checks are a way to eliminate some values of the hot water inlet temperature which lead to a cycle that cannot be implemented.

In connection with those checks, some limits were set to the generator and hot water inlet temperatures. Since the absorber temperature is constant, as the condenser temperature is constant (40 ℃), and the evaporator temperature is constant for during the calculations, the weak concentration doesn't change during the calculation. The strong concentration changes with the generator temperature. So, the above-mentioned checks impose limits to the acceptable generator temperature (or equally to the hot water inlet temperature). The low limits are set by the demand that the strong concentration must be higher than the weak, while the high limits are set by the demand for operation away from the crystallization line. For different evaporator temperature, the acceptable range changes. As can be seen from the Dühring diagram (Figure 19), while the evaporator temperature increases, the weak concentration decreases. That brings the low temperature limit in lower values. Those limits can be seen in the results of the absorption cycle (3.3).

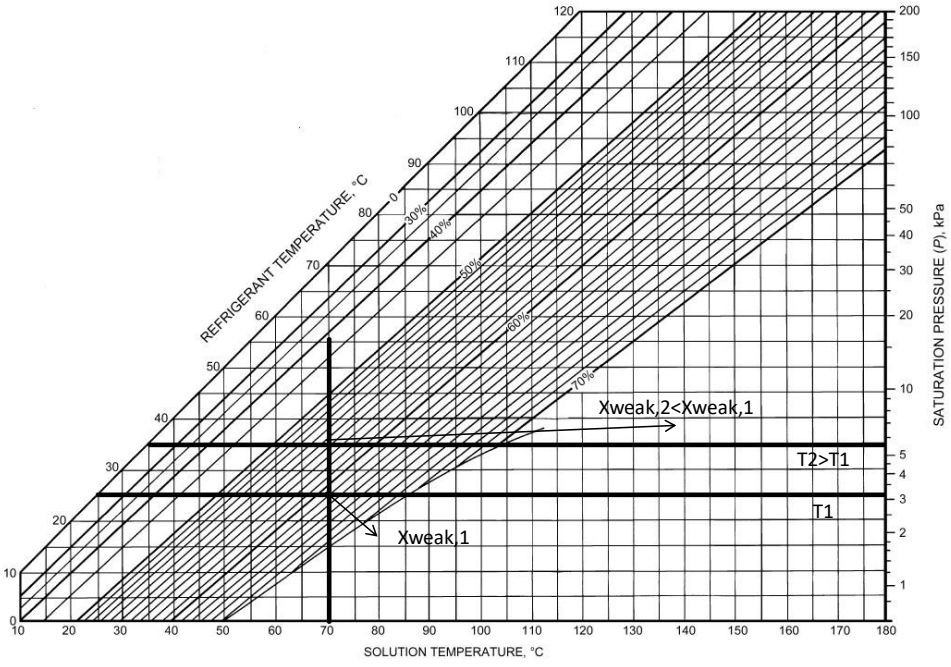

Figure 19 : Change of X_{weak} with the evaporation temperature

Point 7

This point represents the second outlet from the generator, which consists only of the refrigerant. As mentioned in the assumptions, this point is considered to have zero concentration of lithium-bromide. This is an assumption not far from the reality, since the difference in the boiling point between Lithium-Bromide and water is high and allows no evaporation of the absorbent. However, in mixtures like water/ammonia, this assumption cannot be made. Furthermore, the point is considered to be superheated vapor, with pressure equal to that of the condenser and temperature defined as:

$$t_7 = t(P = P_{high}, x = x_{weak}) \quad 2.93$$

From these properties, all the other properties can be calculated.

Point 8

This point represents the outlet from the condenser. It is considered as saturated liquid, so its properties cab be calculated.

Point 9

This point represents the outlet from the throttling valve. As mentioned in the assumptions, the process of throttling is considered isenthalpic, so the enthalpy and pressure of the point are known. This point usually has a small percentage of vapor, as by throttling, given the form of the saturated liquid curve of water (as well as all fluids in general), the fluid enters the two-phase region.

Point 10

This point represents the outlet of the evaporator and its properties are calculated based on the assumption that it is in saturated vapor state.

Point 2

This point represents the outlet of the pump. The modeling of the pump has been explained before. From equation 2.90, for the process 1-2, the following equation can be derived:

$$h_2 - h_1 = \frac{P_{cond} - P_{evap}}{n_{pump}\,\rho} \quad 2.94$$

Moreover, the power required for the pump operation is:

$$\dot{P}_{pump} = \dot{m}\frac{P_{cond} - P_{evap}}{n_{pump}\,\rho} \quad 2.95$$

Here, it must be noted that due to the fact that the density of the mixture is very high (about 1700 $\frac{\text{kg}}{\text{m}^3}$), while the pressure difference is low, the enthalpy difference and the required power of the pump will be very low. Thus, the properties of point 2 will be similar to those of point 1. Finally, it must be noted that many studies consider the work of the pump totally negligible.

For point 2, the enthalpy is known from the pump model and the pressure is equal to the high pressure of the system. From these, the temperature can be calculated from the h-x diagram.

Heat exchanger

From equation 2.91, the effectiveness of the heat exchanger can be expressed as:

$$\varepsilon = \frac{(T_{h,in} - T_{h,out})}{(T_{h,in} - T_{c,min})} = \frac{(T_4 - T_5)}{(T_4 - T_2)} \quad 2.96$$

Moreover, from energy balance at the heat exchanger (at which zero heat losses are considered):

$$\dot{m}_w(h_3 - h_2) = \dot{m}_s(h_4 - h_5) \quad 2.97$$

From equation 2.96, the temperature at point 5 can be calculated and then, by assuming that it is saturated, its enthalpy can be derived from the h-x diagram. Then, from equation 2.97, the enthalpy of point 3 is calculated. Finally, by considering point 3 as saturated, its temperature can be derived from the h-x diagram.

<u>Point 6</u>

That point represents the outlet from the throttling valve and has known pressure, concentration and enthalpy (since throttling is isentropic). If it is considered saturated as well, its temperature can come from diagram h-x.

With the calculation of the properties in each point, the mass flows and the power in each component can be calculated from mass and energy balances in the heat exchangers of the system. These are demonstrated with the following equations.

- Generator
    - Mass balance

$$\dot{m}_7 + \dot{m}_3 = \dot{m}_4 \quad 2.98$$

    - Lithium-bromide Balance

$$x_3\dot{m}_3 = x_4\dot{m}_4 \quad (2.99)$$

- Energy balance

$$Q_{gen} = \dot{m}_4 h_4 - \dot{m}_3 h_3 - \dot{m}_7 h_7 = \dot{m}_s h_4 - \dot{m}_w h_3 - \dot{m}_r h_7 \quad (2.100)$$

- Absorber
  - Energy balance

$$Q_{abs} = \dot{m}_{10} h_{10} + \dot{m}_6 h_6 - \dot{m}_1 h_1 = \dot{m}_r h_{10} + \dot{m}_s h_6 - \dot{m}_w h_1 \quad (2.101)$$

- Condenser
  - Energy balance

$$Q_{cond} = \dot{m}_7 h_7 - \dot{m}_8 h_8 = \dot{m}_r (h_7 - h_8) \quad (2.102)$$

- Evaporator
  - Energy balance

$$Q_{evap} = \dot{m}_{10} h_{10} - \dot{m}_9 h_9 = \dot{m}_r (h_{10} - h_9) \quad (2.103)$$

From these equations, with the previous calculations, the cooling capacity of the system is calculated, and the COP can be expressed as:

$$COP = \frac{Q_{evap}}{Q_{gen}} \quad (2.104)$$

A final remark must be made for the cooling of the condenser and absorber. Both heat exchangers are considered to be cooled by water in the same inlet temperature. Moreover, the fixed pinch point value in the condenser results in a temperature difference for the water in the condenser. It was considered that the same water temperature difference goes for the absorber as well. So, the mass flows and condenser power in both heat exchangers were calculated.

For the exergy calculations of the absorption cycle, the entropy of the lithium-bromide/water must be calculated first. The calculation was done based on the correlations given in [93]. When the entropy of the mixture is known, the calculations can continue in the same way as in the other cases.

Flue gases-water heat exchanger

$$\dot{E}_{d,he} = \dot{m}_g \left(e_{g,in} - e_{g,out}\right) + \dot{m}_{hw} (e_{hw,in,he} - e_{hw,out,he}) \quad (2.105)$$

Generator

$$\dot{E}_{d,gen} = \dot{m}_{hw}\left(e_{hw,in,gen} - e_{hw,out,gen}\right) + \dot{m}_w e_3 - \dot{m}_s e_4 - \dot{m}_r e_7 \quad (2.106)$$

Absorber

$$\dot{E}_{d,abs} = \dot{m}_{cool,w}\left(e_{cool,w,in} - e_{cool,w,out}\right) - \dot{m}_w e_1 + \dot{m}_s e_6 + \dot{m}_r e_{10} \quad (2.107)$$

Evaporator

$$\dot{E}_{d,e} = \dot{m}_{cw}\left(e_{cw,in} - e_{cw,out}\right) + \dot{m}_r(e_9 - e_{10}) \quad (2.108)$$

Condenser

$$\dot{E}_{d,cond} = \dot{m}_{cool,w}\left(e_{cool,w,in} - e_{cool,w,out}\right) + \dot{m}_r(e_7 - e_8) \quad (2.109)$$

Pump

$$\dot{E}_{d,pump} = \dot{m}_w(e_1 - e_2) + \dot{P}_{pump} \quad (2.110)$$

Mixture heat exchanger

$$\dot{E}_{d,mhe} = \dot{m}_w(e_2 - e_3) + \dot{m}_s(e_4 - e_5) \quad (2.111)$$

Valve 5-6

$$\dot{E}_{d,v56} = \dot{m}_s(e_5 - e_6) \quad (2.112)$$

Valve 8-9

$$\dot{E}_{d,v89} = \dot{m}_r(e_8 - e_9) \quad (2.113)$$

The total exergy destruction is equal to:

$$\dot{E}_{dtot} = \dot{E}_{d,he} + \dot{E}_{d,gen} + \dot{E}_{d,e} + \dot{E}_{d,cond} + \dot{E}_{abs} + \dot{E}_{d,pump} + \dot{E}_{d,v56} + \dot{E}_{d,v89} + \dot{E}_{mhe} \quad (2.114)$$

Finally, it must be mentioned that the total exergy destruction can be calculated from the following equation:

$$\sum \dot{E}_{in} = \sum \dot{E}_{out} + \dot{E}_{dtot} \quad (2.115)$$

In 2.79, the exergy inlets include the pump power, which in this case is an inlet to the system.

Exergetic efficiency

The exergetic efficiency in this case is calculated by the following equation:

$$n_{ex} = \frac{\dot{E}_{cw,out}}{\dot{E}_{g,in} + \dot{P}_{pump}} \quad 2.116$$

2.6 Adsorption chiller

As mentioned before, the adsorption chiller was not modeled as the other systems. Data from manufacturers were found instead, which describe the relationship between the heat source temperature and the efficiency of the system (COP, cooling product).

Generally, adsorption chillers are designed for relatively low cooling capacities, instead of absorption chillers, which are designed for a wide range of cooling capacities.

In any case, data from two manufacturers were acquired, whose adsorption chillers could operate in higher cooling capacities. Given that a typical COP for an adsorption chiller is about 0.6 and that the heat input is 1592 kW, the expected cooling capacity was about 950 kW.

2.6.1 ECO-MAX adsorption chiller

The first manufacturer that was chosen was ECO-MAX. The information about the chiller's efficiency were taken from the manufacturer's web page [57]. There, diagrams were found, which depict the capacity which the chiller achieves as percent of the nominal capacity when operating under specific hot water inlet, cooling water inlet and chilled water outlet temperature. The diagrams that are given refer to two specific chilled water temperatures, 45 F (Figure 20) and 50 F (Figure 21) (7 and 10 ℃), five cooling water inlet temperatures 65, 75, 80, 85, 90, 95 F (18.33, 23.88, 26.66, 29.44, 32.22, 35 ℃) and hot water inlet temperatures ranging from 150 to 200 F (65.55 to 93.33 ℃). These figures are shown below:

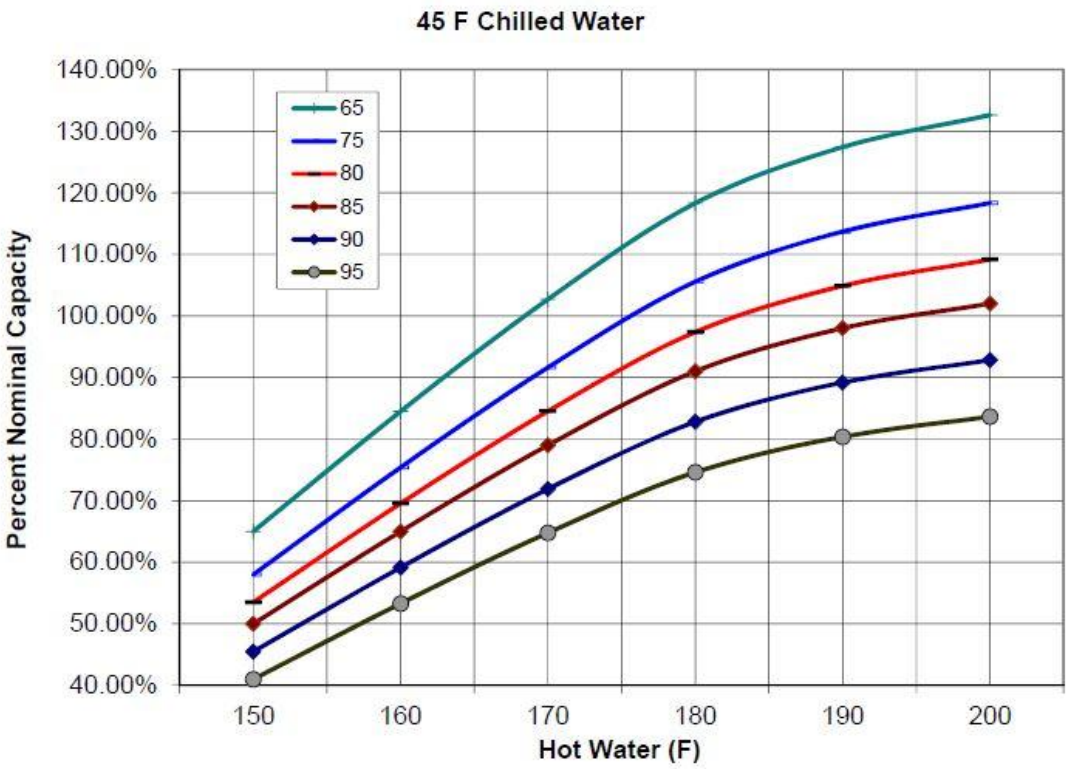

Figure 20 : Percentage of nominal capacity-Hot water temperature diagram for ECO-MAX absorption chiller at 45 F chilled water outlet [57]

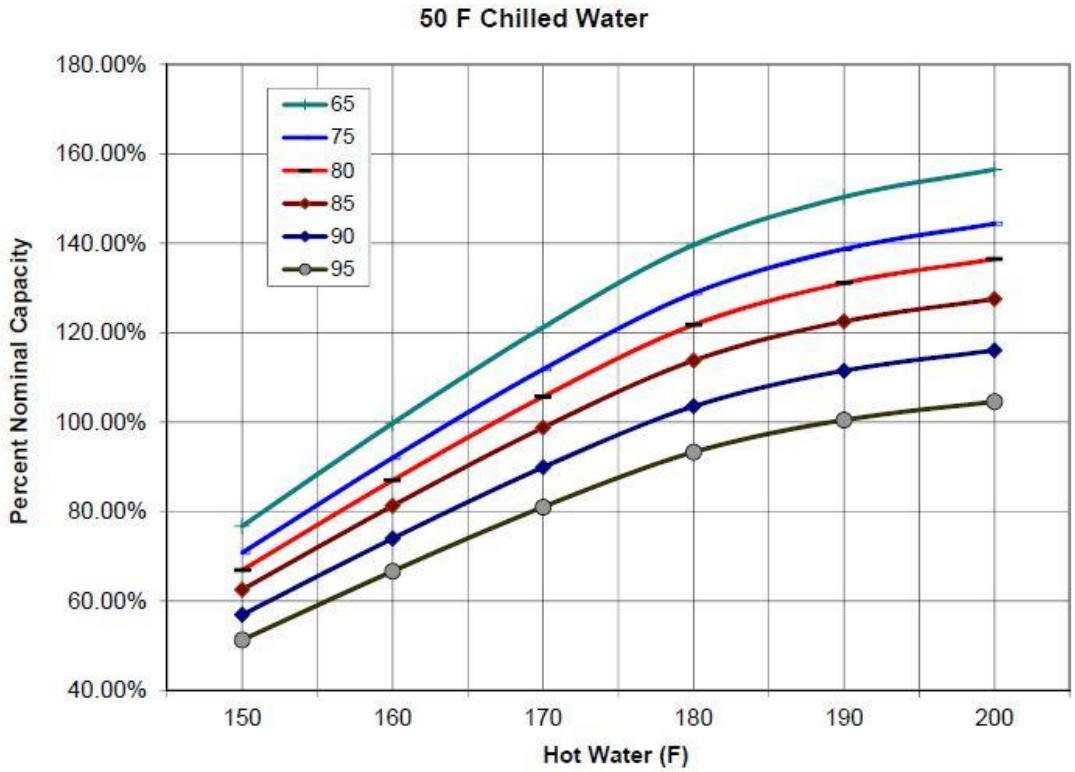

Figure 21: Percentage of nominal capacity-Hot water temperature diagram for ECO-MAX absorption chiller at 50 F chilled water outlet [57]

The two diagrams were used in order to plot the variation of the COP with the hot water inlet temperature, for specific chilled water outlet temperatures, like the result of the calculations from the other systems is, in order to compare the adsorption chillers with the other systems.

In order to do that, the assumption that the COP changes in the same way as the capacity of the chiller was made. Then, a specific cooling water inlet temperature was chosen and the diagram was plotted. For cooling water inlet temperature of 30 ℃, the following diagram was plotted:

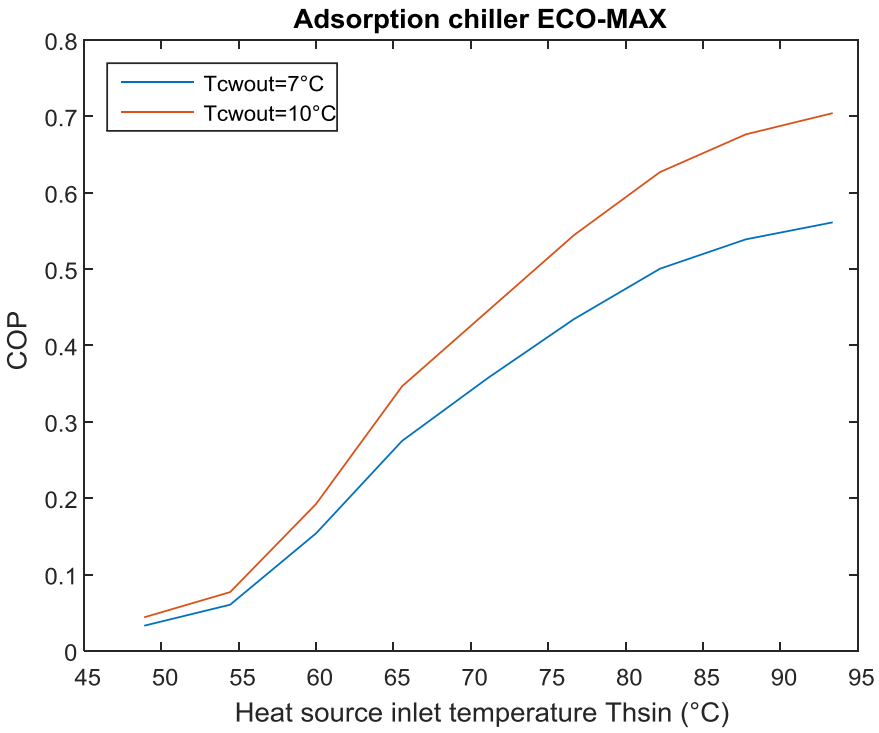

Figure 22: COP-Heat source inlet temperature diagram for ECO-MAX adsorption chiller, for cooling water inlet temperature of 30 ℃

By plotting such diagrams, the comparison among the adsorption chiller and the other chillers is possible.

This chiller has several different models. From the data of the manufacturer [57], it seems that the F300 model, with a capacity of 1073 kW, is the most appropriate model for this case. In the manufacturer's data sheet, other information like the nominal working conditions, temperature differences and electrical consumption are given as well.

2.6.2 GBU NAK Adsorption chiller

The second company, of which information about the adsorption chillers were taken, is GBU. GBU, as long as adsorption chillers are concerned, is agent of a Japanese manufacturing company of adsorption chillers. In its web page [52], information about the operation and efficiency of the NAK adsorption chiller are given. The chillers are available for cooling capacities of 71, 177, 354, 1061 kW. That means for this case, the 1061 kW chiller is an acceptable choice.

In the technical description of the chiller, diagrams of the variation of the cooling capacity (as percentage of the nominal capacity) with the hot water inlet temperature are given, with the cooling water inlet temperature as a parameter. Five diagrams are given, for chilled water outlet temperatures of 5-9 ℃ and range of 5 K. The cooling water inlet temperatures range from 28-32 ℃, while the heat source inlet temperature ranges from 65 to 100 ℃. Furthermore, the variation of the COP with the heat source inlet temperature is given in tabulated form. An example of the above is given with Figure 23 and Figure 24:

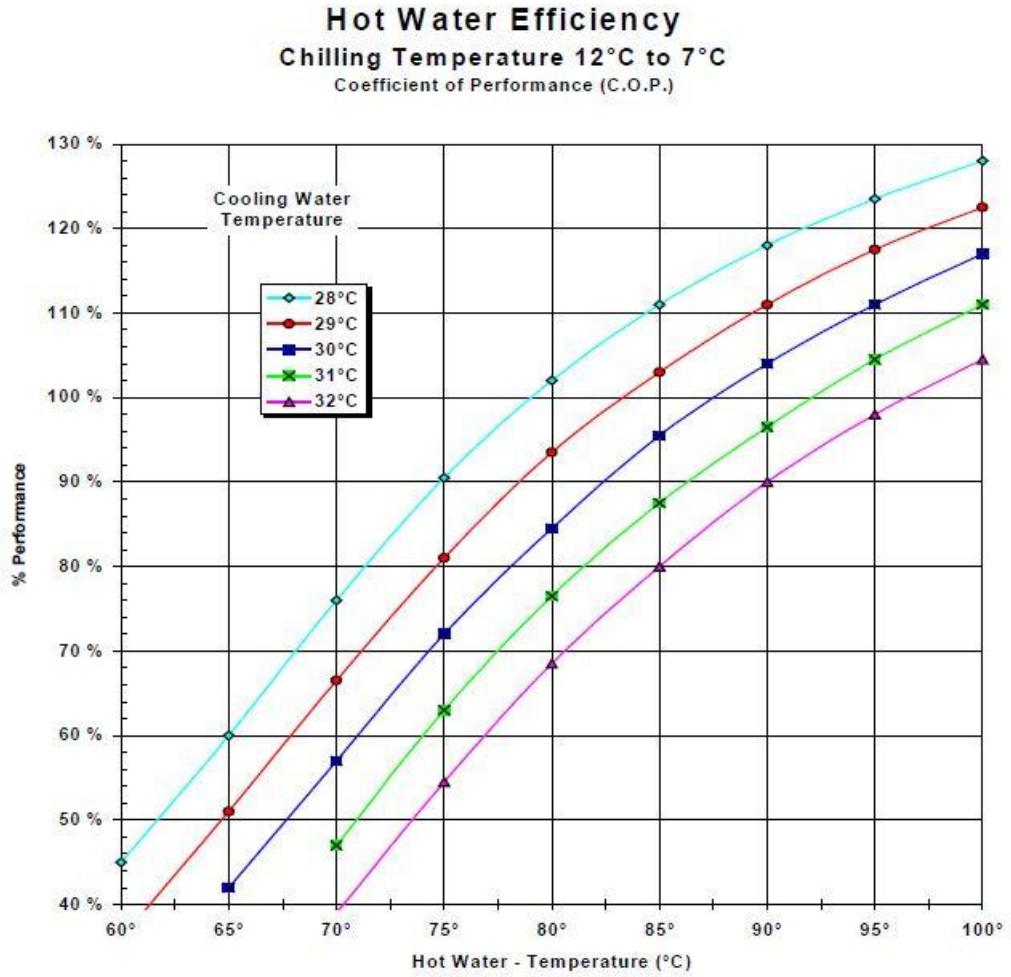

Figure 23 : Performance percentage-Heat source inlet temperature diagram for NAK adsorption chiller, for chilled water temperatures 12 to 7 ℃

Cooling Water Temperature	Hot Water - Temperature							
	65°C	70°C	75°C	80°C	85°C	90°C	95°C	100°C
28°C	0,56	0,57	0,58	0,61	0,63	0,64	0,65	0,66
29°C	0,44	0,51	0,55	0,59	0,61	0,63	0,64	0,65
30°C		0,47	0,53	0,56	0,59	0,61	0,63	0,64
31°C		0,44	0,50	0,54	0,57	0,60	0,61	0,63
32°C			0,46	0,51	0,55	0,58	0,60	0,61

Figure 24 : COP-Heat source inlet temperature data for NAK adsorption chiller, for chilled water temperatures 12 to 7 ℃

Since the COP and the cooling capacity don't have the exact same variation with the heat source inlet temperature, the tabulated information for the COP was taken, and the respective diagrams were plotted. These diagrams have the chilled water temperatures as a parameter and are plotted for a specific cooling water inlet temperature. Figure 25 shows such a diagram, for the nominal cooling water temperature of the chiller (28 ℃).

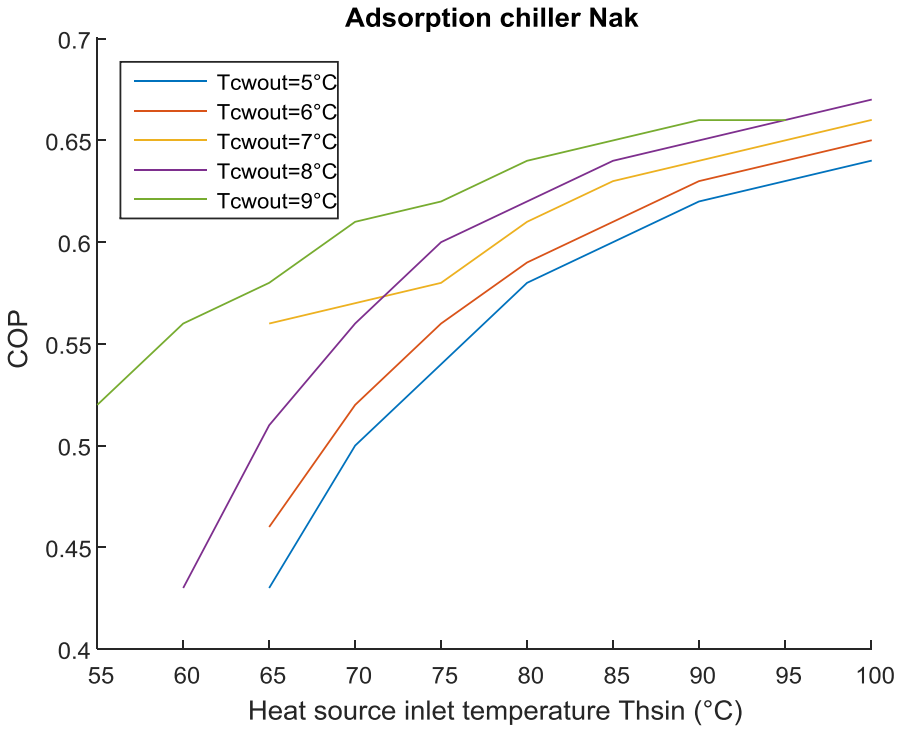

Figure 25 : COP-Heat source inlet temperature variation for five chilled water temperatures for NAK adsorption chiller, for cooling water temperature of 28 ℃

Finally, it must be mentioned that an extra 1.1 kW were considered as a power demand for the operation of the chiller, as mentioned in the manufacturer's technical data.

2.6.3 Calculation of efficiency of the adsorption chillers

Given the variation of the COP with the hot water inlet temperature, the cooling capacity and exergetic efficiency can be calculated for each case and be compared with those of the other chillers. For a specific heat source inlet temperature, the COP of the chiller is known. Since the input heat is constant in each case, the cooling capacity can be calculated as:

$$Q_{ref} = COP * Q_{in} \quad 2.117$$

Furthermore, the temperature differences for the hot and the chilled water are given for each chiller. These are:

Table 19: Range of streams of water for the two chillers

Range of stream (K)	ECO-MAX	NAK
Hot water	6.7	5.6
Chilled water	5.6	5
Cooling water	5.6	3.8
Cooling water inlet temperature	29.4	28

Since the ranges are known, the mass flow for both streams can be calculated. With that, some calculations related to exergy are possible. Since the inlet and outlet temperatures and mass flows in the heat exchangers are known, the total exergy input and output can be calculated. So, the exergy destruction in the fue gases-water heat exchanger and the total exergy destruction in the chiller can be calculated as:

Flue gases-water heat exchanger

$$\dot{E}_{d,he} = \dot{m}_g\left(e_{g,in} - e_{g,out}\right) + \dot{m}_{hw}\left(e_{hw,in,I} - e_{hw,out,I}\right) \quad 2.118$$

$$\sum \dot{E}_{in} = \sum \dot{E}_{out} + \dot{E}_{dtot} \quad 2.119$$

Finally, the exergy efficiency can be calculated as:

$$n_{ex} = \frac{\dot{E}_{cw,out}}{\dot{E}_{g,in} + \dot{P}_{pump}} \quad 2.120$$

3. Results

3.1 ORC-VCC Results

As mentioned before, the ORC-VCC system's efficiency is investigated for a range of temperatures, with an optimization taking place as well, which calculates the COP of the system for several evaporator I temperatures in a specific range. The optimization is independent of the heat source temperature. However, the heat source temperature determines whether each case of evaporator I temperature is possible, based on the heat transfer results. The results of the inner optimization can be seen in Figure 26 and Figure 27.

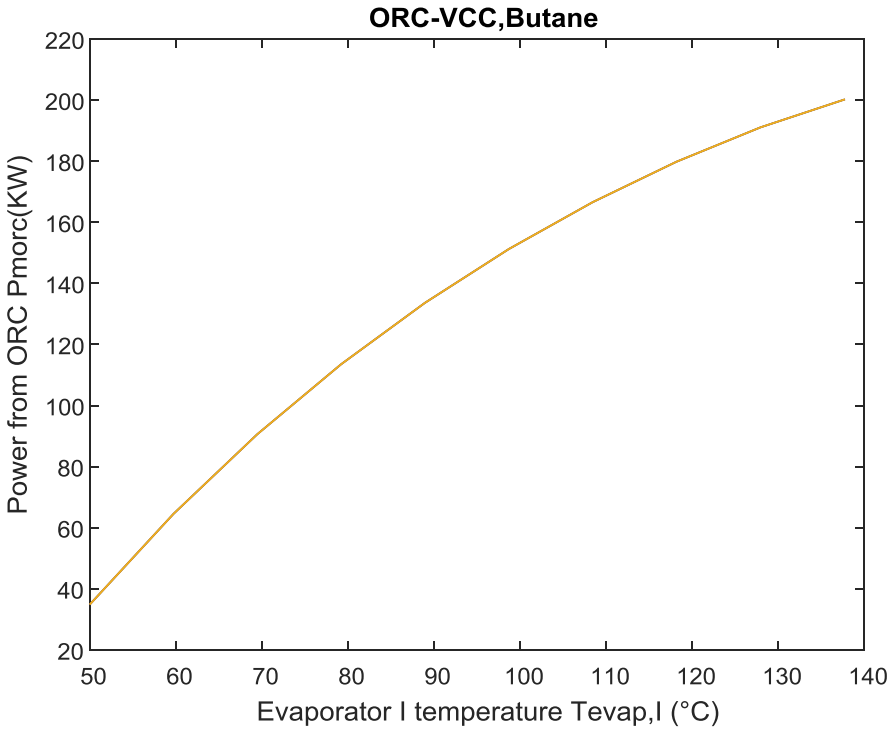

Figure 26 : ORC power variation with the evaporator I temperature

As it can be seen from Figure 26, the mechanical work of the ORC is increasing as the temperature of evaporator I increases. That is due to the fact that the increase in the temperature of evaporator I increases the pressure of point 2, thus increasing the power produced by the turbine.

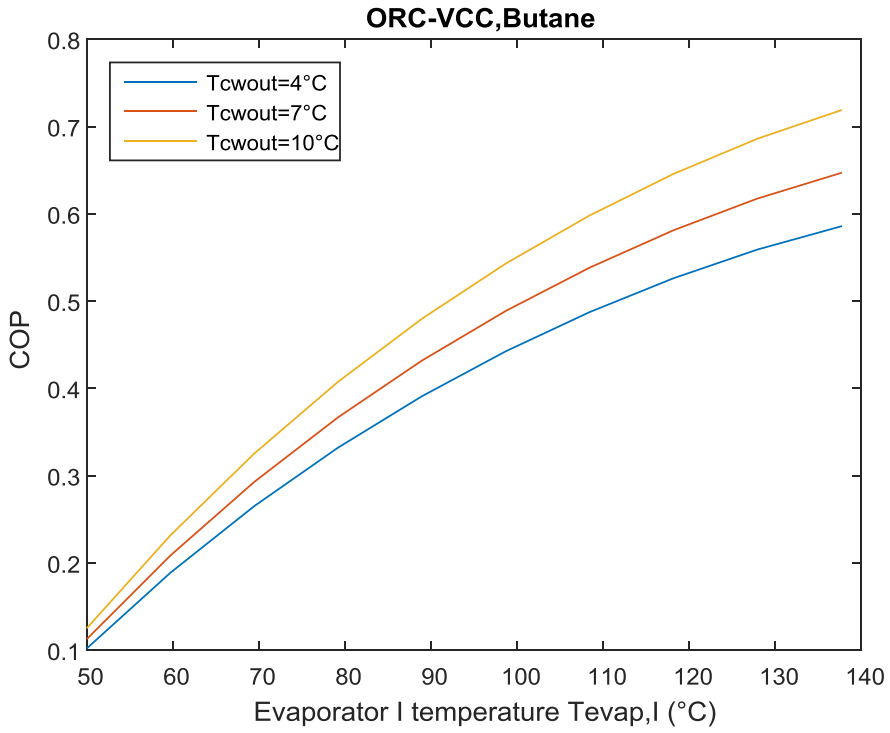

Figure 27 : COP variation with the evaporator I temperature for three different chilled water outlet temperatures

As it can be seen from Figure 27, the COP is also increasing as the evaporator I temperature increases. Since the mechanical work that is given to the compressor increases and the pressures in the VCC are constant, the mass flow in the VCC increases and thus the cooling capacity increases as well. Finally, since the input heat is constant, the COP is increased. Furthermore, the increase in the evaporation temperature increases the COP, something that is expected since the pressure difference between the condenser and the evaporator decreases.

The main purpose of the ORC-VCC modeling was to calculate the variation of the COP, cooling power and exergetic efficiency with the hot water temperature. The diagrams can be seen in Figure 28, Figure 29 and Figure 30 for the fluids that were investigated for the ORC-VCC system, for chilled water outlet temperature of 10 ℃.

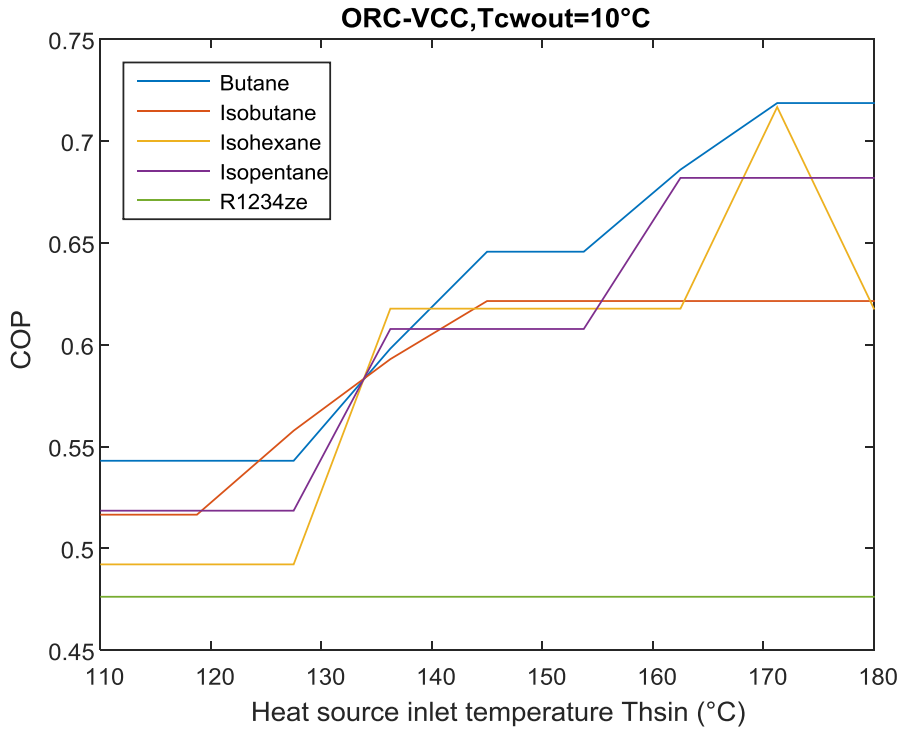

Figure 28 : Variation of the COP of the ORC-VCC system with the heat source inlet temperature for chilled water outlet temperature of 10 °C

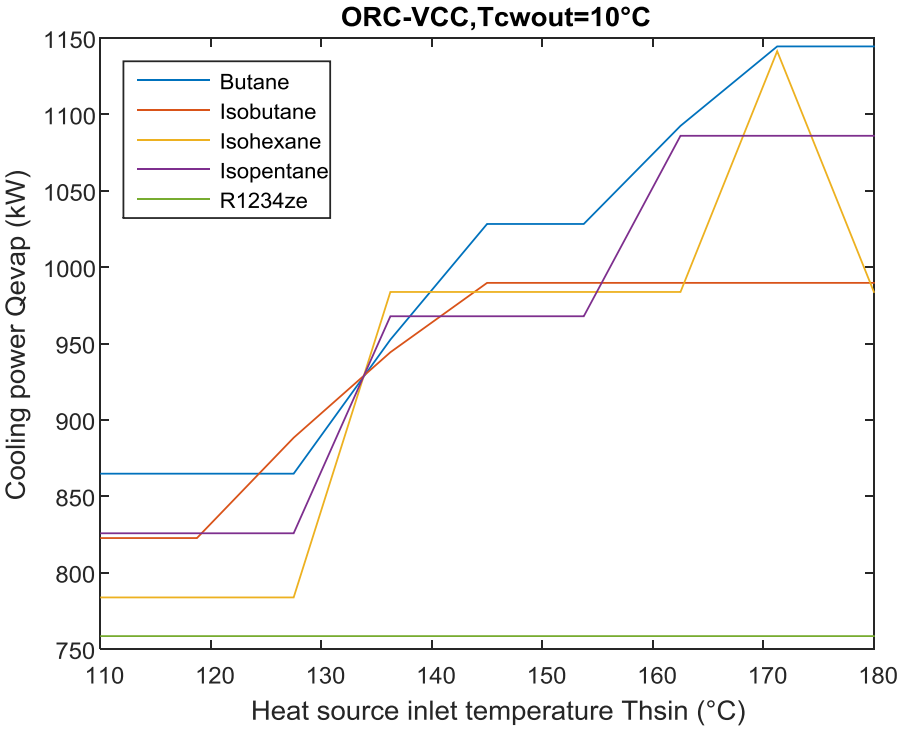

Figure 29: Variation of the cooling power of the system with the heat source inlet temperature for chilled water outlet temperature of 10 °C

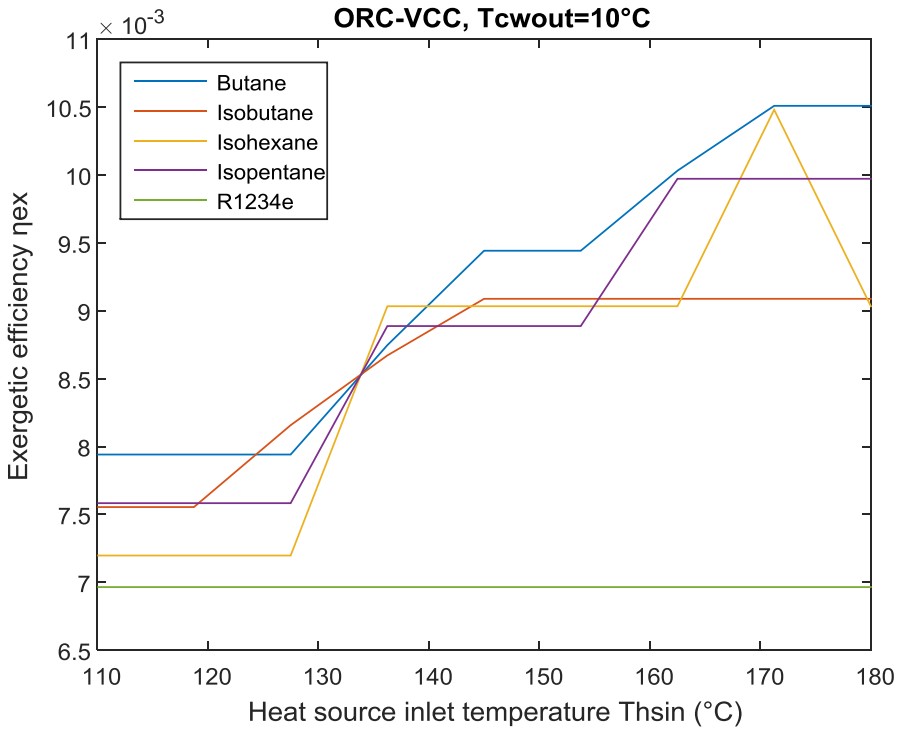

Figure 30 : Variation of the exergetic efficiency of the system with the heat source inlet temperature for chilled water outlet temperature of 10 ℃

The diagrams stop at a temperature value of 110 ℃. That happens because a pinch point of 20 K has been considered, which can be achieved only for the specific range of temperatures.

The form of the diagrams can be explained by using Figure 27, as well as the explanation of the modeling of the cycle. It must be mentioned that Figure 28 and Figure 29 have the same form, since the input heat of the cycle is constant and thus the cooling power is directly proportional to the COP. As it can be seen in Figure 27, the COP increases with the temperature of evaporator I, but it is not certain if all cases of heat transfer are possible. Whether the heat transfer is possible is determined by calculating the pinch point of the evaporator I. That means that for each heat source inlet temperature examined, the maximum temperature of evaporator I for which the heat transfer is possible is determined (taking into consideration the superheating of the working fluid as well), and in this way the maximum COP of the cycle for the specific heat source inlet temperature is found. In Figure 28, it can be seen that in some cases the COP doesn't increase, even though the temperature increases. That happens because the possible heat transfer allows the same maximum COP value to be obtained. However, what changes in such cases is that the pinch point in the case of the higher temperature is higher, something that requires smaller heat exchanger area and thus reduces the cost of the heat exchanger. The most representative example is that of R1234ze, which achieves its highest COP value (in the examined evaporator I temperature range) from the lowest examined heat source inlet temperature. Isobutane and Butane eventually reach their maximum COP, while Isopentane and Isohexane don't reach the maximum values, as the heat transfer required to achieve them is

impossible even for the maximum water inlet temperature examined. Same thing goes for the cooling power.

The exergetic efficiency has the same variation as the COP as well. That happens because the exergy rate of the input stream (gas) is the same for all cases, while the exergy rate of the chilled water outlet is proportional to the mass flow of the chilled water, since the exergy is constant. The mass flow is proportional to the cooling power, so the exergetic efficiency has the same variation as the cooling power.

As for the efficiency of each fluid, it can be concluded that Butane has the highest efficiency among the examined fluids, reaching a maximum COP of 0.7187, even though at some temperatures Isobutane, Isopentane and Isohexane have higher COP than Butane. Isobutane has a relatively high efficiency comparing to the other fluids for low temperatures, but for higher temperatures it is overtaken by Isopentane and Isohexane, since its highest COP value is 0.6215. Finally, Isopentane and Isohexane have lower efficiency at lower temperatures, but as the temperatures rise, their COP reaches 0.6819 and 0.7167 respectively. R1234ze has the lowest efficiency for the whole range of examined temperatures, with a COP of 0.4763. The trend doesn't change for the exergetic efficiency, with the maximum value of efficiency achieved being 0.0105 for butane.

In order to examine the difference that the chilled water outlet temperature causes, the same diagrams as those demonstrated before are shown, this time for chilled water outlet temperature of 4 ℃.

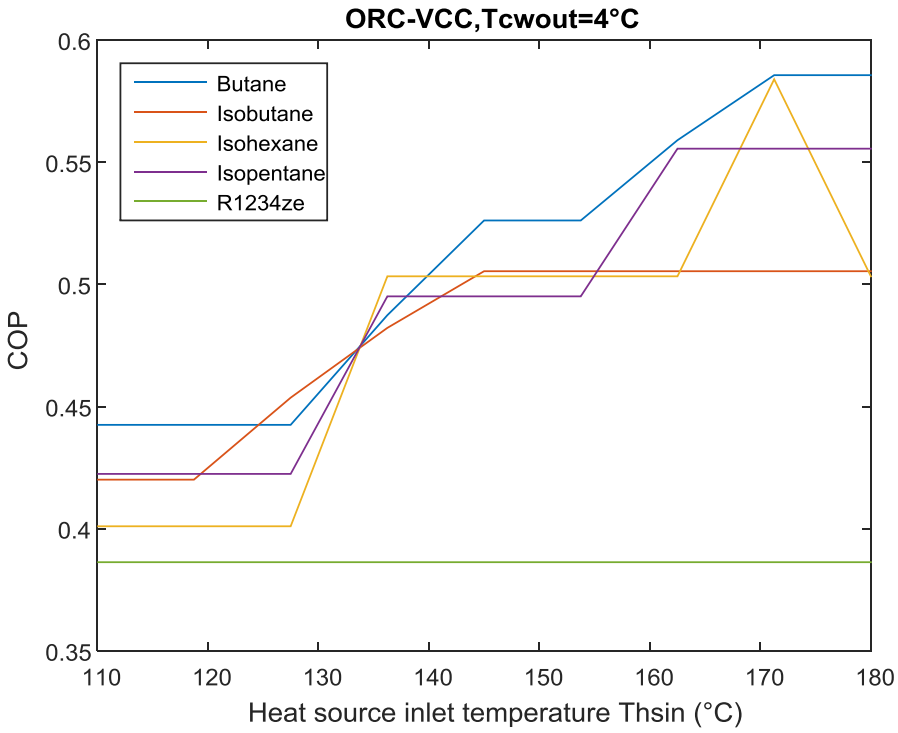

Figure 31: Variation of the COP of the system with the heat source inlet temperature for chilled water outlet temperature of 4 ℃ for the ORC-VCC

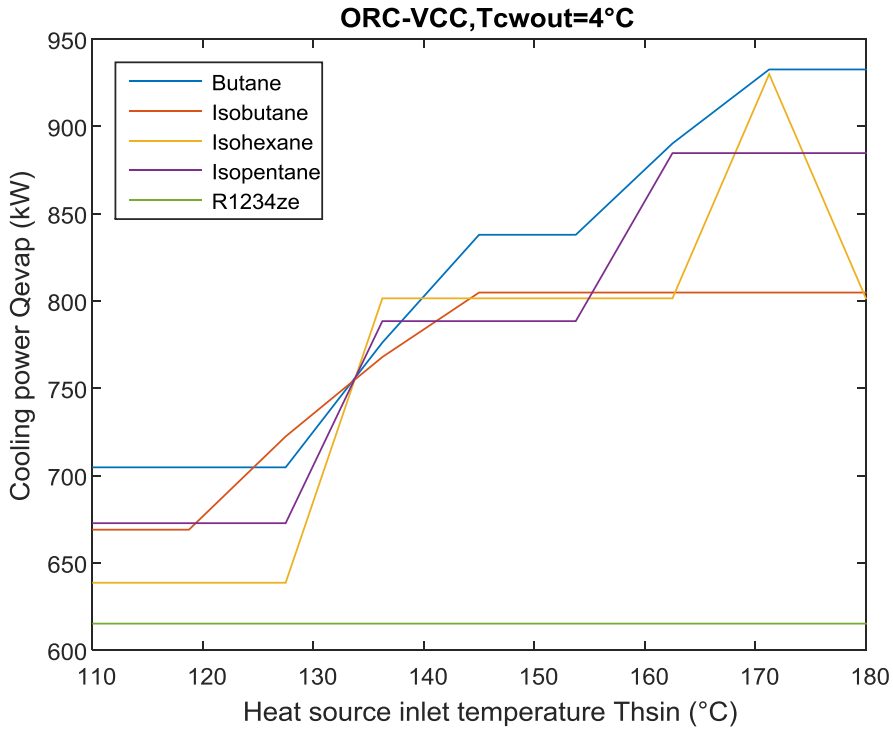

Figure 32 : Variation of the cooling power of the system with the heat source inlet temperature for chilled water outlet temperature of 4 °C for the ORC-VCC

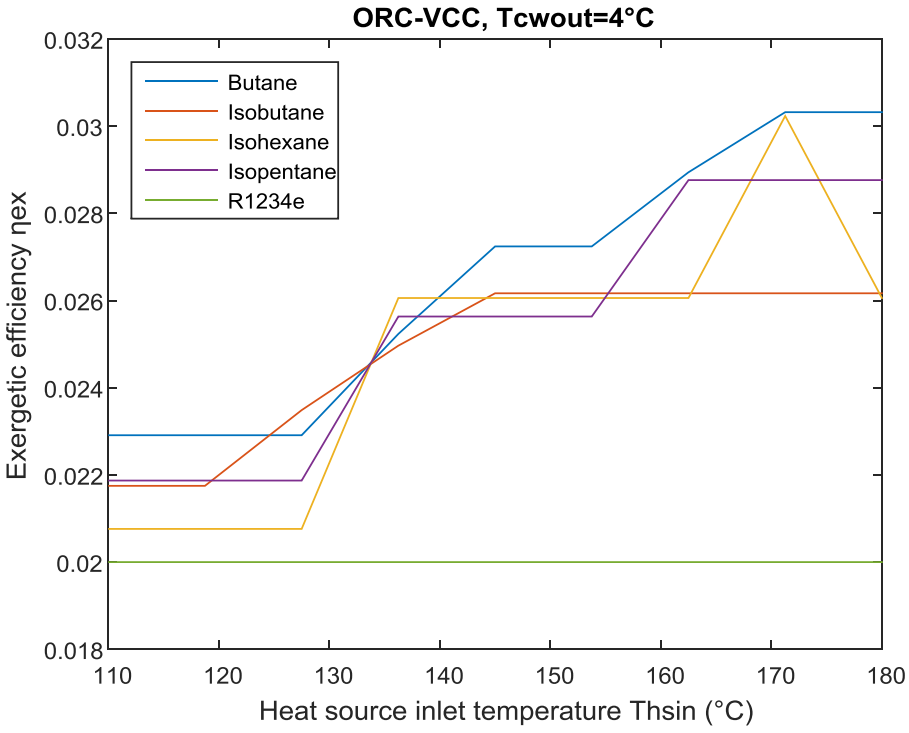

Figure 33 : Variation of the exergetic efficiency of the system with the heat source inlet temperature for chilled water outlet temperature of 4 °C for the ORC-VCC

From Figure 31, Figure 32 and Figure 33 it can be observed that the form of the curves is the same as in the case of chilled water outlet temperature of 10 ℃. However, the values of the variables change. Moreover, the efficiency of each fluid comparing to the others doesn't change either, something that suggests that butane is the best choice among the examined fluids, for every examined cold water outlet temperature.

In order to display the difference in the efficiency of the fluid when changing the cold water outlet temperature, Figure 34 and Figure 35 display the COP and exergetic efficiency of butane for three different temperatures. It can be observed that higher water outlet temperatures lead to higher COP values. That is an expected result, as the COP of the VCC increases when the pressure difference between evaporator and condenser decreases.

The opposite result goes for the exergetic efficiency, whose values decrease as the chilled water outlet temperature increases. Since the exergy of the gas inlet stream is the same, the chilled water stream's exergy obtains higher values for lower outlet temperatures. That is an expected result as well.

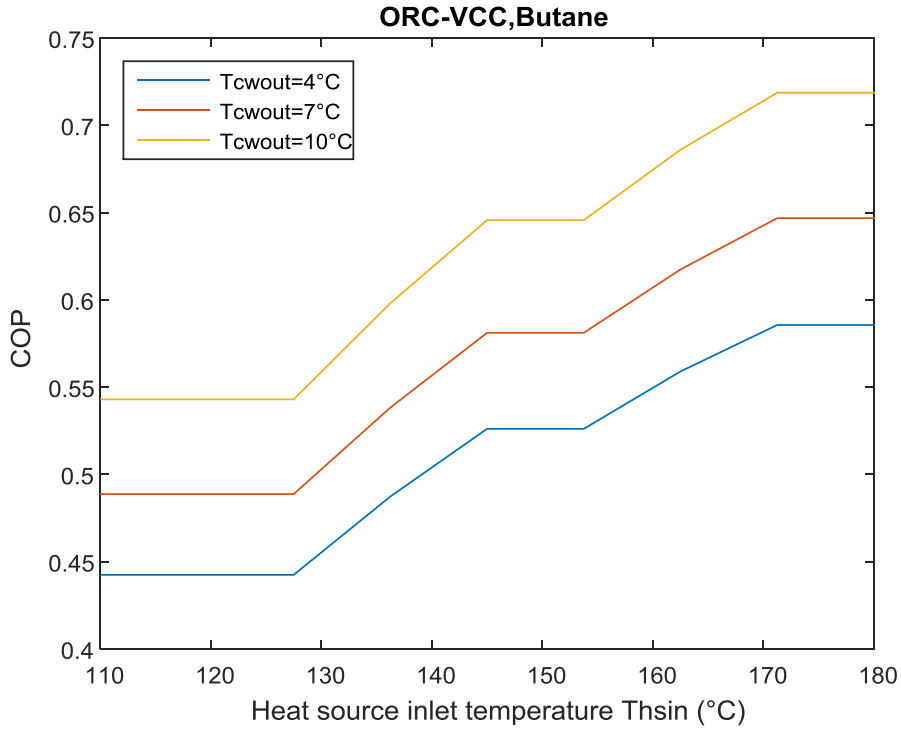

Figure 34 : COP-Heat source inlet temperature curve variation with the chilled water outlet temperature

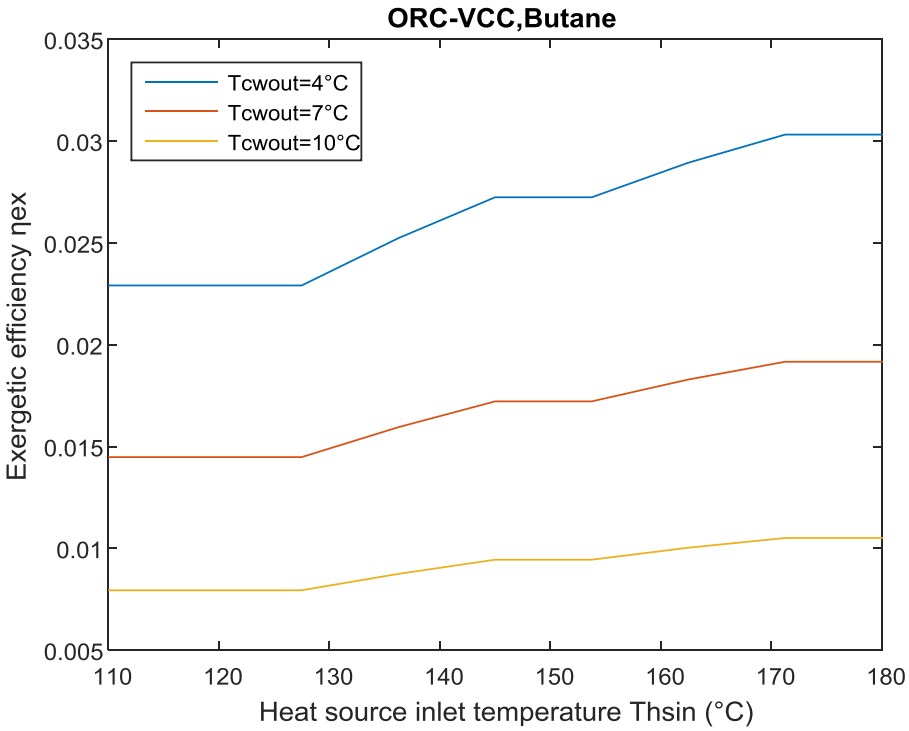

Figure 35 : Exergetic efficiency-Heat source inlet temperature curve variation with the chilled water outlet temperature

In general, the obtained results, which demonstrate that the cooling power and COP generally increase as the heat source inlet temperature increases, are expected. However, an interesting fact can be observed for the case of Isohexane. Its value of maximum COP decreases between the last two investigated temperatures, something which is unexpected. However, an explanation for that can be given considering the pinch point limitation that is set for the flue gas-hot water heat exchanger. In the case of 180 ℃ inlet temperature, the position of the pinch point changes from the inlet to the outlet of the heat exchanger (inlet and outlet of hot water). That causes a shift in the hot water curve in the Q̇-T diagram, which changes the pinch point value in the second heat exchanger. This displayed in Figure 36, where the Q̇-T diagram for both the heat exchanger and for evaporator I is plotted.

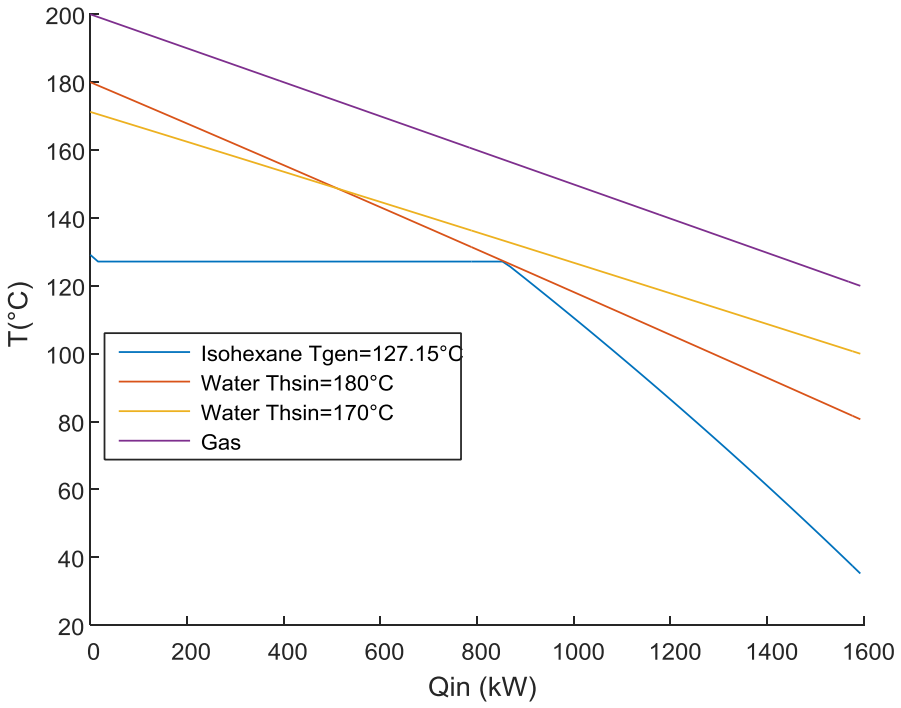

Figure 36 : Change of pinch point location in the flue gases-water heat exchanger and effect on the pinch point of evaporator I for Isohexane

In relation to the latter remark, it must be mentioned that even though this change in the pinch point location occurs for all the investigated fluids, in the other cases it doesn't cause a fall in the COP value.

To sum up, for the ORC-VCC case, the examination of several fluids resulted in butane being the most suitable fluid, as it obtains the highest efficiency. The fluids with lower critical temperatures, namely R1234ze and Isobutane reached their maximum efficiency (the former from the beginning, the latter eventually), which was lower than that of butane. Butane reached its maximum efficiency as well. The fluids with higher critical temperature, Isopentane and Isohexane, couldn't reach their maximum efficiency because they required higher heat source temperatures. The efficiency they could achieve was lower that the efficiency of Butane. So, when comparing the different technologies, the ORC-VCC system's working fluid will be butane. Finally, it can be concluded that in the specific temperature range and with the specific modeling process, working fluids with medium and medium to high critical temperatures are preferable.

3.2 ECC Results

The results for the ECC system are similar to those of the ORC-VCC. To begin with, the diagrams which describe the inner optimization of the system are given, like in the case of ORC-VCC. Figure 37 and Figure 38 display the variation of the COP and entrainment ratio of the system with the generator temperature. As can be seen, the ECC cannot operate for 50 ℃ generator temperature, as its COP and entrainment ratio are negative. However, from the temperature of 60 ℃ it can operate normally. From the diagrams, it can be concluded that a rise in both the generator and the chilled water outlet temperature cause a rise in both variables.

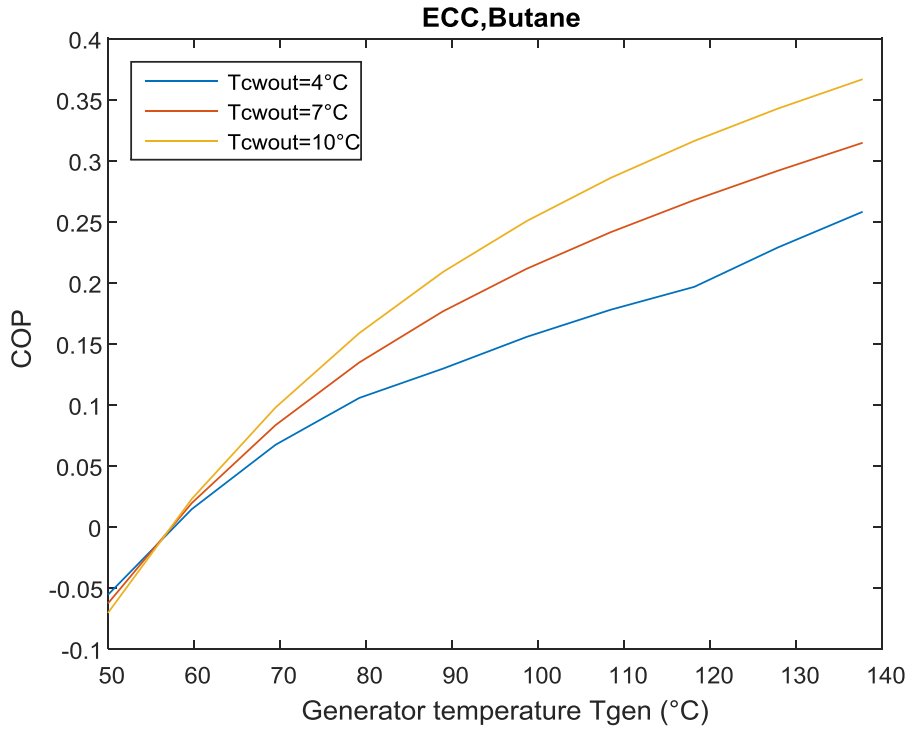

Figure 37 : COP variation with the generator temperature for three different chilled water outlet temperatures for the ECC

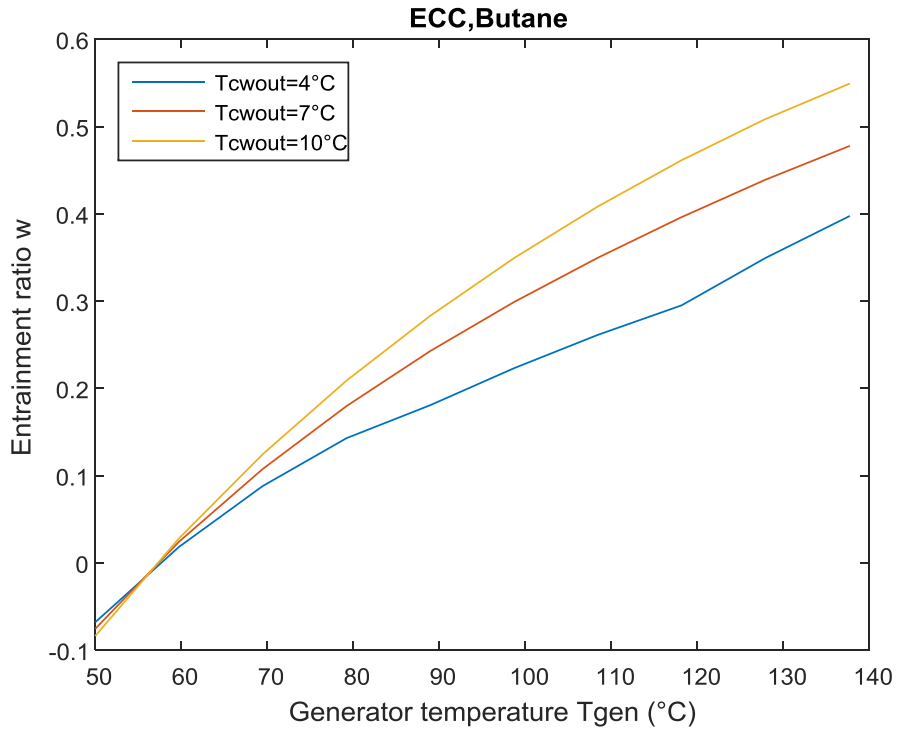

Figure 38 : Entrainment ratio variation with the generator temperature for three different chilled water outlet temperatures for the ECC

Similar diagrams to those of the ORC-VCC are displayed here as well. The same working fluids were investigated. First, the COP, cooling power and exergetic efficiency diagrams are displayed in Figure 39, Figure 40 and Figure 41.

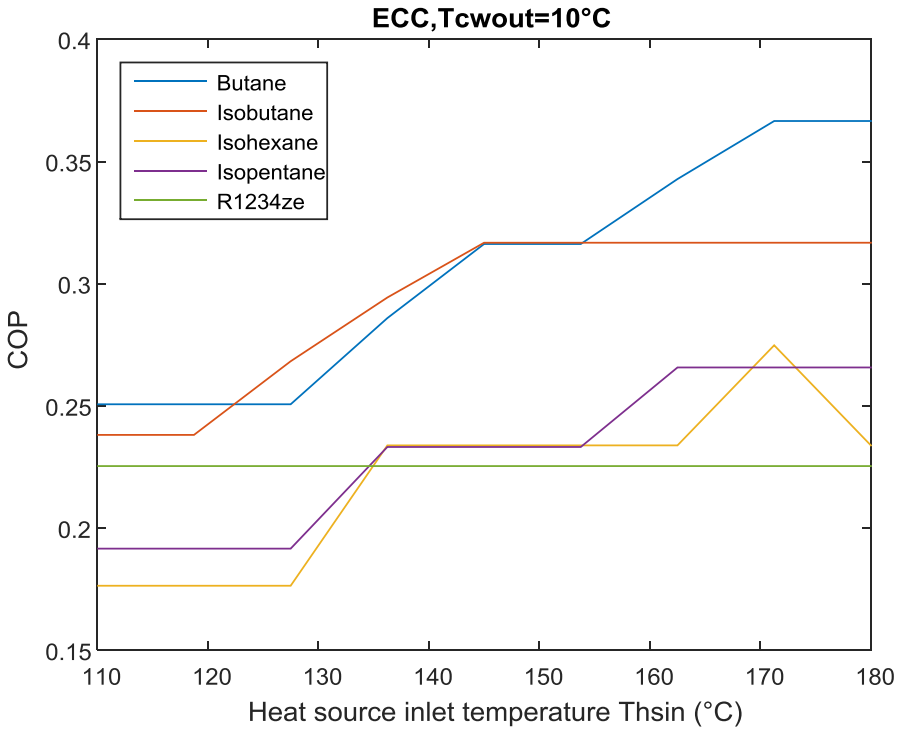

Figure 39 : Variation of the COP of the ECC system with the heat source inlet temperature for chilled water outlet temperature of 10 °C

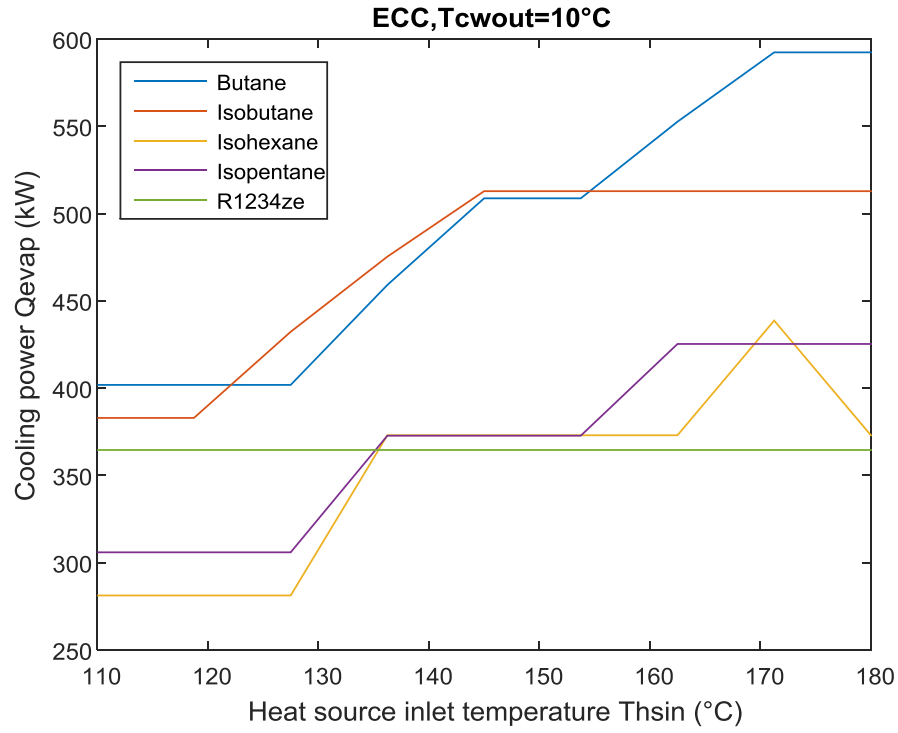

Figure 40 : Variation of the cooling power of the ECC system with the heat source inlet temperature for chilled water outlet temperature of 10 °C

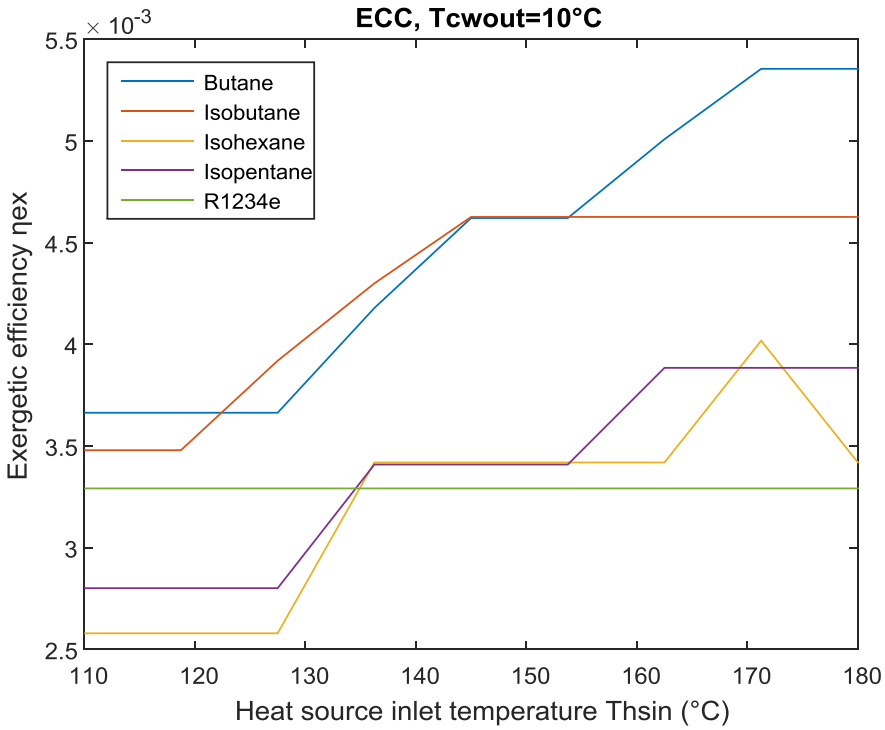

Figure 41 : Variation of the exergetic efficiency of the ECC system with the heat source inlet temperature for chilled water outlet temperature of 10 ℃

From the diagrams, it can be seen that the form of the curves of the fluids is similar to the case of ORC-VCC. The COP and cooling power values don't change along with the temperature increase for some cases, as was happening in the previous case. Also, the exergetic efficiency displays that attribute. The similarity is caused by the similarity of modeling of each system. Since both systems have a heat exchanger to transfer the heat from the hot water to the working fluid and both heat exchangers are modeled with the same way, a similarity between the results of the two systems was expected. However, the efficiency of this system is much lower than the ORC-VCC, as it can be seen from the obtained values. Moreover, a difference can be spotted in the comparison between the several working fluids. Even though Butane seems to be the most appropriate fluid for the ECC in the whole range of temperatures, Isobutane has a better performance in the ECC than in the ORC-VCC and its efficiency is higher than that of the others, reaching a maximum value of 0.3168. Moreover, in lower temperatures it is slightly higher than Butane. Furthermore, R1234ze, which had by far the lowest performance among the fluids for the ORC-VCC case, has a better performance than Isopentane and Isohexane for low heat source temperatures. Its COP has a constant value of 0.2254. Finally, Isopentane and Isohexane have the same efficiency difference when comparing to each other, even though it is the lowest among the fluids for low temperatures and slightly rises in higher temperatures, overtaking R1234ze and reaching a value of 0.2657 and 0.2338 respectively. For this chilled water temperature, R1234ze reaches its maximum COP from the beginning; Isobutane and Butane reach it eventually and Isopentane and Isohexane cannot reach it. The highest COP

value obtained is 0.366 and is obtained for Butane. The same trends among the fluids can be observed for the exergy efficiency, where the maximum obtained value is 0.0054 for Butane.

Finally, it must be mentioned that the same decrease in the COP of Isohexane is happening in this case as well. That is something expected, since the two heat exchangers (flue gases-water heat exchanger and evaporator I (generator for the ECC)) are modeled in the same way and the explanation is the same.

The respective diagrams in the temperature of 4 ℃ are presented below, followed by the diagrams which show the change that the chilled outlet temperature induces to the curves.

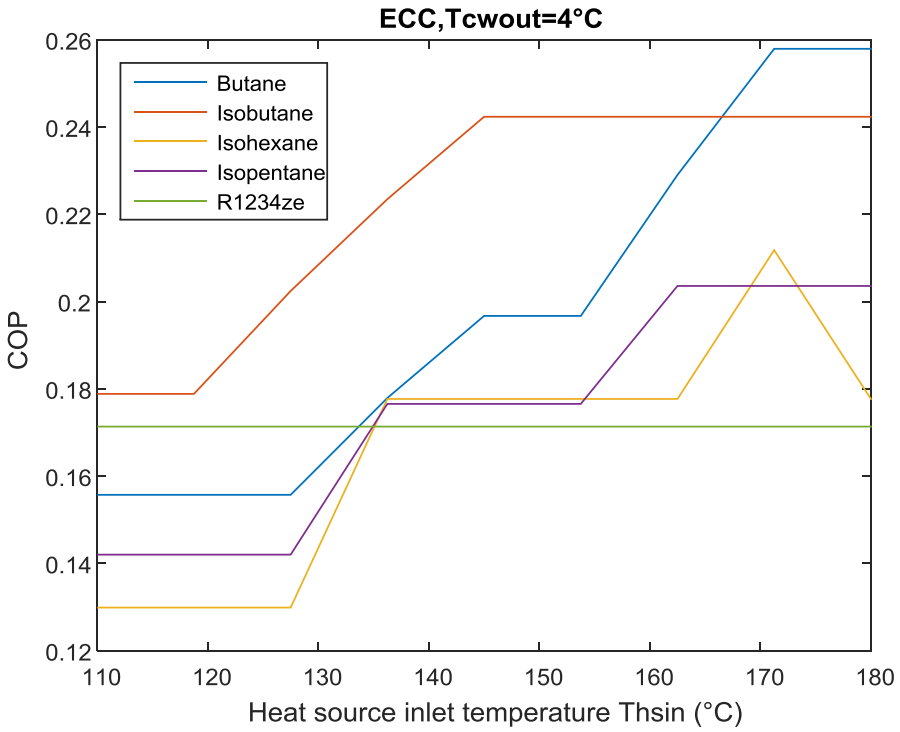

Figure 42 : Variation of the COP of the system with the heat source inlet temperature for chilled water outlet temperature of 4 ℃ for the ECC

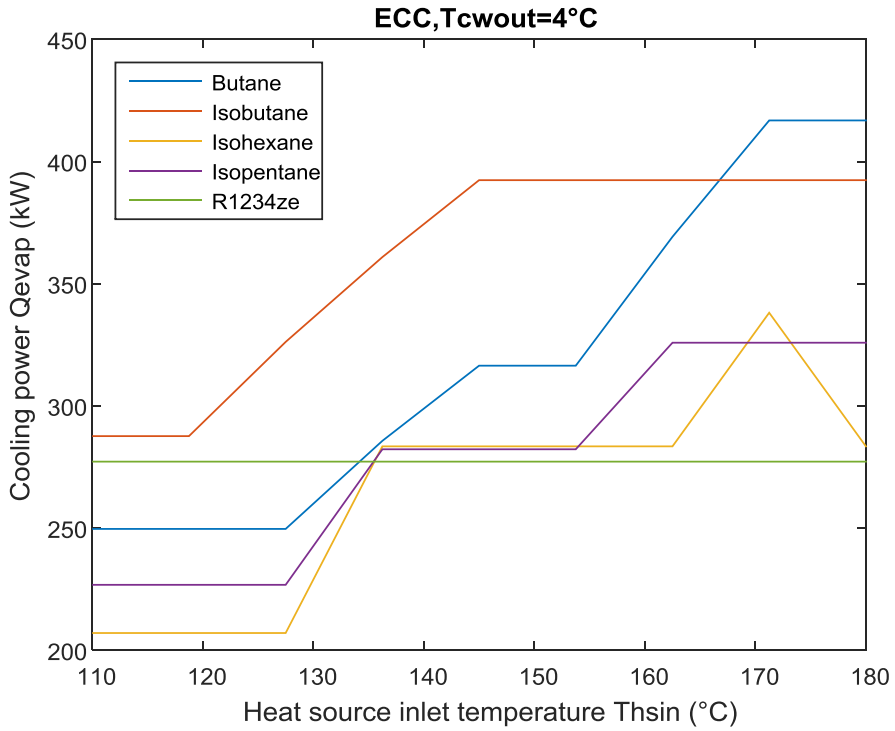

Figure 43 : Variation of the cooling power of the system with the heat source inlet temperature for chilled water outlet temperature of 4 °C for the ECC

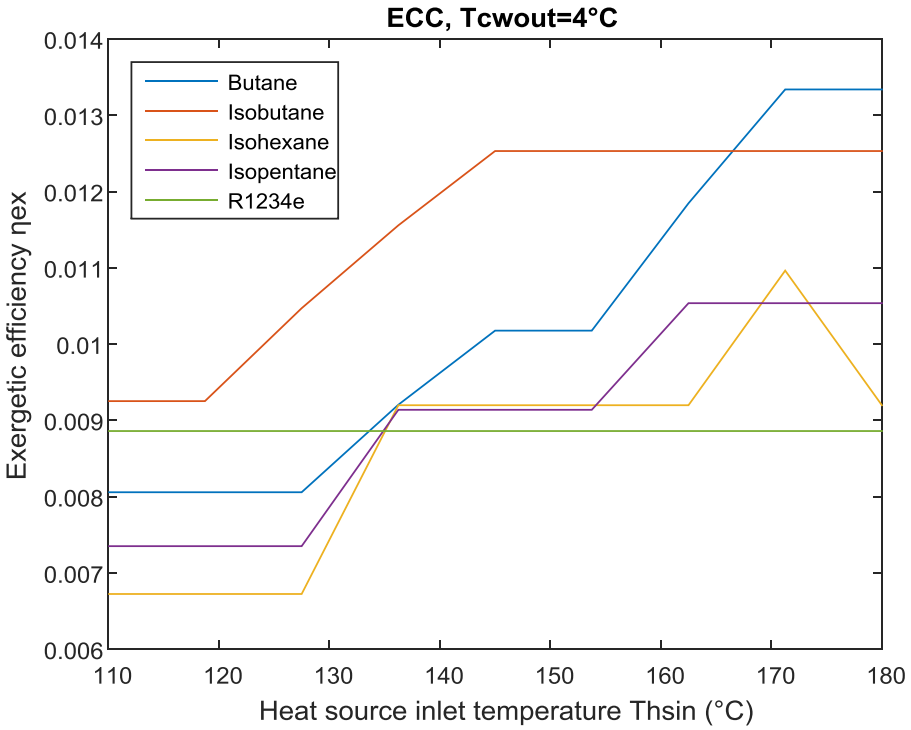

Figure 44 : Variation of the exergetic efficiency of the system with the heat source inlet temperature for chilled water outlet temperature of 4 °C for the ECC

As it was expected, the form of the curves doesn't change with the change in the chilled water outlet temperature. A change can be observed in the comparison between Butane and Isobutane, as Isobutane has a much better performance in lower temperatures than Butane. Moreover, even R1234ze has a higher COP than Butane in lower temperatures. However, in higher temperatures Butane achieves the highest performance and has the highest COP and cooling power among the fluids, achieving a COP value of 0.2579. Finally, Isopentane and Isohexane have the lowest performance in smaller temperatures, which rises slightly as the temperature increases, being 0.2036 and 0.2118 respectively. The exergy efficiency has a similar performance, with its higher value being 0.0133 for Butane.

By comparing the efficiency of the cycle in the two temperatures and by observing Figure 45 and Figure 46, it can be concluded that the reduction of the chilled water outlet temperature induces a fall in the COP and cooling power and a rise of the exergetic efficiency. The latter conclusion is expected, as by reducing the temperature, the exergy of the chilled water stream rises, while the exergy of the gas inlet stream remains constant for each hot water temperature; the former conclusion could be expected as well, since by lowering the pressure difference between condenser and evaporator, the COP of the system is expected to increase.

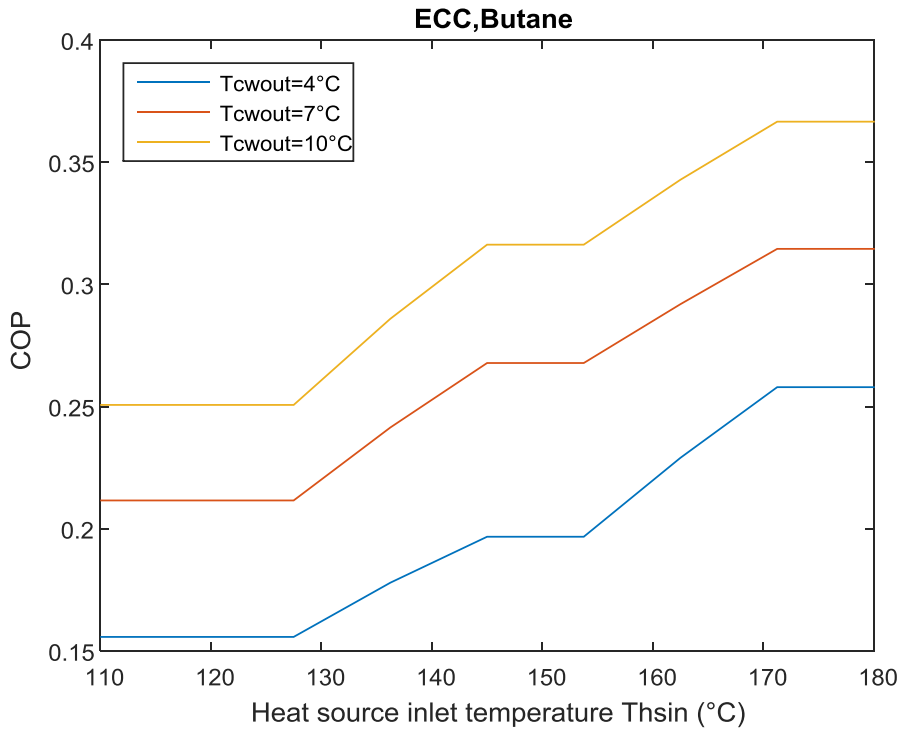

Figure 45 : COP-Heat source inlet temperature curve variation with the chilled water outlet temperature for the ECC

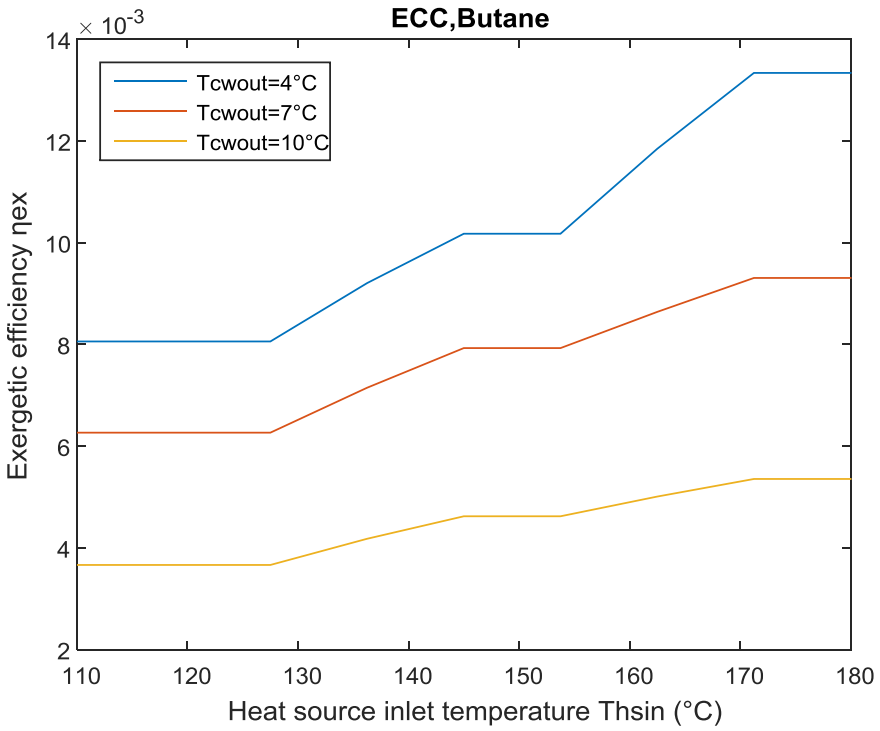

Figure 46 : Exergetic efficiency-Heat source inlet temperature curve variation with the chilled water outlet temperature for the ECC

To sum up, for the ECC case, Butane was found to be the most suitable fluid, as it obtains the highest efficiency. So, when comparing the different technologies, the ECC system's working fluid will be butane. Finally, it can be suggested that for this temperature range and for this specific modeling process, working fluids with medium and medium to low critical temperatures are more preferable for the ECC system.

3.3 Absorption chiller results

The results for the absorption chiller are presented in a similar way to the results of the other two systems. However, since the examined working fluid of the absorption chiller is lithium-bromide/water only, the diagrams of the comparison of the efficiency in the examined hot water inlet and chilled water outlet temperature are directly presented (Figure 47, Figure 48 and Figure 49).

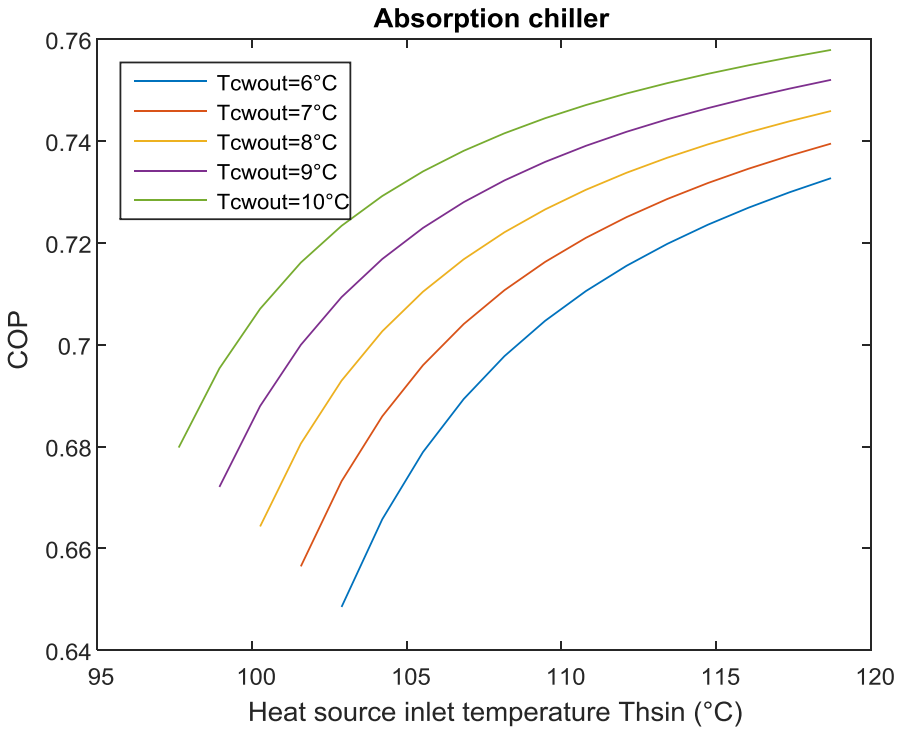

Figure 47 : COP variation with the hot water inlet and chilled water outlet temperatures for the absorption chiller

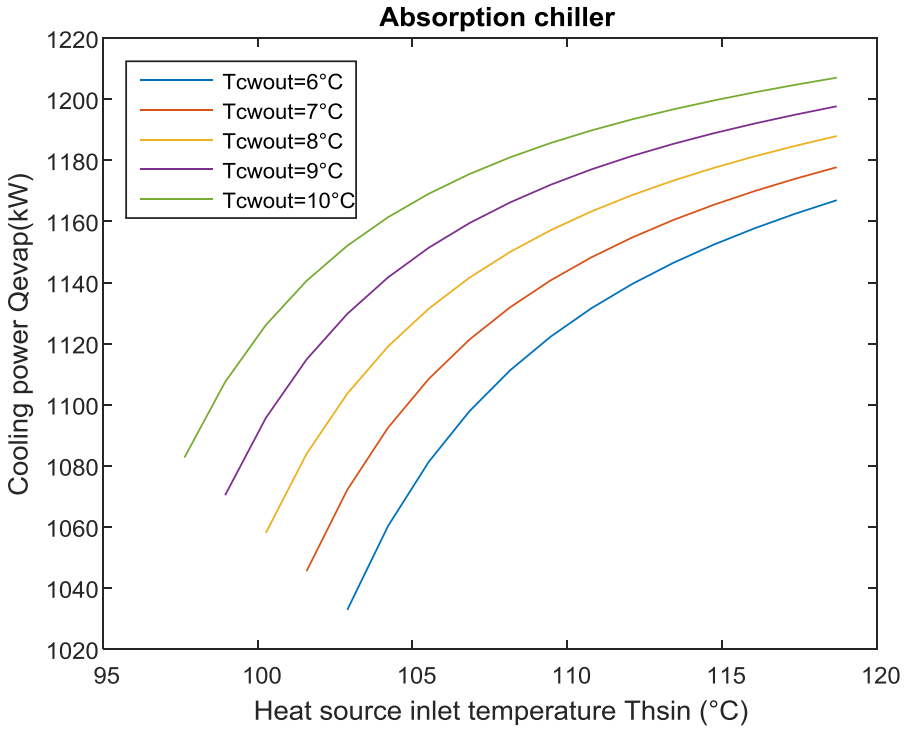

Figure 48 : Cooling power variation with the hot water inlet and chilled water outlet temperatures for the absorption chiller

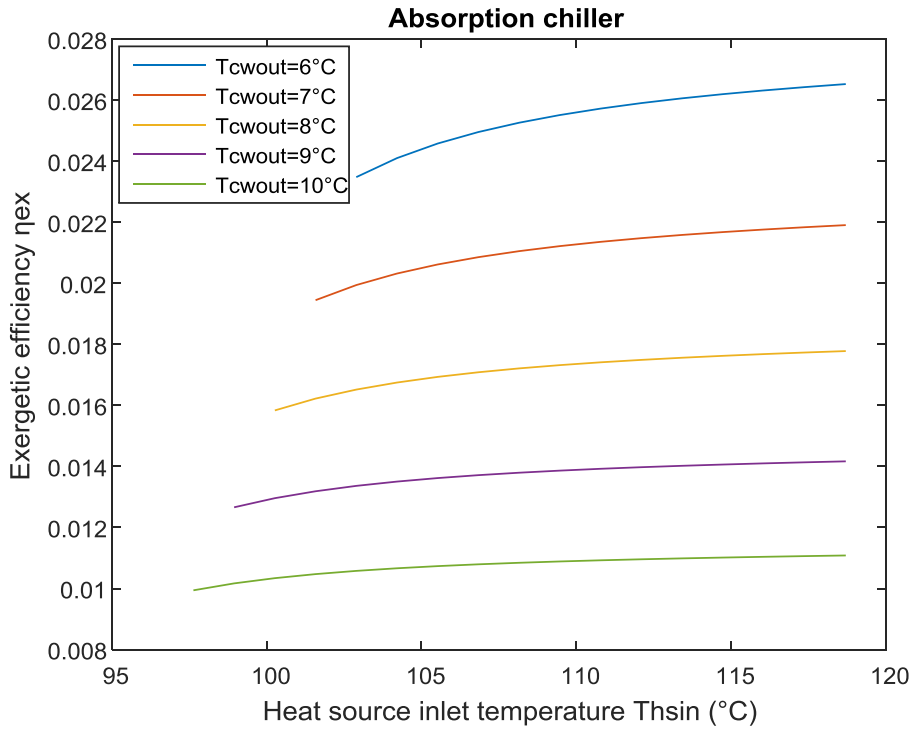

Figure 49 : Exergetic efficiency variation with the hot water inlet and chilled water outlet temperatures for the absorption chiller

To begin with, it must be mentioned that with the modeling of the cycle that was considered, the absorption chiller can operate for chilled water outlet temperatures up to 6 ℃. That is happening because of the approach value of 5 K, which demands water temperatures (evaporator temperatures) lower than 1 ℃ for chilled water temperatures lower than 6 ℃, something that can't be achieved due to the freezing point of water. In any case, the comparisons between absorption chiller and the other chillers will be done for this range of chilled water temperatures.

An interesting point that should be mentioned is that, as mentioned in the modeling process of the chiller, the lowest heat source inlet temperature changes with the cold water temperature. There are two reasons for that. The first reason is that the reduction of the cold water temperature (and thus of the evaporator temperature) causes an increase in the weak concentration of the mixture. So, the check which ensures that the strong concentration is higher than the weak doesn't allow the operation for low heat source temperatures. The other reason is that for low temperatures, the pinch point may occur in the other side of the heat exchanger, something unacceptable due to the assumption made in the modeling of the cycle. The lowest possible heat source inlet temperature is approximately 97 ℃, for cold water temperature of 10 ℃. Moreover, the maximum heat source temperature for all cases is approximately 119 ℃. That restriction occurs because in higher temperatures the strong solution concentration is higher than 70 %, something unacceptable for the absorption chiller operation.

Figure 47 and Figure 48, which have the same form, show an expected increase of the COP of the cycle with the hot water temperature. Furthermore, the COP increases with the chilled water outlet temperature as well, something which was expected. The maximum COP that can be reached is 0.7579 for cold water temperature of 10 ℃ and the maximum cooling power is 1207 kW.

From Figure 49, two conclusions can be extracted. First, the exergetic efficiency rises with the drop of the chilled water temperature; that is an expected result as explained before. The other fact is that the increase in the hot water temperature causes an increase in the exergetic efficiency, as it is the case for the COP and cooling power. In general, the curve of the exergetic efficiency has the same form as that of the COP and cooling power.

3.4 Adsorption chiller results

The data acquired by the manufacturers were presented in paragraph 2.6. However, the final results are given here, including the results for the COP, cooling power and exergetic efficiency for the two chillers.

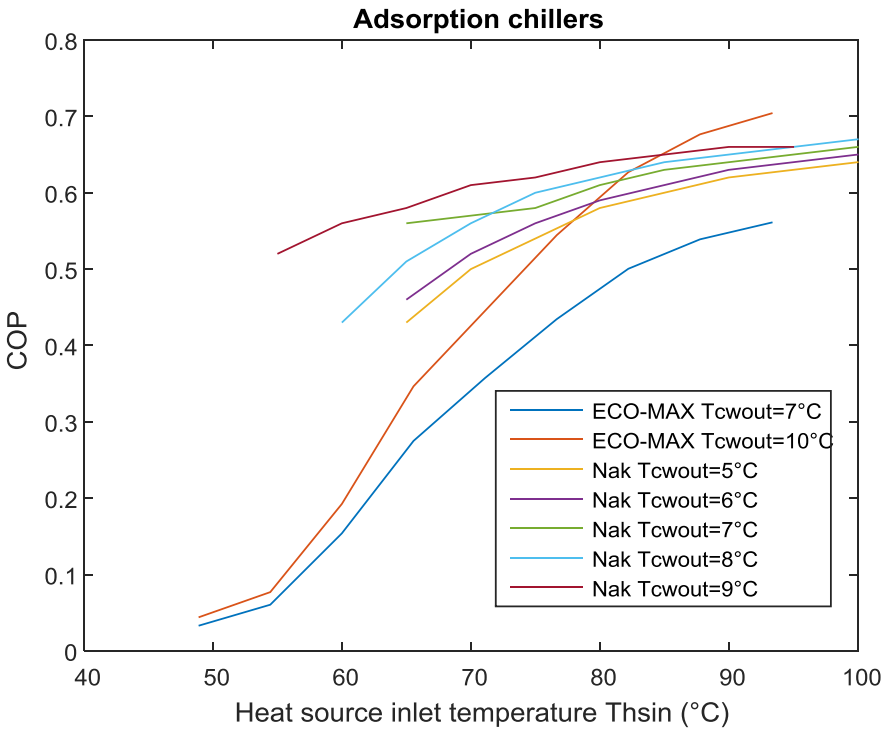

Figure 50 : COP variation with the hot water inlet and chilled water outlet temperatures for the adsorption chillers

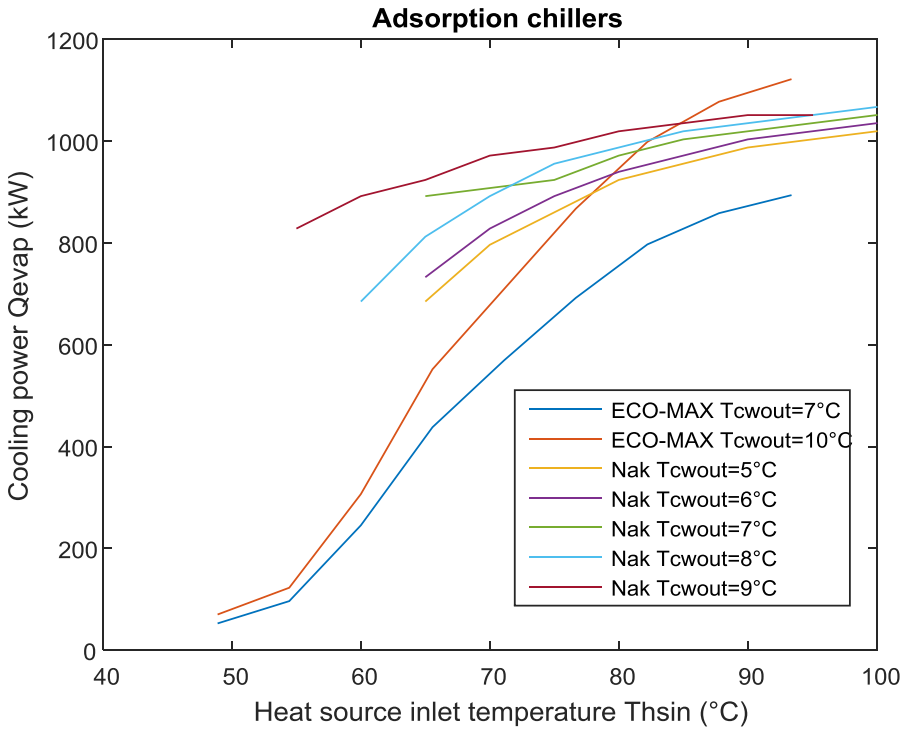

Figure 51 : Cooling power variation with the hot water inlet and chilled water outlet temperatures for the adsorption chillers

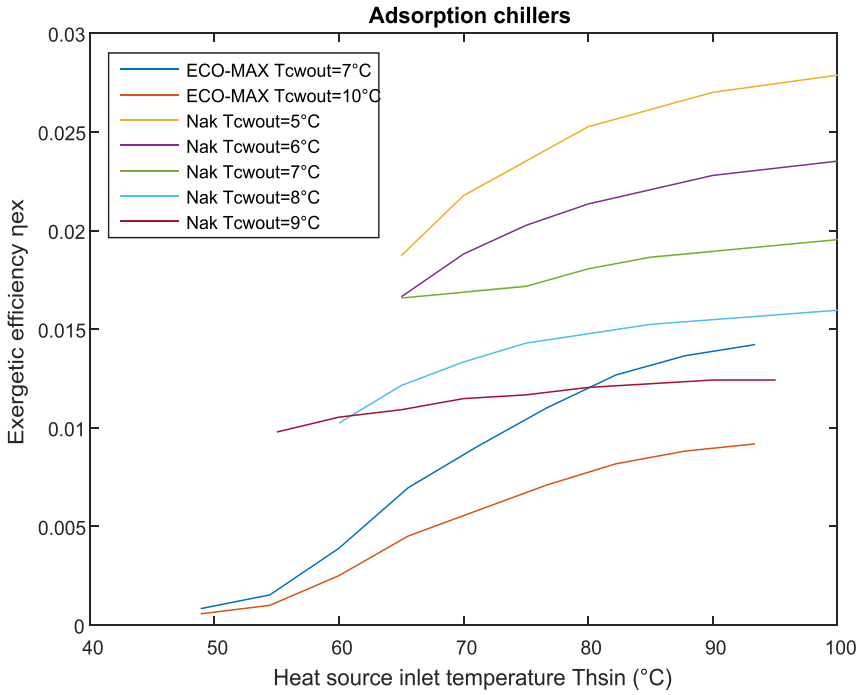

Figure 52 : Exergetic efficiency variation with the hot water inlet and chilled water outlet temperatures for the absorption chiller

Figure 50 and Figure 51 are displaying the variation of the COP and cooling power and have the same form, as in the other cases. In general, the diagrams show an increase of the efficiency with increase in the heat source inlet temperature. The same thing goes for the increase in the chilled water outlet temperature.

From the diagrams, it can be seen that the chiller from ECO-MAX can operate for heat source temperatures as low as 50 ℃, even though the COP at this case is very low (less than 0.05). However, that chiller can reach the maximum COP observed in Figure 50, which is 0.7040 and is achieved with chilled water outlet temperature of 10 ℃. For 7 ℃ water temperature, the maximum COP that can be achieved is 0.5610.

Nak adsorption chiller doesn't have great difference in its efficiency at different heat source temperatures. As can be seen from Figure 50, the five curves are relatively close to each other. However, it has a slightly smaller working heat source temperature range and can achieve lower maximum efficiency, comparing to ECO-MAX chiller. The lowest heat source temperature at which it can operate is 55 ℃ but only for cold water temperature of 9℃. The highest COP value achieved is 0.67 for heat source temperature of 100 ℃ and chilled water temperature of 8 ℃.

As long as the exergetic efficiency is concerned, an increase is observed with the decrease of the chilled water temperature, as was the case in the other chillers. The highest efficiency (0.0279), which is achieved by the Nak chiller, occurs at 5 ℃ chilled water temperature for 100 ℃ heat source temperature. Moreover, as the heat source temperature increases, an upward trend of the exergy efficiency is observed for the Nak chiller. Same thing goes for the ECO-MAX chiller's exergy efficiency, which achieves a maximum value at 94 ℃ for both chilled water outlet temperature cases.

3.5 Comparison among the technologies

Finally, after the demonstration of the results of all the technologies, a comparison among the four technologies was done, in order to find out which of them has the best efficiency and at which temperature. Since the different technologies cannot operate in the same range of temperatures, the comparison was made for three cases of specific chilled water temperature demand.

3.5.1 1st case-Chilled water outlet temperature of 10 ℃

For that case, all four technologies can be implemented. As for the adsorption chiller, only the ECO-MAX chiller can be used, as there are no data for the Nak chiller at that temperature. So, for the given heat input the comparison among the technologies is displayed in the following figures:

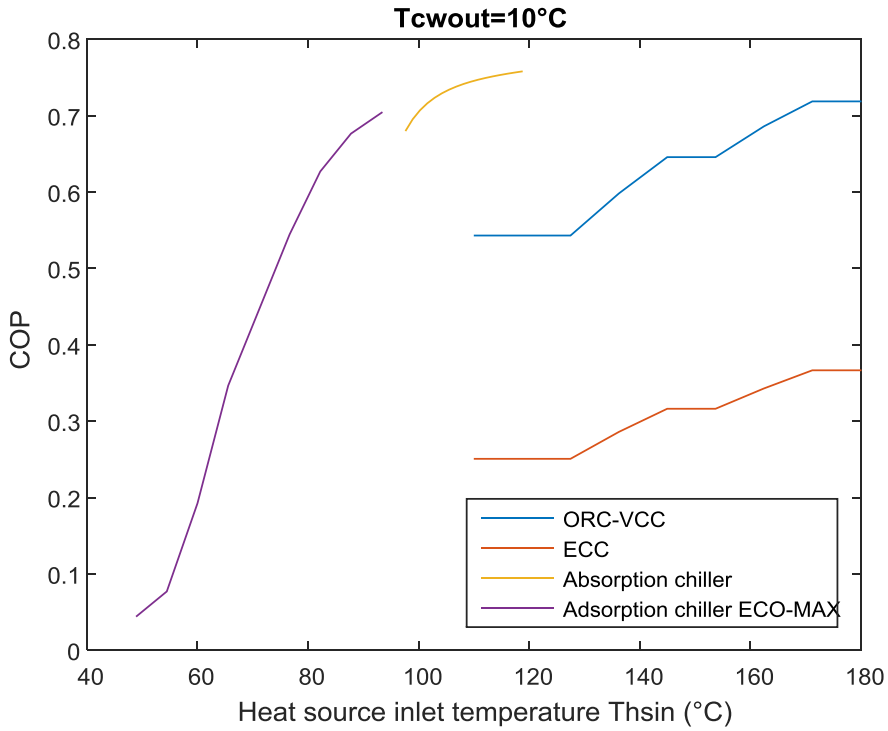

Figure 53 : Comparison of the COP of the four technologies for a chilled water outlet temperature demand of 10 °C

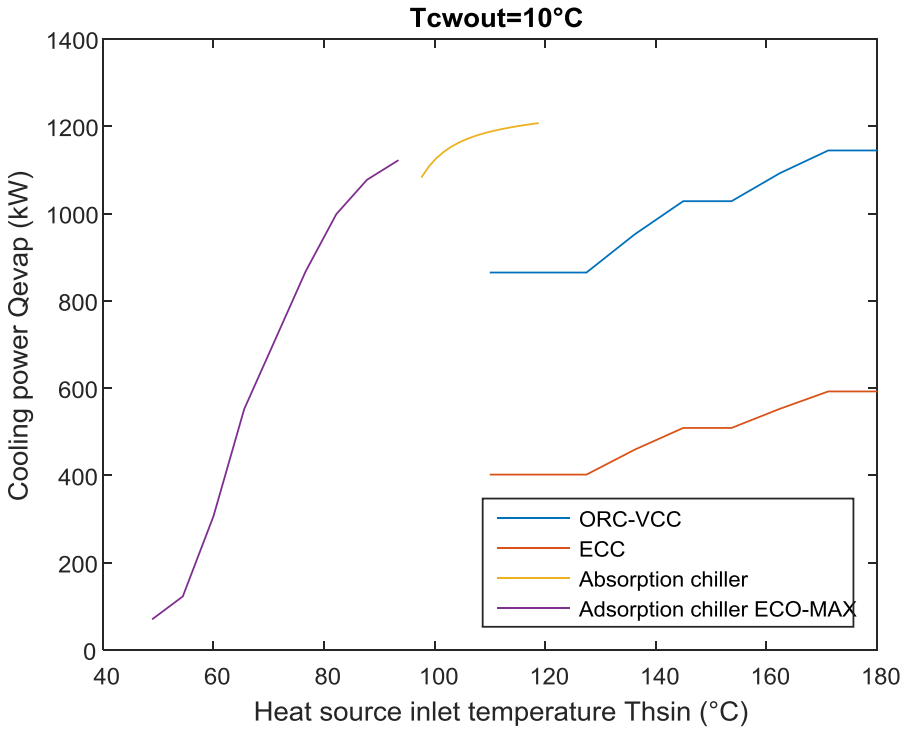

Figure 54 : Comparison of the cooling power of the four technologies for a chilled water outlet temperature demand of 10 °C

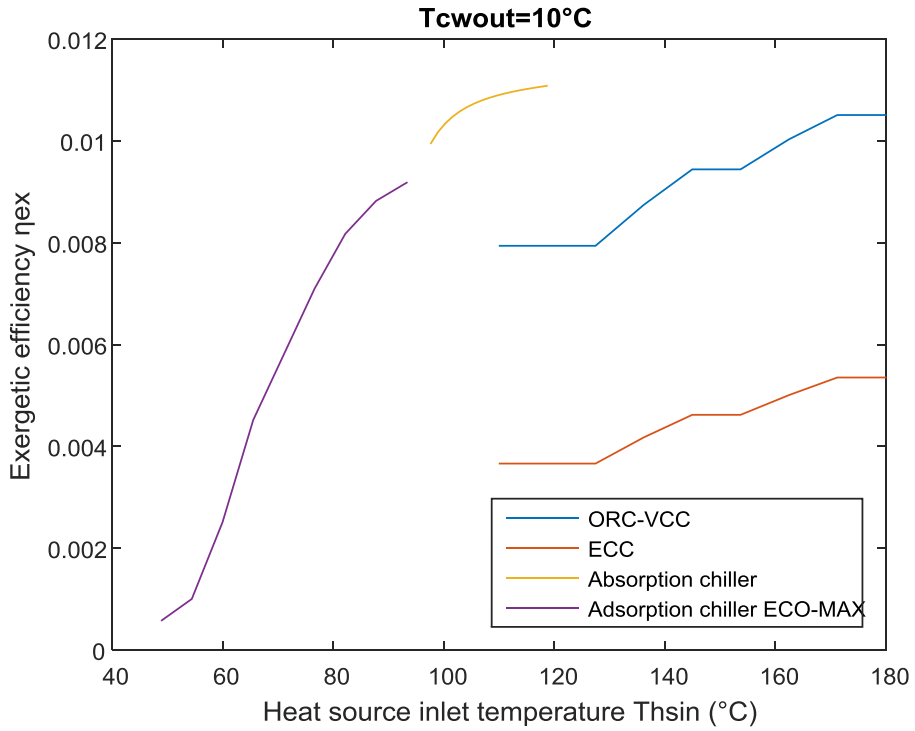

Figure 55 : Comparison of the exergetic efficiency of the four technologies for a chilled water outlet temperature demand of 10 ℃

From Figure 53 and Figure 54, it seems that the absorption chiller achieves the highest COP and cooling power, reaching 0.7579 for a heat source temperature of approximately 119 ℃. The ORC-VCC system can achieve a COP of 0.7187 for a temperature of 180 ℃ and it is the second most efficient system. The adsorption chiller has a maximum COP of 0.7040 for approximately 93 ℃ and the ECC system has the lowest efficiency, reaching a COP value of only 0.366 at 180 ℃. As long as the exergetic efficiency is concerned, the results are similar. The ORC-VCC system achieves an efficiency of 0.0105. The ECC system has an exergetic efficiency of 0.0054. The absorption and adsorption chiller's maximum efficiency is 0.0111 and 0.0092 respectively. The temperature of maximum exergetic efficiency of the systems coincides with the temperature of maximum COP, since the diagrams have the same form. Finally, an important conclusion is that the absorption chiller has a relatively small operational temperature range, while the ORC-VCC and ECC have much bigger operational range. Their range is even bigger than that displayed here, but as explained before, this range was imposed due to the pinch point limitation. However, their efficiency would reduce further with the reduction in the hot water inlet temperature. The adsorption chiller has also a bigger range than the absorption chiller, which however is limited by the silica gel operating temperature (must be lower than 120 ℃) and by the minimum heat source temperature in order to make the system operate.

To sum up, from the energy and exergy point of view, absorption chiller can reach the highest efficiency and the ECC the lowest, with ORC-VCC and adsorption chiller having values in between and closer to the absorption chiller's values.

Exergy results

From the exergetic analysis of the system, the results are shown here. More specifically, a table is presented for each case, to demonstrate the exergy inlet, outlet and destruction in each case. Following that, the Sankey and Grassman diagrams for each case are presented.

ORC-VCC

Table 20 : Exergy results for the ORC-VCC (Butane) for the 10 ℃ chilled water outlet temperature case

	Exergy destruction (kW)		Exergy input (kW)	Exergy output (kW)
Heat exchanger	79,7179	Heat exchanger	1469,6	939,2891
Evaporator I	72,4182	Evaporator I	557	106,4073
Condenser	147,5381	Condenser	0,7	75,1472
Evaporator	30,82	Evaporator	5,4	15,4449
Turbine	54,051			
Pump	4,0987			
Compressor	40,4106			
Valve	15,3998			
Mixing	1,3816			
Total	445,8359			

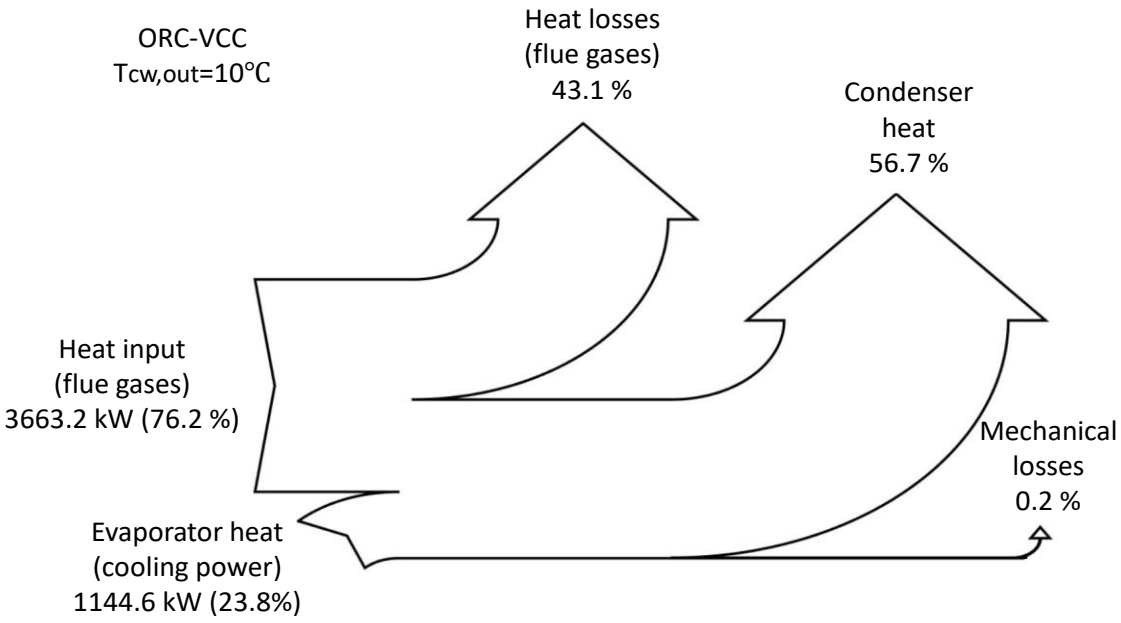

Figure 56 : Sankey diagram for the ORC-VCC for the 10 ℃ chilled water outlet temperature case

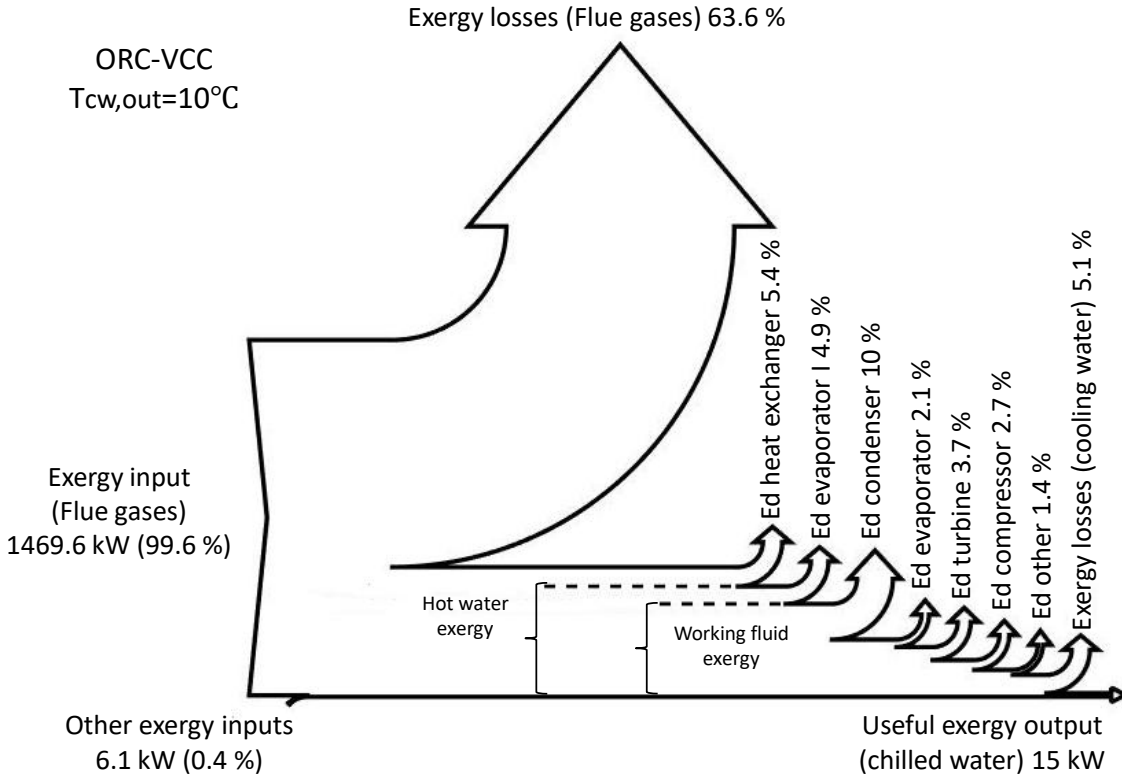

Figure 57 : Grassman diagram for the ORC-VCC for the 10 °C chilled water outlet temperature case

ECC

Table 21 : Exergy results for the ECC (Butane) for the 10 °C chilled water outlet temperature case

	Exergy destruction (kW)		Exergy input (kW)	Exergy output (kW)
Heat exchanger	79,7179	Heat exchanger	1469,6	939,2891
Generator	72,4182	Generator	557	106,4073
Condenser	124,3567	Condenser	0,6	65,1124
Evaporator	15,95	Evaporator	2,8	7,993
Ejector	176,27	Pump	23,3462	
Pump	7,1957			
Valve	7,9698			
Total	483,8783			

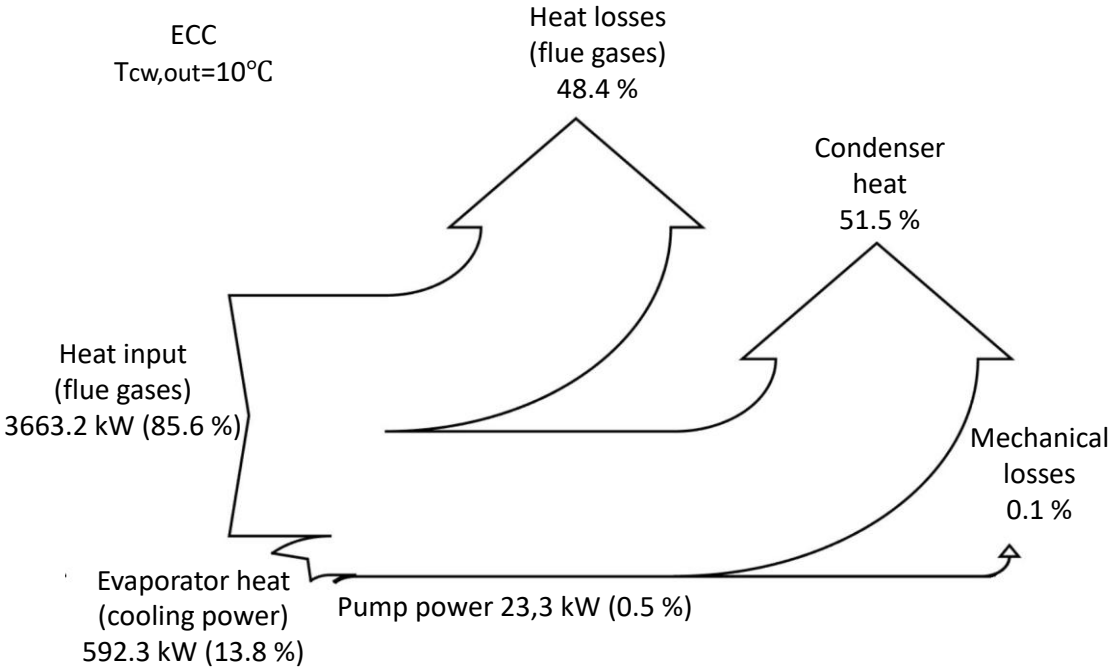

Figure 58 : Sankey diagram for the ECC for the 10 °C chilled water outlet temperature case

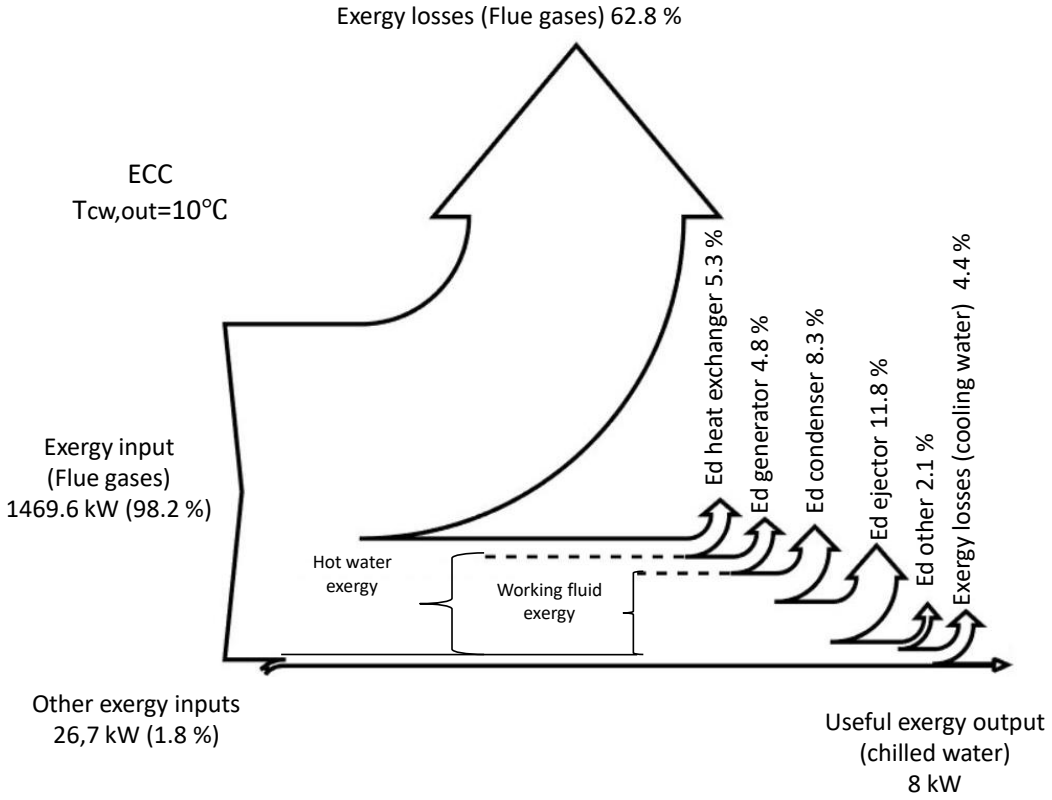

Figure 59 : Grassman diagram for the ECC for the 10 °C chilled water outlet temperature case

From the exergy results of the ECC and its Grassman diagram, it can be seen that the ejector's exergy destruction has the highest value, followed by the destruction in the condenser and in the heat exchanger and the generator. That is an expected result [94],[95].

Absorption chiller

Table 22 : Exergy results for the Absorption chiller for the 10 °C chilled water outlet temperature case

	Exergy destruction (kW)		Exergy input (kW)	Exergy output (kW)
Heat exchanger	119,4511	Heat exchanger	1469,6	939,3
Generator	89,42	Generator	3429,5	3018,7
Condenser	70,5604	Condenser	0,4	33,5
Evaporator	32,7523	Evaporator	5,7	16,3
Absorber	116,4923	Absorber	0,4	40,2
Heat Exchanger	14,7886	Pump	0,0141	
Pump	0,0126			
Valve 5-6	0			
Valve 8-9	3,3323			
Total	446,8096			

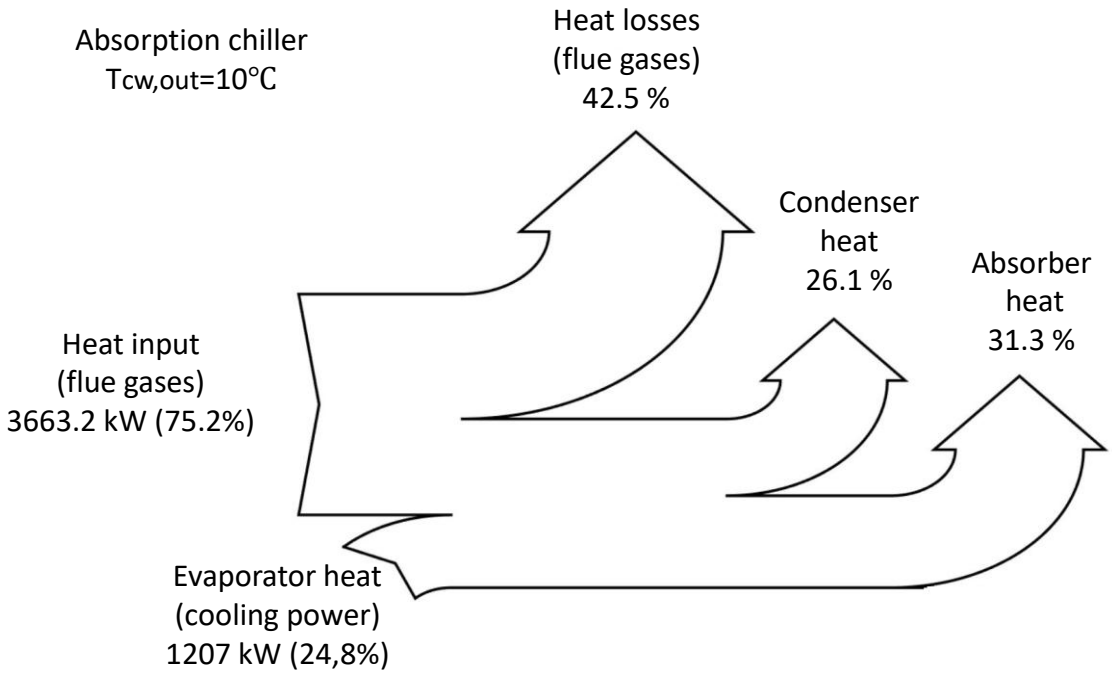

Figure 60: Sankey diagram for the Absorption chiller for the 10 °C chilled water outlet temperature case

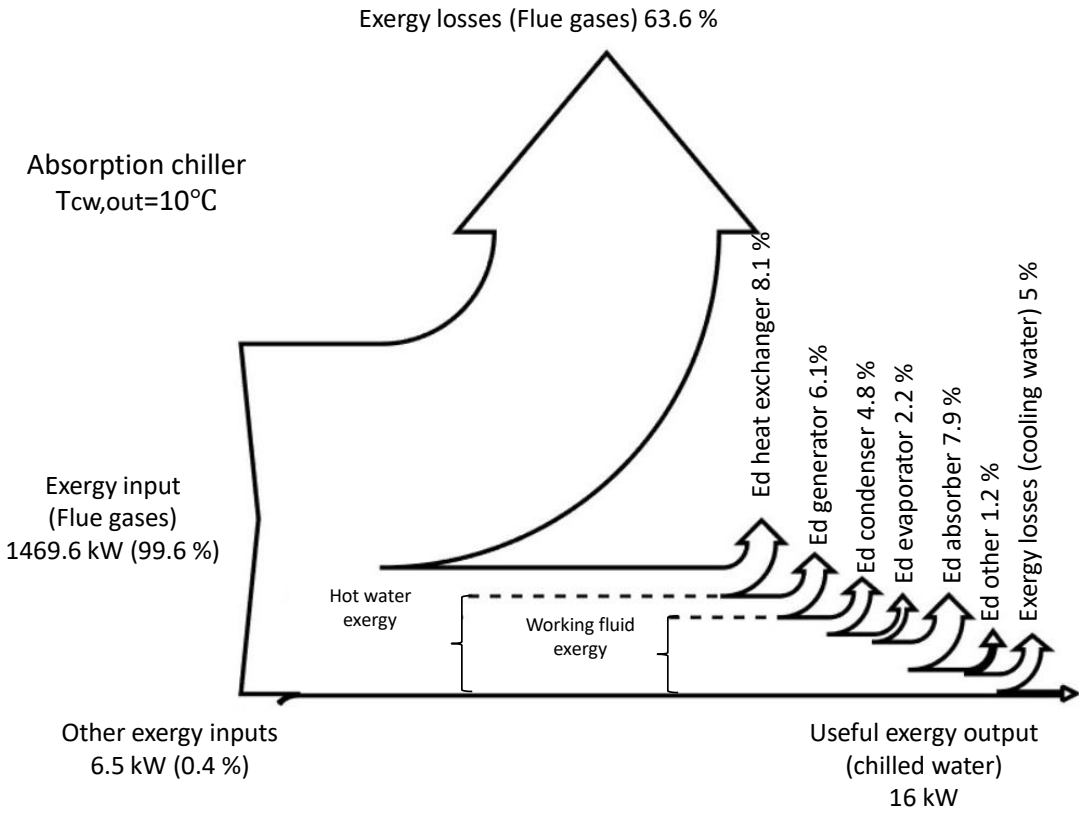

Figure 61 : Grassman diagram for the absorption chiller for the 10 ℃ chilled water outlet temperature case

Adsorption chiller (ECO-MAX)

Table 23 : Exergy results for the Adsorption chiller for the 10 ℃ chilled water outlet temperature case

	Exergy destruction (kW)		Exergy input (kW)	Exergy output (kW)
Heat exchanger	201,4659	Heat exchanger	1469,6	939,3
Other	169,0616	Condenser	171,1	324,0324
Total	370,5275	Evaporator	4,8	13,5094
		Pump	1,8	

For the case of the adsorption chiller, the exergy destruction in each component is not known, since there has not been a detailed modeling of the cycle. However, the exergy inputs and outputs can be calculated based on the data of the manufacturer (cooling water temperatures, chilled water range etc.) and the total exergy destruction can be calculated. Moreover, since the flue gases and hot water temperatures are known, the exergy destruction in the heat exchanger of the system can be calculated.

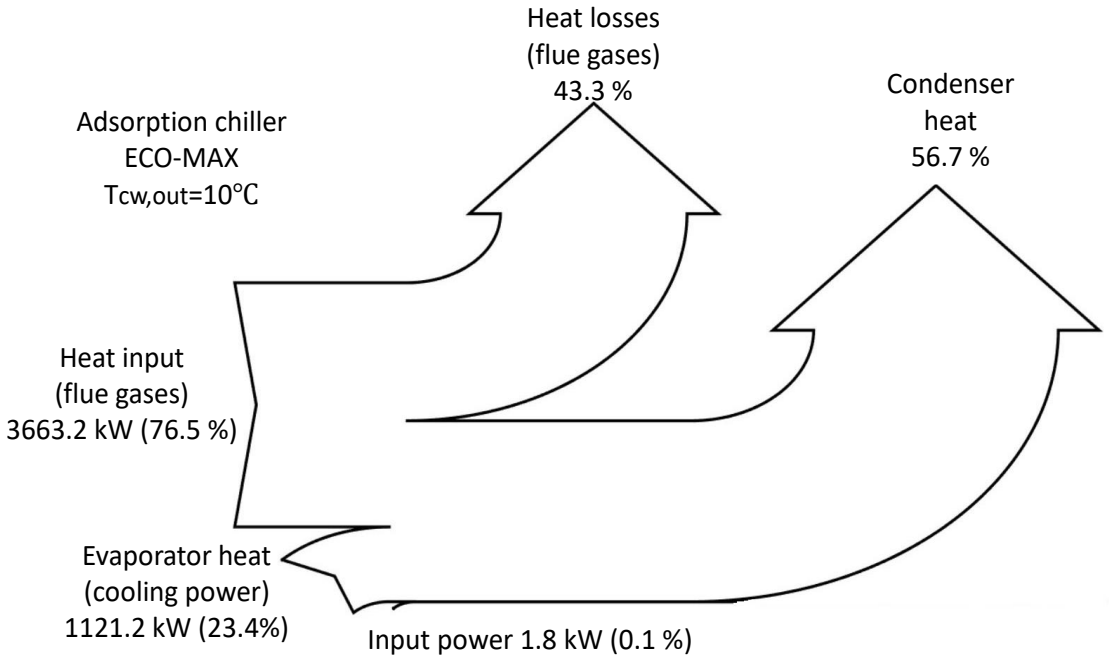

Figure 62 : Sankey diagram for the Adsorption chiller (ECO-MAX) for the 10 °C chilled water outlet temperature case

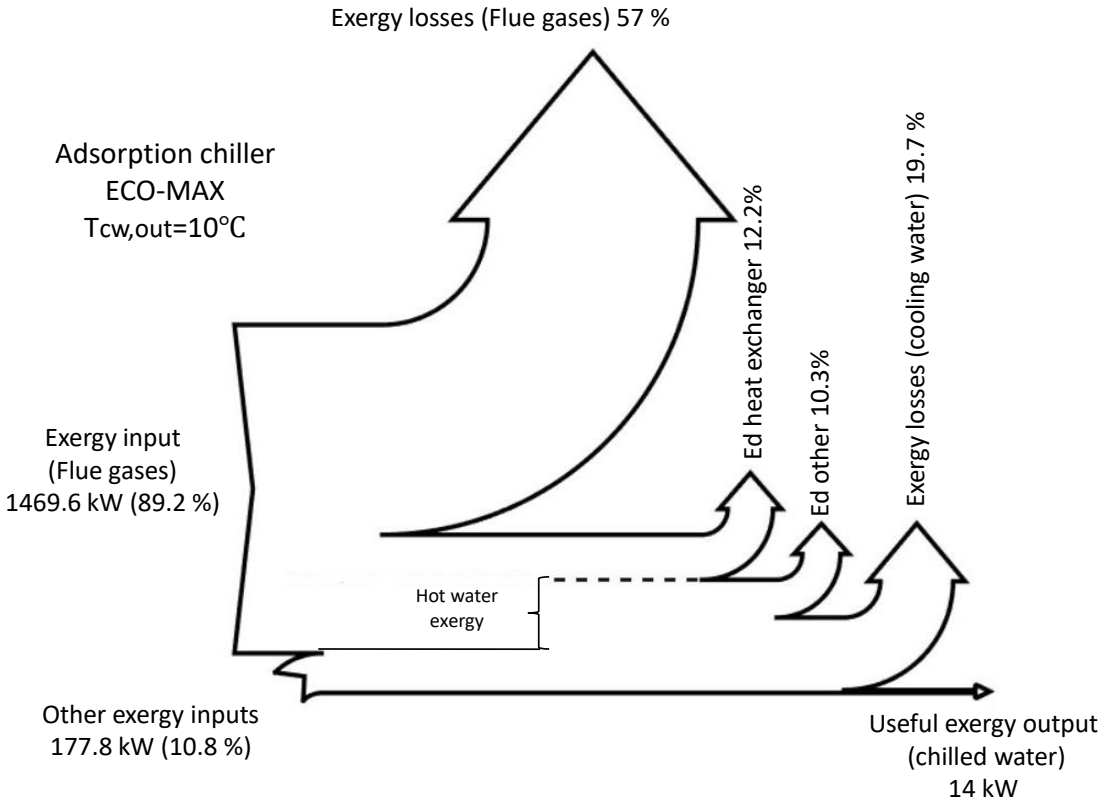

Figure 63 : Grassman diagram for the Adsorption chiller (ECO-MAX) for the 10 °C chilled water outlet temperature case

A remark that can be done related with the Sankey diagrams is that big amounts of heat are rejected. On one hand, those that have to do with the flue gases cannot be used in another way, since the lowest temperature that the gases can reach is usually imposed by their composition (dew point). On the other hand, the heat rejected by the condenser could be used in other ways, for example for heating. However, the cooling water's outlet temperature is low, at about 30-31 ℃.

From the Grassman diagrams, it can be seen that the larger losses are related with the flue gases outlet, which is unavoidable. Moreover, in all cases, in the heat exchanger, a big proportion of the exergy destruction takes place, which is more intense for the absorption and adsorption chillers, since in these the temperature differences are greater. Finally, the condenser is another component responsible for high exergy destruction.

3.5.2 2nd case-Chilled water outlet temperature of 7 ℃

For that case as well, all four technologies can be implemented. As for the adsorption chiller, both chillers can be used. So, for the given heat input, the comparison among the technologies is displayed in the following figures:

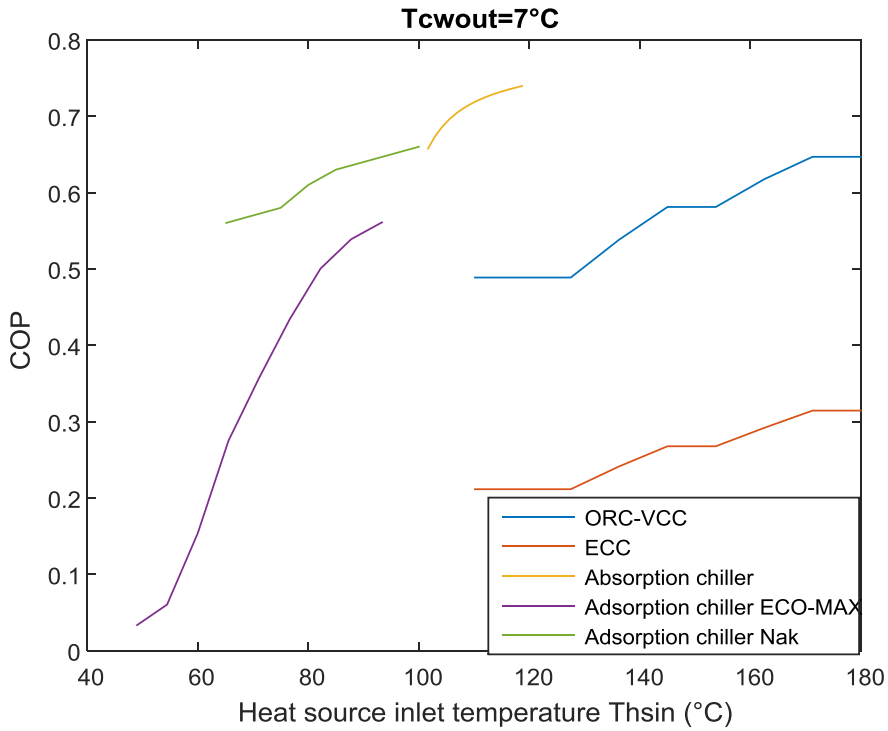

Figure 64 : Comparison of the COP of the four technologies for a chilled water outlet temperature demand of 7 ℃

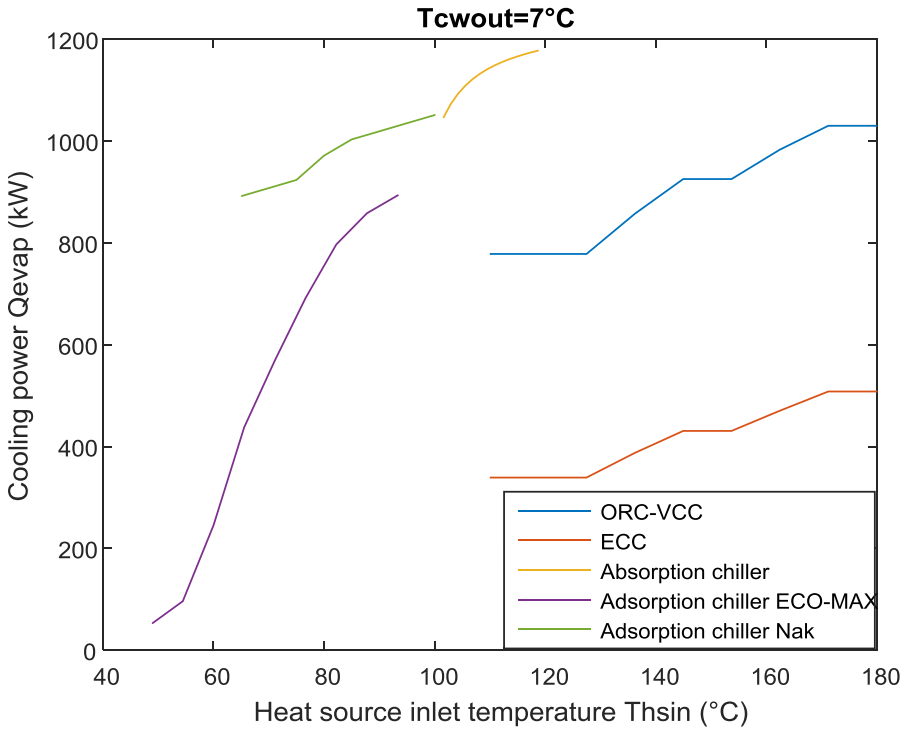

Figure 65 : Comparison of the cooling power of the four technologies for a chilled water outlet temperature demand of 7 °C

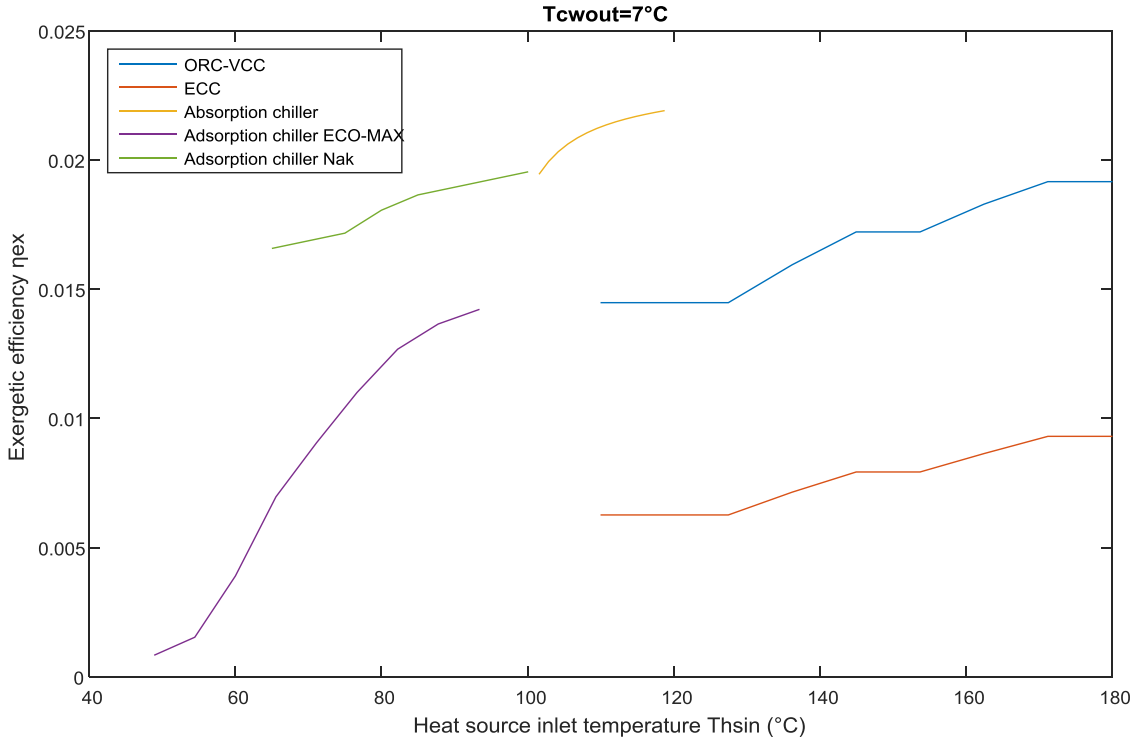

Figure 66 : Comparison of the exergetic efficiency of the four technologies for a chilled water outlet temperature demand of 7 °C

For that case, the results are similar. The absorption COP reaches 0.7395. The ORC-VCC system's COP reaches 0.6468 and it is overweighed by Nak Adsorption chiller, which achieves a COP of 0.66.

In general, in that case, the COPs were lower than in the previous case, due to the lower evaporator temperature. Absorption chiller has again the highest COP. For that case, the Nak adsorption chiller had relatively high efficiency.

As in the previous case, tables with the exergy inlet, outlet and destruction are shown below, followed by Sankey and Grassman diagrams.

ORC-VCC

Table 24 : Exergy results for the ORC-VCC (butane) for the 7 °C chilled water outlet temperature case

	Exergy destruction (kW)		Exergy input (kW)	Exergy output (kW)
Heat exchanger	79,7179	Heat exchanger	1469,6	939,2891
Evaporator I	72,4182	Evaporator I	557	106,4073
Condenser	141,3332	Condenser	0,7	72,3689
Evaporator	28,337	Evaporator	8,1	28,1626
Turbine	54,051			
Pump	4,0987			
Compressor	40,3864			
Valve	16,9656			
Mixing	1,2445			
Total	438,5525			

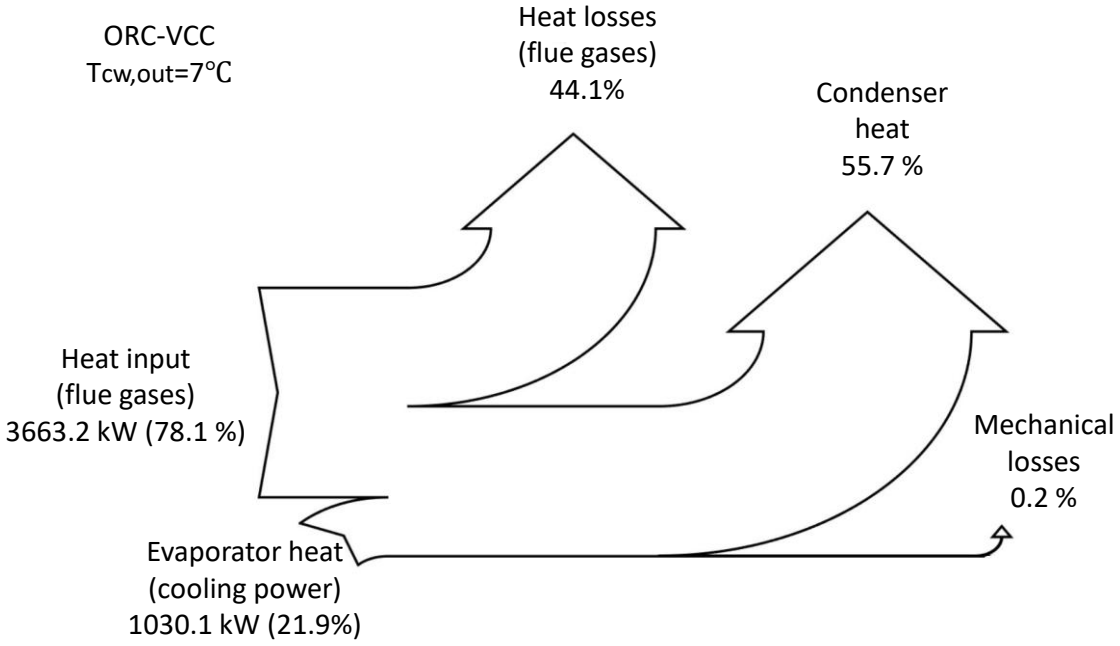

Figure 67 : Sankey diagram for the ORC-VCC (butane) for the 7 °C chilled water outlet temperature case

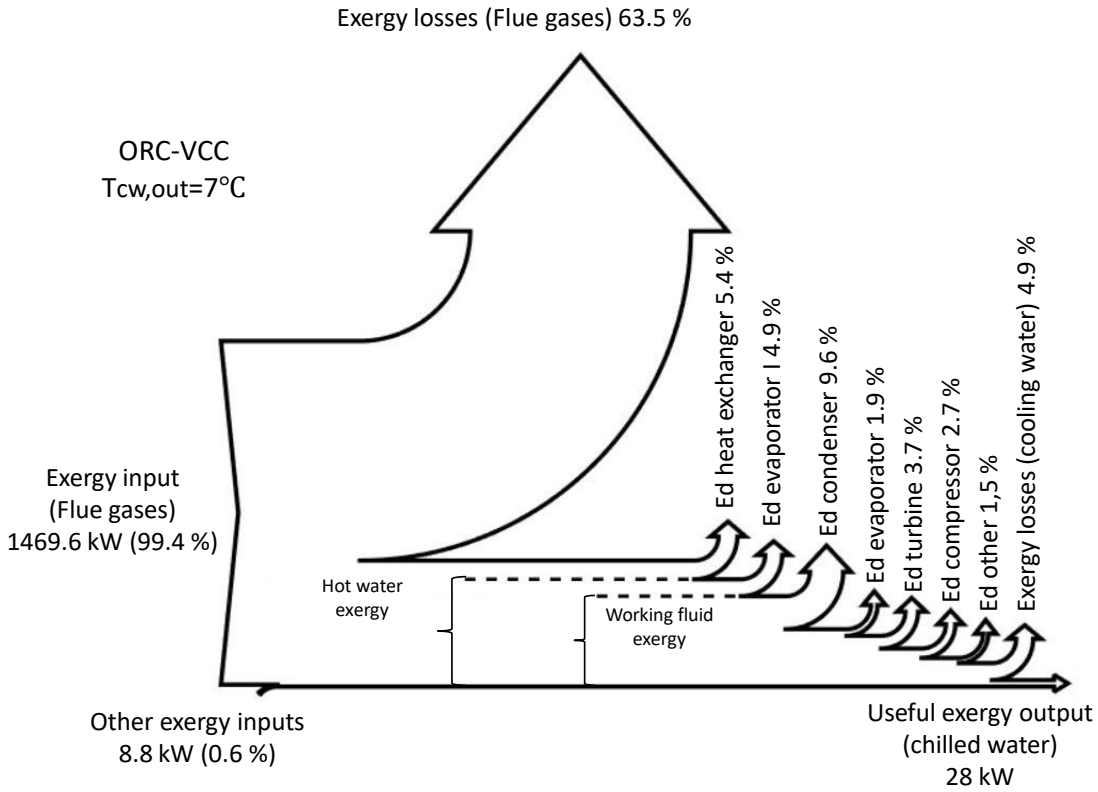

Figure 68 : Grassman diagram for the ORC-VCC (butane) for the 7 °C chilled water outlet temperature case

Table 25 : Exergy results for the ECC (butane) for the 7 °C chilled water outlet temperature case

	Exergy destruction (kW)		Exergy input (kW)	Exergy output (kW)
Heat exchanger	79,7179	Heat exchanger	1469,6	939,2891
Generator	72,4182	Generator	557	106,4073
Condenser	120,6267	Condenser	0,5	62,9784
Evaporator	13,9802	Evaporator	4	13,8941
Ejector	178,9759	Pump	23,3462	
Pump	7,1957			
Valve	8,37			
Edtot	481,2846			

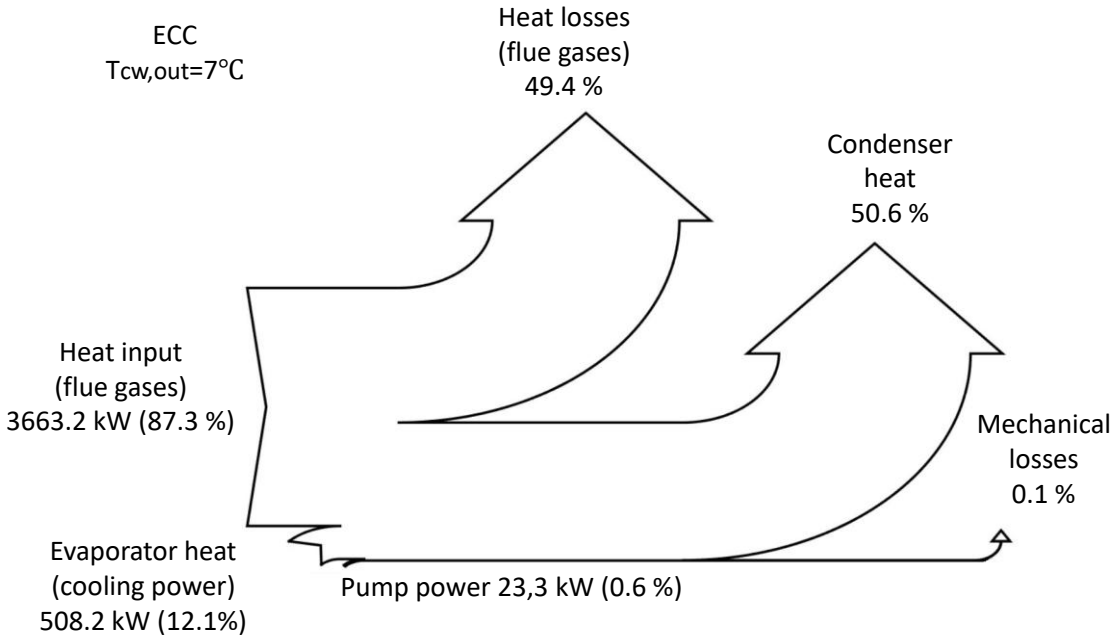

Figure 69 : Sankey diagram for the ECC (butane) for the 7 °C chilled water outlet temperature case

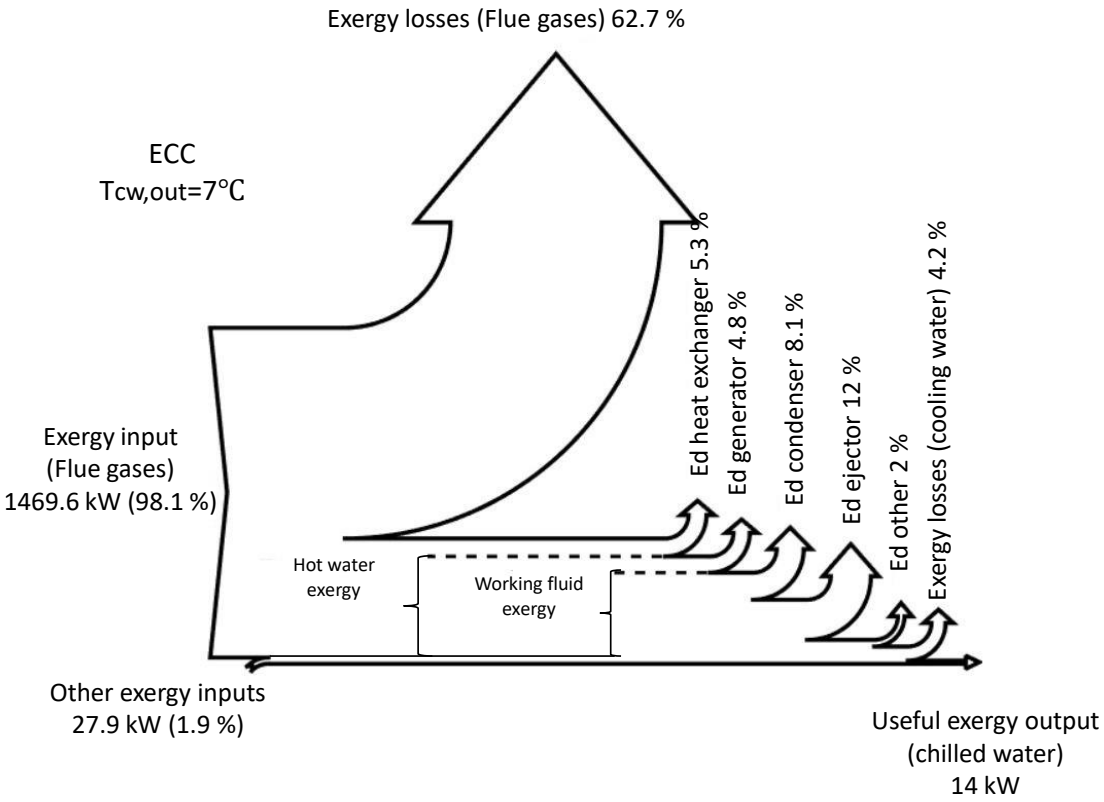

Figure 70 : Grassman diagram for the ECC (butane) for the 7 °C chilled water outlet temperature case

Table 26 : Exergy results for the Absorption chiller for the 7 °C chilled water outlet temperature case

	Exergy destruction (kW)		Exergy input (kW)	Exergy output (kW)
Heat exchanger	119,4511	Heat exchanger	1469,6	939,3
Generator	86,2423	Generator	3429,5	3018,7
Condenser	69,603	Condenser	0,4	32,9
Evaporator	32,6464	Evaporator	9,2	32,2
Absorber	106,0932	Absorber	0,4	40
Heat Exchanger	17,1716	Pump	0,0163	
Pump	0,0146			
Valve 5-6	0			
Valve 8-9	4,0004			
Edtot	435,2226			

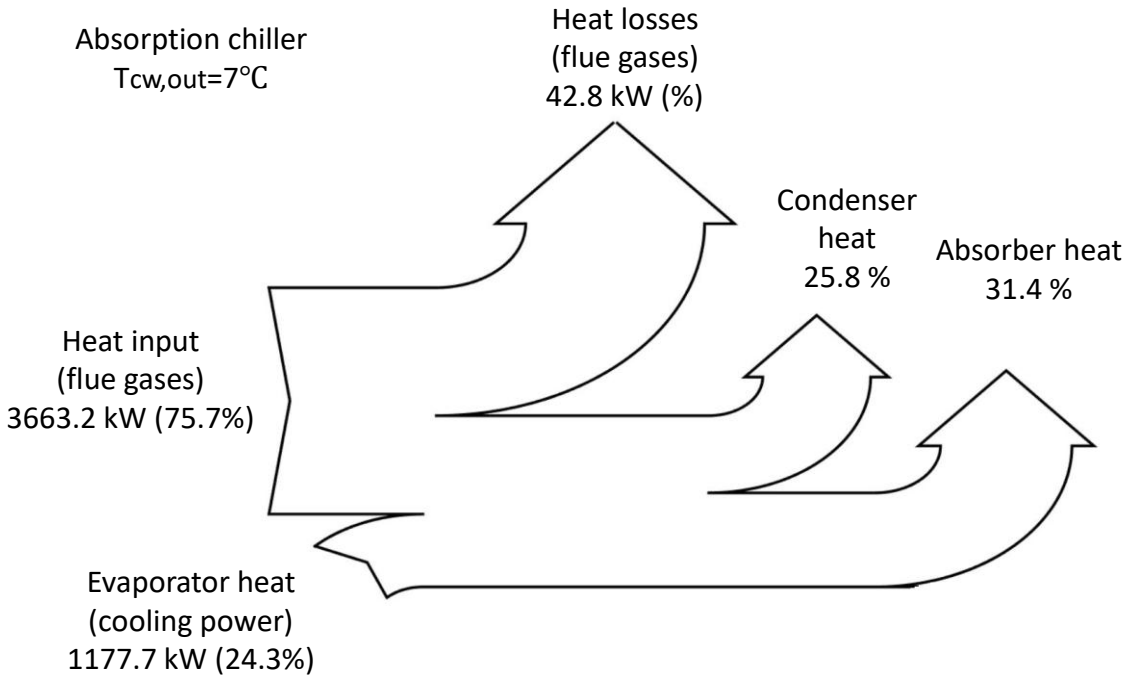

Figure 71 : Sankey diagram for the Absorption chiller for the 7 °C chilled water outlet temperature case

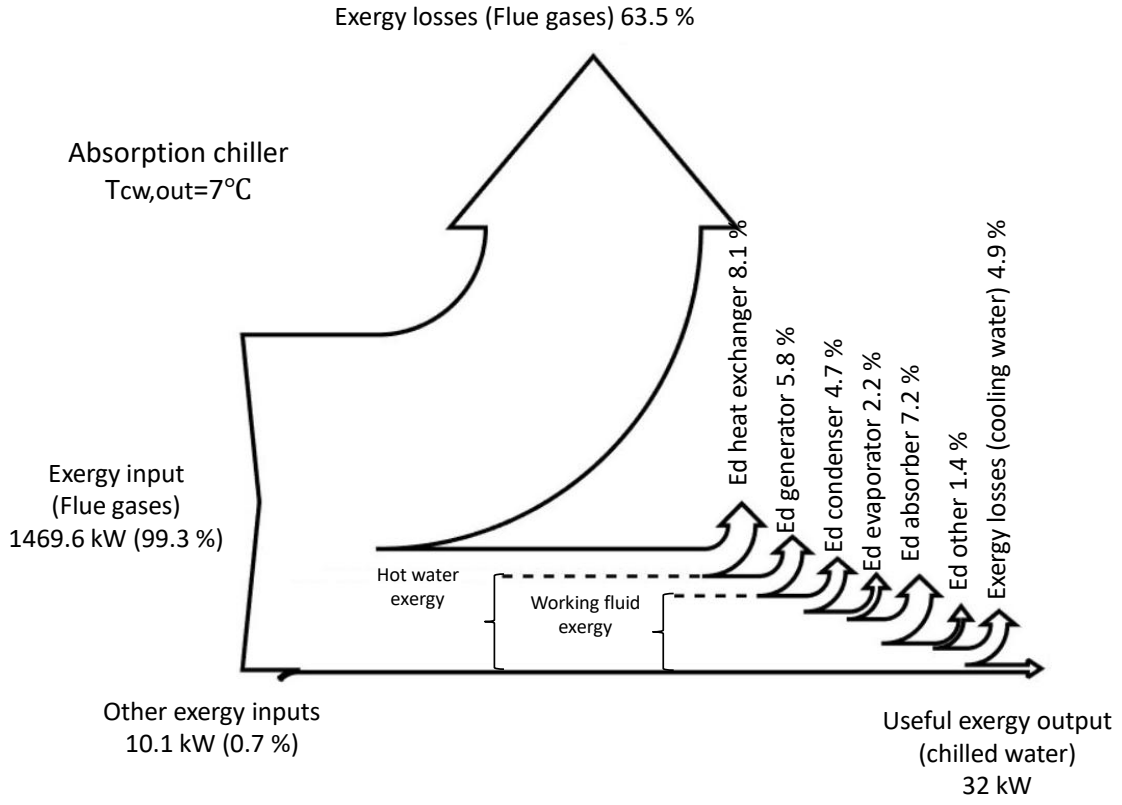

Figure 72 : Grassman diagram for the Absorption chiller for the 7 °C chilled water outlet temperature case

Table 27 : Exergy results for the Adsorption chiller (ECO-MAX) for the 7 °C chilled water outlet temperature case

	Exergy destruction (kW)		Exergy input (kW)	Exergy output (kW)
Heat exchanger	201,4659	Heat exchanger	1469,6	939,3
Ed,other	174,7394	Condenser	156,8	296,8576
Total	376,2053	Evaporator	5,1	20,9118
		Pump	1,8	

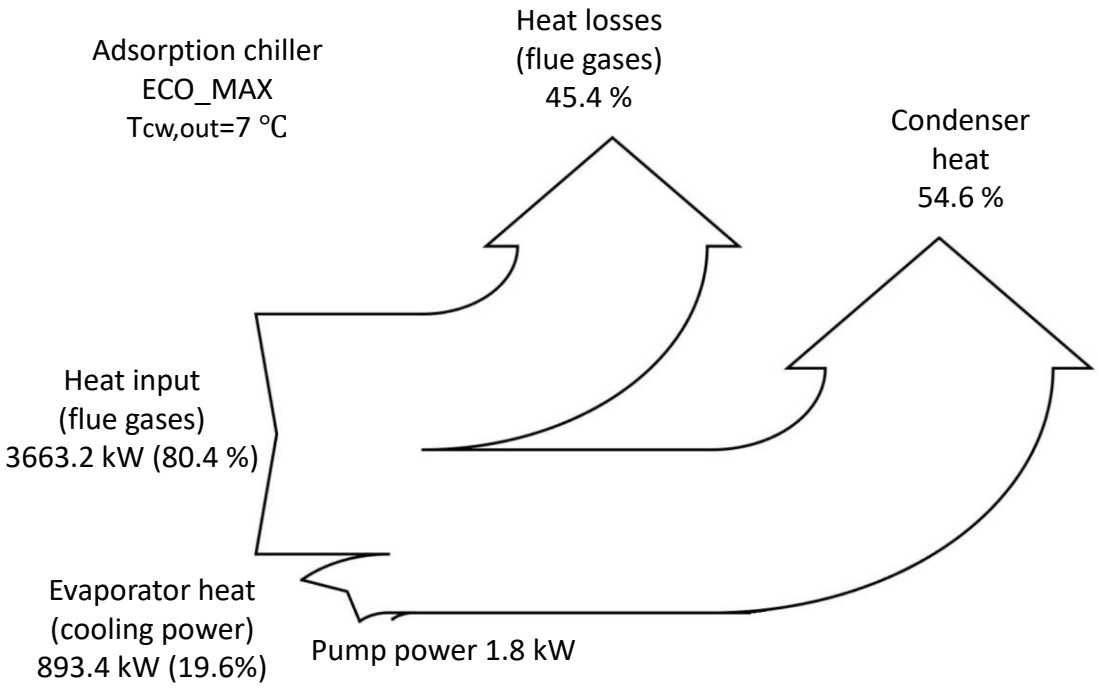

Figure 73 : Sankey diagram for the Adsorption chiller (ECO-MAX) for the 7 °C chilled water outlet temperature case

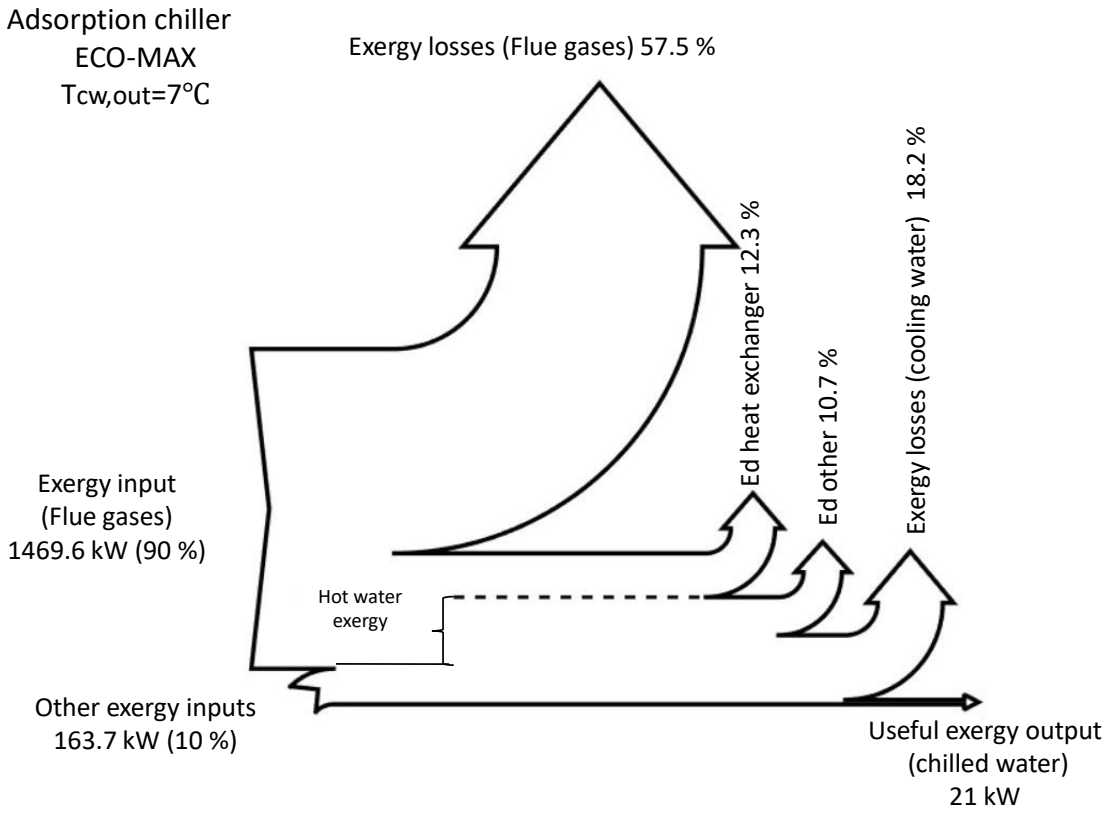

Figure 74 : Grassman diagram for the Adsorption chiller (ECO-MAX) for the 7 °C chilled water outlet temperature case

Table 28 : Exergy results for the Adsorption chiller (Nak) for the 7 °C chilled water outlet temperature case

	Exergy destruction (kW)		Exergy input (kW)	Exergy output (kW)
Heat exchanger	176,8292	Heat exchanger	1469,6	939,2891
Ed, other	178,3816	Condenser	301,3	455,9056
Edtot	355,2108	Evaporator	8,3	28,7355

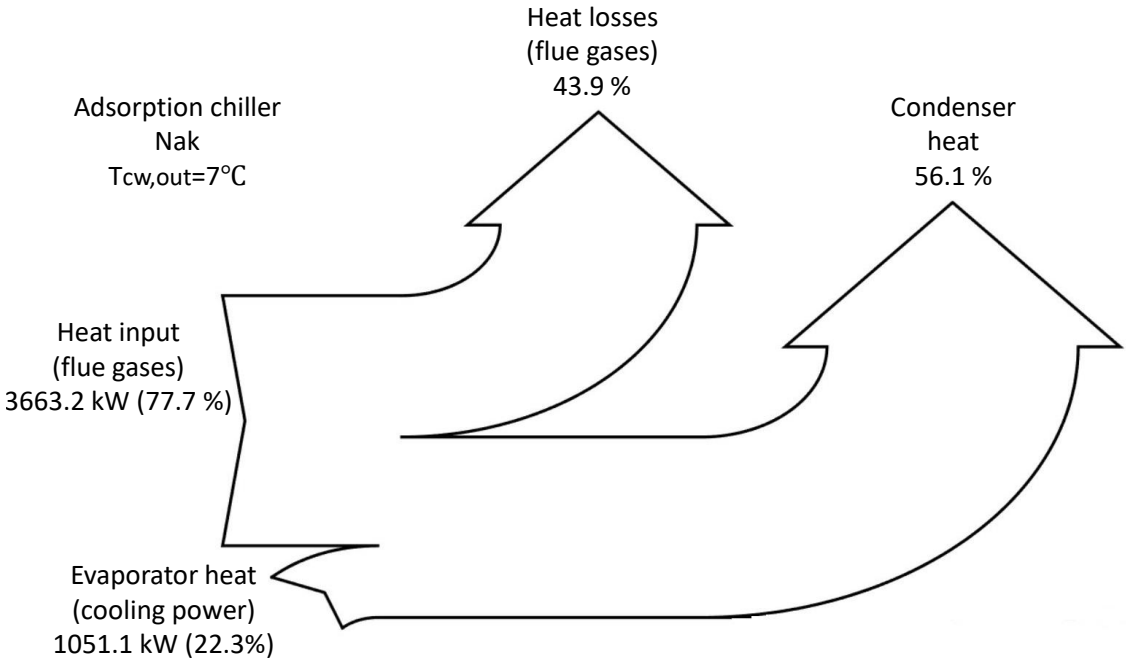

Figure 75 : Sankey diagram for the Adsorption chiller (Nak) for the 7 °C chilled water outlet temperature case

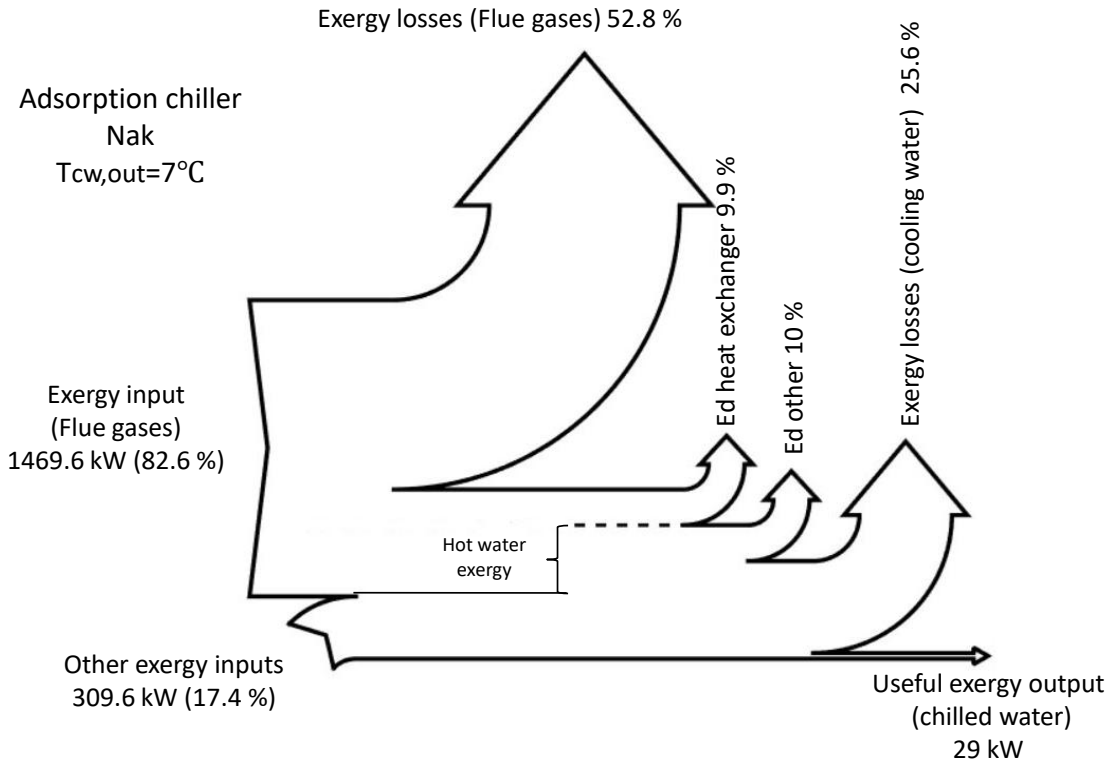

Figure 76 : Grassman diagram for the Adsorption chiller (Nak) for the 7 °C chilled water outlet temperature case

3.5.3 3rd case-Chilled water outlet temperature of 4 °C

For that case, only the ORC-VCC and ECC can operate. As for the absorption and adsorption chiller, both chillers cannot be used, since they use water as refrigerant and its freezing point restricts the operation at low evaporator temperatures. So, for the given heat input the comparison among the two technologies is displayed in the following figures:

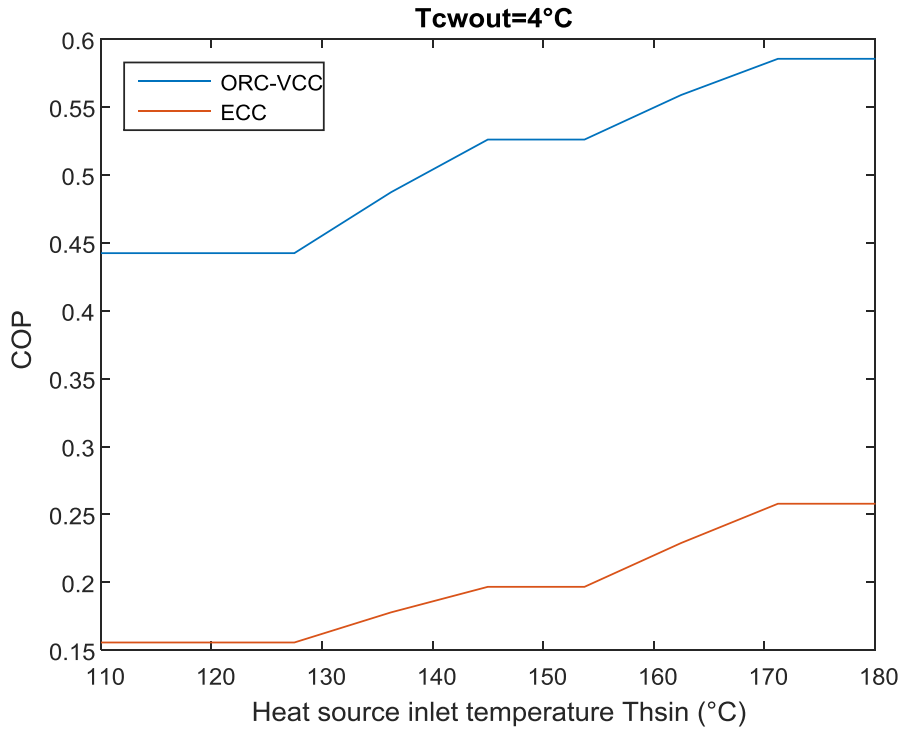

Figure 77 : Comparison of the cooling power of the two technologies that can operate for a chilled water outlet temperature demand of 4 °C

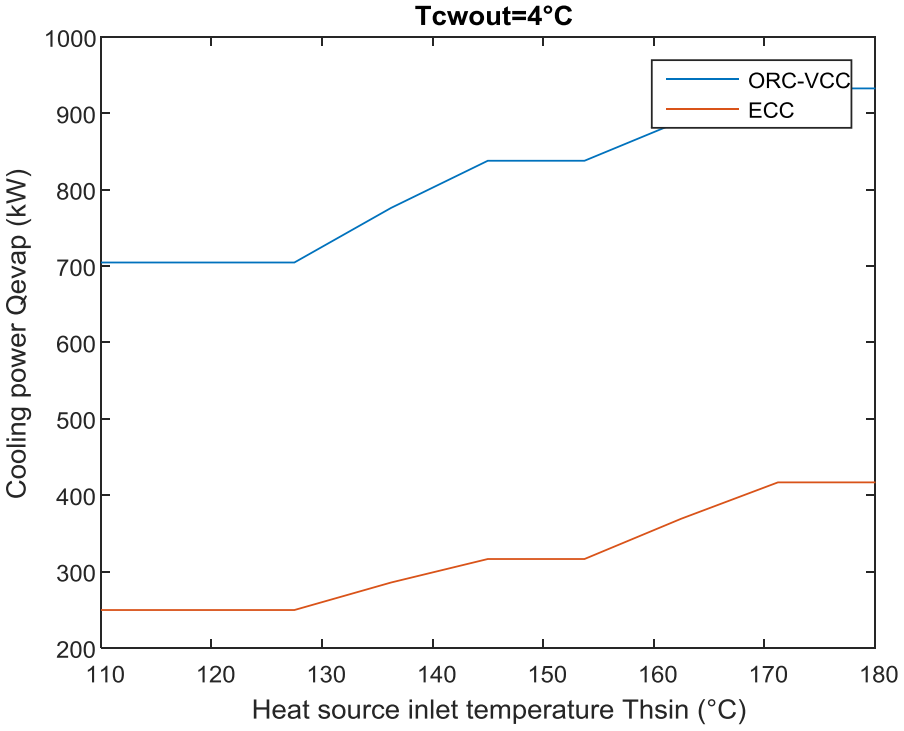

Figure 78 : Comparison of the cooling power of the two technologies that can operate for a chilled water outlet temperature demand of 4 °C

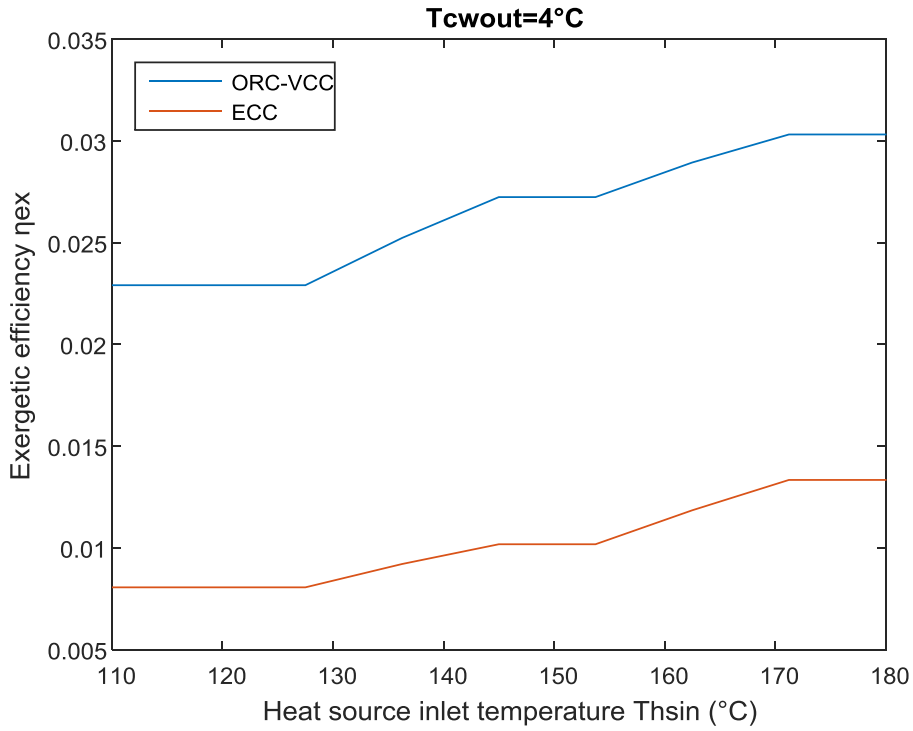

Figure 79 : Comparison of the exergetic efficiency of the two technologies that can operate for a chilled water outlet temperature demand of 4 °C

From Figure 77, Figure 78 and Figure 79, it is obvious that the ORC-VCC system has the highest energetic and exergetic efficiency between the two systems. Both systems reach their maximum efficiencies at 180 °C. As for the COP, the maximum value achieved is 0.5856 and the maximum value of exergy efficiency is 0.0303, which is the highest value among the three cases, due to the low evaporator temperature. So, it can be concluded that for cases where absorption and adsorption cannot operate, the ORC-VCC system is the best choice.

Table 29 : Exergy results for the ORC-VCC (butane) for the 4 °C chilled water outlet temperature case

	Exergy destruction (kW)		Exergy input (kW)	Exergy output (kW)
Heat exchanger	79,7179	Heat exchanger	1469,6	939,2891
Evaporator I	72,4182	Evaporator I	557	106,4073
Condenser	136,408	Condenser	0,7	69,6696
Evaporator	26,2143	Evaporator	16,2	44,5568
Turbine	54,051			
Pump	4,0987			
Compressor	40,3562			
Valve	18,5467			
Mixing	1,1126			
Edtot	432,9236			

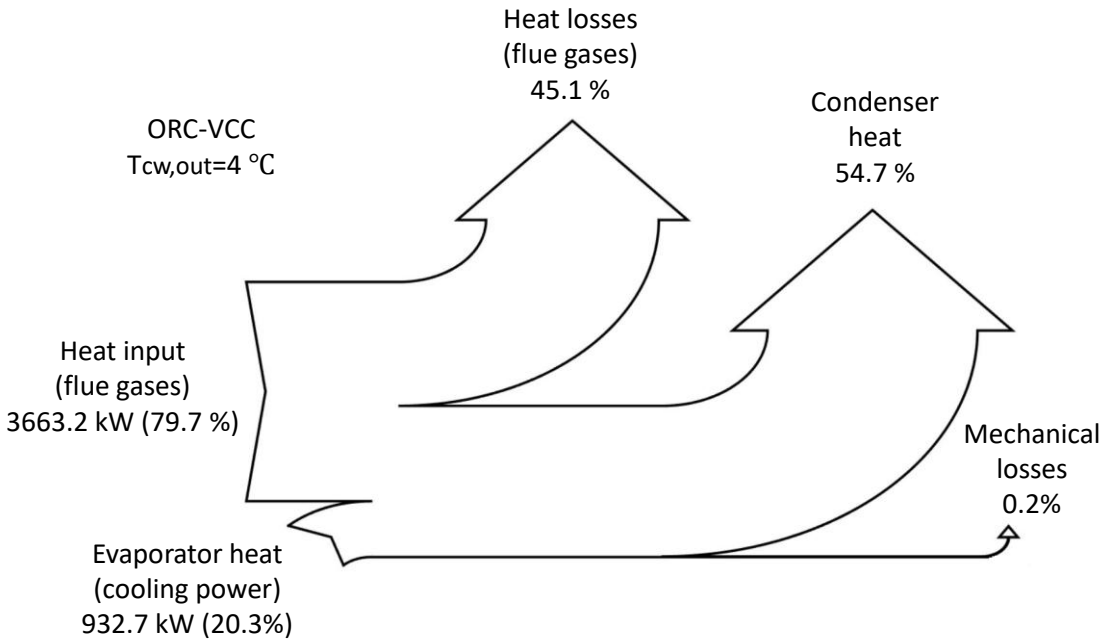

Figure 80 : Sankey diagram for the ORC-VCC (butane) for the 4 ℃ chilled water outlet temperature case

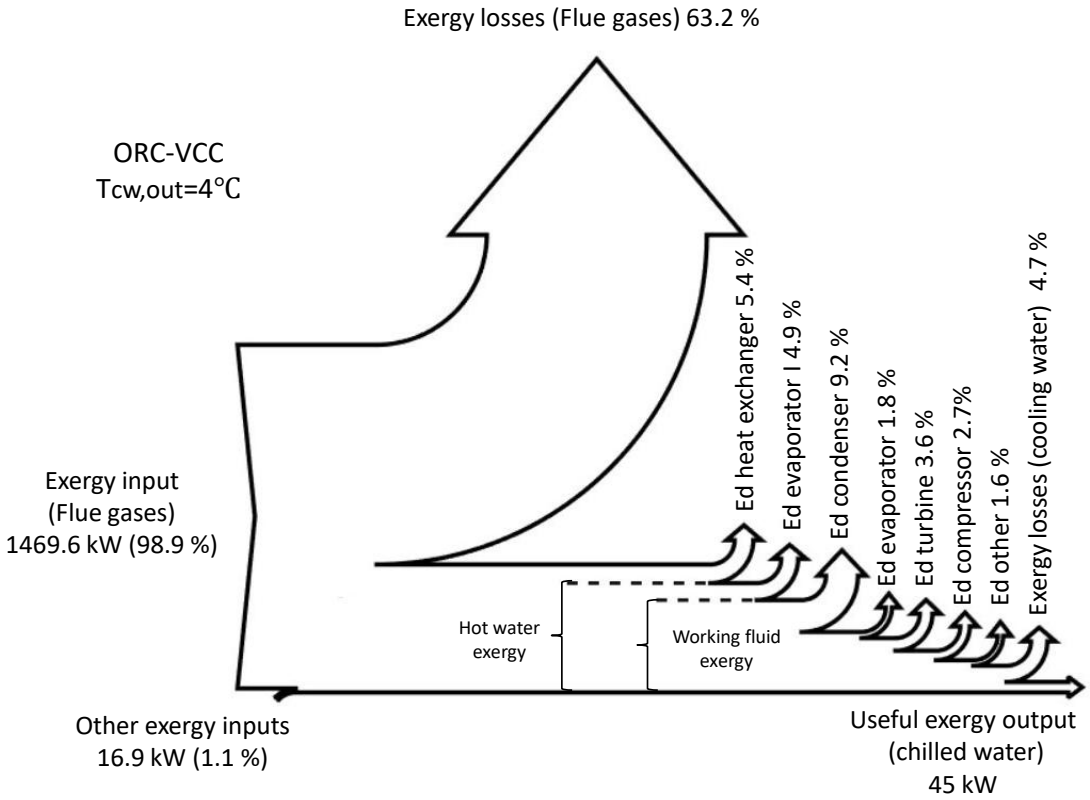

Figure 81 : Grassman diagram for the ORC-VCC (butane) for the 4 ℃ chilled water outlet temperature case

Table 30 : Exergy results for the ECC (butane) for the 4 °C chilled water outlet temperature case

	Exergy destruction (kW)		Exergy input (kW)	Exergy output (kW)
Heat exchanger	79,7179	Heat exchanger	1469,6	939,2891
Generator	72,4182	Generator	557	106,4073
Condenser	116,7179	Condenser	0,5	60,945
Evaporator	11,715	Evaporator	7,2	19,9121
Ejector	184,4587	Pump	23,3462	
Pump	7,1957			
Valve	8,2884			
Edtot	480,5118			

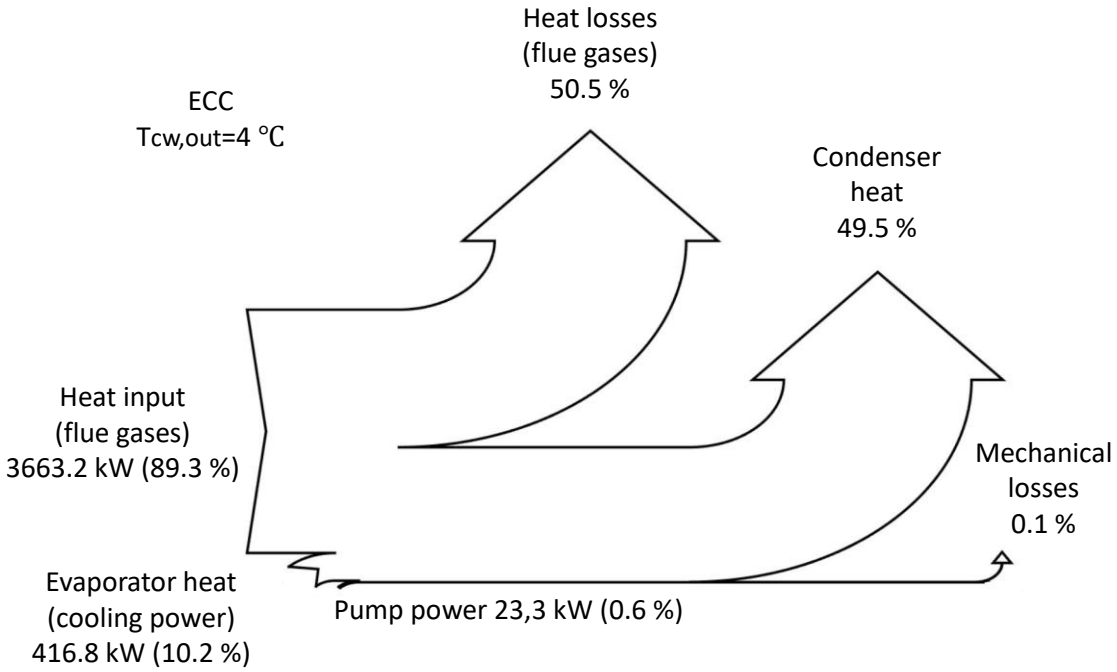

Figure 82: Sankey diagram for the ECC (butane) for the 4 °C chilled water outlet temperature case

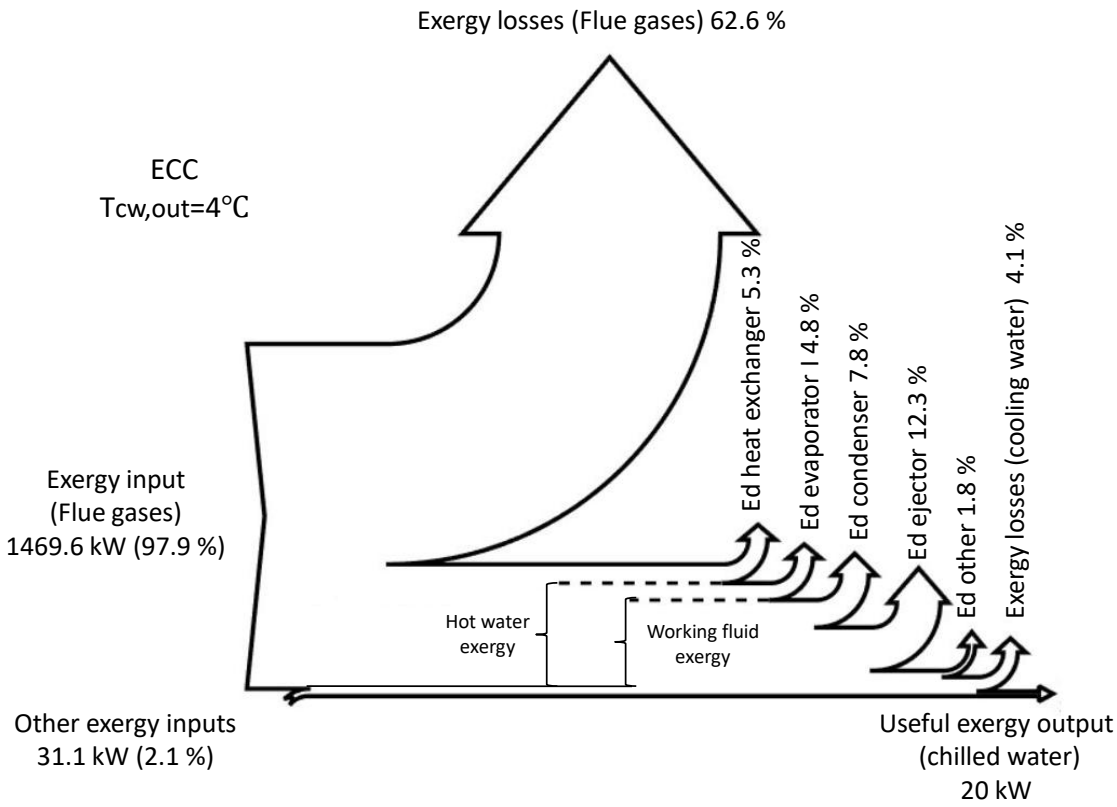

Figure 83 : Grassman diagram for the ECC (butane) for the 4 °C chilled water outlet temperature case

From the above three cases, the following conclusion can be extracted for each technology:

- ORC-VCC: The system can operate in a big range of chilled water temperatures and can achieve relatively high COP and exergetic efficiency in all cases comparing to the other technologies.
- ECC: The system can operate in a big range of chilled water temperature as well. However, its efficiency is in most occasions lower than those of the other technologies.
- Absorption chiller: The system can operate in a small range of chilled water temperature, due to its limitations. In the cases it can be used, it can achieve high values of COP and cooling power. Its exergetic efficiency is also high comparing to the other systems.
- Adsorption chiller: The system can operate in a relatively big range of chilled water temperature, comparing to the absorption chiller. The chillers used displayed relatively good performance. Even though they didn't have the highest efficiency, their efficiency was close to the highest, especially in the case of 7 °C. Its most important feature is that it can operate in low temperatures, where the absorption chiller cannot work and the ORC-VCC and ECC systems would have much lower efficiency than the efficiency they have in higher temperatures. That practically makes the adsorption chiller the only practical solution for heat recovery in that range of temperatures.

4. Economic analysis

In order to complete the analysis between the four systems, an economical comparison was made. In order to do that, an economical analysis of each system was made. First, the Specific Investment Cost (SIC), operational and maintenance costs for each system were estimated, based on several studies or data from manufacturers. Then, the installation of each system was considered. The case that was used was the first case examined in the previous chapter (3.5.1); namely demand of chilled water outlet temperature of 10 °C. With the calculations made in the previous chapter, the cooling power that each system can produce is known. So, the substitution of the cooling power produced from an electricity-powered VCC by each cooling system was considered. The incomes from such an investment are calculated as the savings from electricity, which would be consumed by the VCC in order to produce the same amount of cooling. Finally, three representative economical performance measures were calculated for each system. Those were the net present value (NPV), the internal rate of return (IRR) and the payback period (PBP). With those measures, a comparison among the investment of each technology is possible.

4.1 ORC costs

In order to calculate the costs for the ORC, the power production of the system must be known. For the case which is under consideration, a mechanical power of 200 kW is produced by the ORC. In general, the ORC is a system studied extensively and several studies include economical analysis of it. Figures like Figure 84 have been made by several researchers. Lemmens [96] reviewed several studies with economical results. From this review, it can be concluded that for waste heat recovery application with a power production of about 200 kW, a cost of about 2000 $\frac{€}{kW}$ is a reasonable assumption (Figure 85). That is close with the value that can be estimated by Figure 84. Furthermore, the installation cost can be calculated as approximately 30 % of the cost for the equipment [97]. That leads to a total investment cost of 2600 $\frac{€}{kW}$.

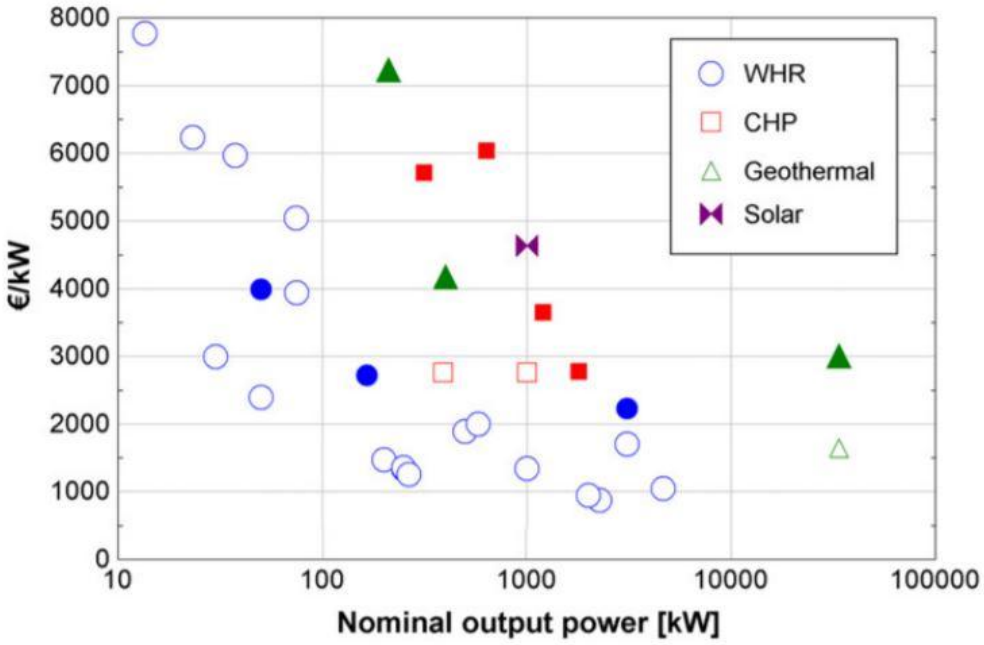

Figure 84 : ORC costs [5]

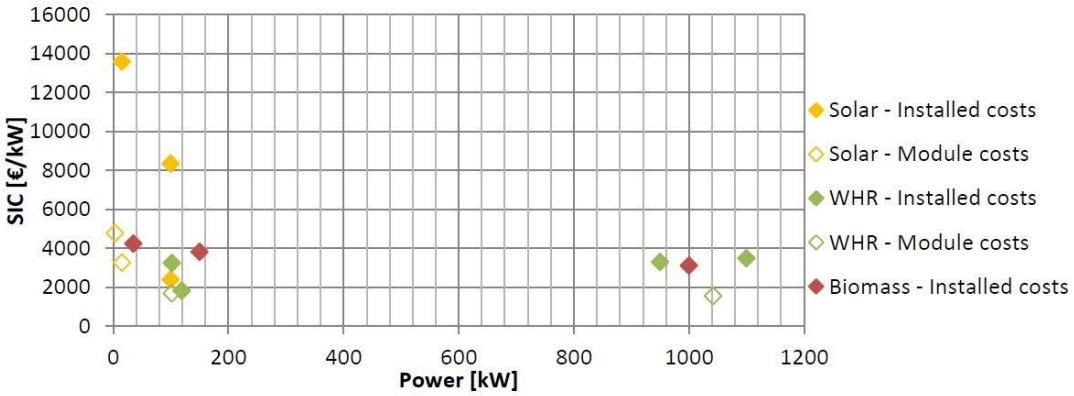

Figure 85 : ORC costs [96]

Finally, according to Southon [98], the maintenance cost can be calculated as a proportion of the total investment cost. That proportion is given by the following relationship

$$y = 0{,}039Q(MW)^{-0.1698} \qquad 4.1$$

That gives a proportion of 0.0513 (5,13 %) of the investment cost. This cost is considered to include the operational costs of the ORC-VCC system.

4.2 VCC costs

For the VCC case, there are economical data in several studies, as well as data from manufacturers. The cost of the VCC is generally lower than that of the other cooling systems. Murugavel and Saravanan [99] estimated the price of a VCC of 375 RT to be $106{,}26\ \frac{€}{kW}$. In [100], a price of $170\ \frac{€}{kW}$ is proposed for a 1 MW VCC. Finally, from the GSA schedules price list of Daikin Applied products [101], the price of a chiller with cooling capacity of about 326 RT (1144 kW), as the case of the VCC in the ORC-VCC system, has a cost of about $122\ \frac{€}{kW}$. The latter cost is considered, as it is close to the costs found in the previous studies. By adding the installation cost, a total investment cost of $158.6\ \frac{€}{kW}$ is considered for the VCC

The maintenance costs of the VCC are estimated at 8320 € per year in [99], while in [57], the maintenance cost is estimated as 10000 € per year. The latter value is acquired.

The operational cost of the system is considered to be included in the maintenance cost calculated for the ORC case.

The service life of the chiller is estimated to be 20 and 25 years, for reciprocating and centrifugal compressor respectively [102].

The service life of the ORC-VCC system can be considered to be 20 years [17].

4.3 ECC costs

The ECC is a system which hasn't been implemented extensively, since in its simple configuration, it has low efficiency, as was proved in this thesis as well. Even though there are a number of studies investigating the operation and design of the ejector compression cycle, only few of them involve economic analysis of the system.

Sherif et al.[103] compared the use of a steam jet with an absorption chiller and a vapor compression chiller. In their study, a price of about $380\ \frac{€}{\mathrm{kW}}$ was assumed for a 300 RT steam jet ejector refrigeration system. The system's operating cost was estimated at about 1760 $\frac{€}{\mathrm{a}}$.

Furthermore, Milazzo and Mazzelli [104] mention a price of $400\ \frac{€}{\mathrm{kW}}$ as a minimum achievable price of the ejector compression system.

The latter price is considered as the ECC module cost and by adding the installation costs, a final cost of $520\ \frac{€}{\mathrm{kW}}$ is estimated for the ECC system.

As long as the maintenance costs are concerned, Nguyen et al. [105] proposed that the ECC system has zero maintenance costs, and proposed a lifetime of 30 years for the ECC. However, in this case, the maintenance cost was estimated as a 3 % percentage of the total cost of the system.

Finally, the operational costs can be calculated by the pump required power, which is 23.346 kW for the examined case.

4.4 Absorption chiller costs

There are a lot of studies about the absorption chiller, some of which include cost estimation for the chiller. However, a most secure estimation can be extracted from a manufacturer's data. So, from an absorption chiller manufacturer [80], the following curve can be extracted:

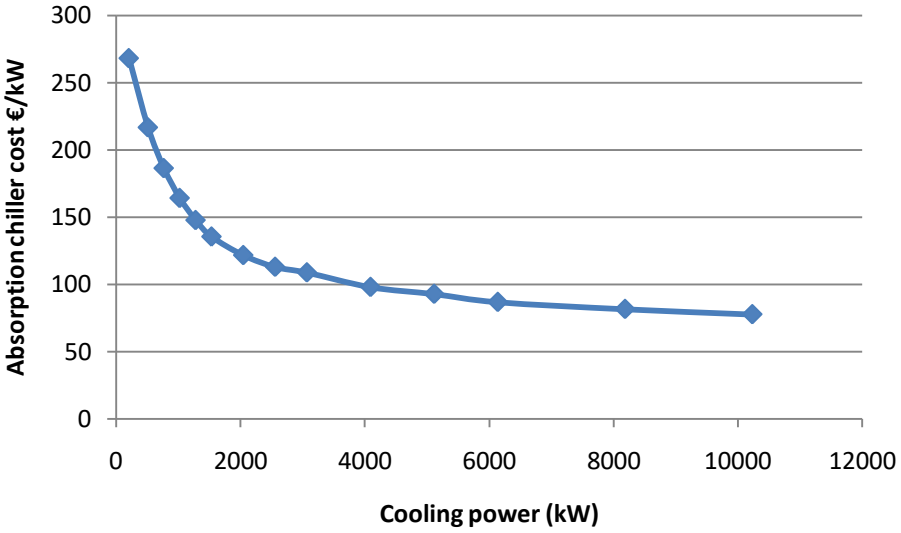

Figure 86 : Cooling power-cost diagram for the Absorption chiller

From the curve, the following equation can be extracted:

$$SIC(\frac{€}{\text{kW}}) = 1674 * Q^{-0.33} \qquad 4.2$$

The cost of the chiller in the examined case can be calculated as 161 $\frac{€}{\text{kW}}$. For the calculations, data for waste heat (hot water) chiller were obtained. With addition of the installation costs, a final cost of 210 $\frac{€}{\text{kW}}$ was considered.

As for the maintenance cost, according to [57], the maintenance cost of an absorption chiller can range from 20.000 to 30.000 € per year. Moreover, a cost of 15000 $ (13400 €) has been recorded in [70] for an 90 RT absorption chiller. In this thesis, a cost of $20000\frac{€}{a}$ was considered.

Finally, in the manufacturer's data, an operational power of 5.7 kW is mentioned. Since this value is greater than the pump's power demand, it was considered the operational power of the chiller.

The service life of the chiller can be estimated to be about 23 years [102].

4.5 Adsorption chiller costs

From the literature, there is a small number of studies concerning the cost of the adsorption chiller, since most of the studies focus on its design and operation. Moreover, since adsorption chillers are generally used in low cooling capacity applications, the existing data refer to low cooling capacity chillers. In [106], the cost for an adsorption chiller of several KW is estimated at approximately $600\ \frac{€}{kW}$. From [107], a price of $500\ \frac{€}{kW}$ is given for a commercial chiller of 70 kW (Mycom chiller). Finally, in[70], the cost of a chiller of 80 RT (280 kW) is estimated to be 191000 $, which is equivalent to $605{,}37\ \frac{€}{kW}$. In the study, this cost corresponded to an ECO-MAX adsorption chiller.

According to [108], when a purchase price for a similar system of different capacity is known, the following correlation can estimate the cost of the system for a specific capacity value (C is the cost, A the capacity and n is the cost exponent):

$$\frac{C_a}{C_b} = (\frac{A_a}{A_b})^n \qquad 4.3$$

A common value for n is often around 0.6 and then the relationship is referred to as “the six tenths rule”. That is also expressing the concept of economy of scale, as the change in the capacity is not proportional to the change of the cost.

In this case, since the value closer to that calculated in 3.5.1 is that given in [70], equation 4.3 is used for this value and in that way, the cost of the chiller is estimated to be 349 $\frac{€}{\text{kW}}$ and by adding the installation cost, the total investment cost is 454 $\frac{€}{\text{kW}}$.

The service life of the system is estimated at about 20 years, while its maintenance costs per year are estimated at 3000 $ (2680 €)[70]. Moreover, from the manufacturers data [57], a maintenance cost of 5000 $ per year are given as a typical case. The latter value is acquired.

Finally, as mentioned before, an operational power of 1.8 kW is acquired from the manufacturer’s data [57].

The difference between the maintenance costs of the chillers can be attributed to the following reasons. The silica gel is non toxic and its initial charge can last for the whole lifetime of the chiller. On the other hand, the lithium-bromide charge changes every 4-5 years. Moreover, since it is corrosive, more usual component replacement is needed, the life time of the components decreases and the maintenance cost increases. Finally, lithium-bromide needs special handling during maintenance and decommissioning, since it is hazardous [70].

The above-mentioned costs are summarized in Table 31 and Table 32. The module SIC refers to the purchase cost of the system, without the extra cost for the installation.

Table 31 : Investment costs for the four chillers

	COP/η_{ORC}	Q (kW)	SIC (€/kW) module	SIC (€/kW) total	IC (€)
ECC	0,366	592,34	400	520	362551
Absorption chiller	0,7579	1207	160,98	209,28	307139
Adsorption chiller	0,704	1121,2	349,11	453,854	563396
ORC-VCC	0,7187	1144,6	471,71	613,226	756432
ORC	*0,1257*	*200,14*	*2000*	*2600*	*520364*
VCC	*5,719*	*1144,6*	*122*	*158,6*	*181534*

Table 32 : Maintenance and operating costs per year for the four chillers

	Maintenance (€/a)	Operational power (kW)	Operational cost (€/a)	Total cost (€/a)
ECC	10876,52457	23,346	15679,3	26555,83
Absorption chiller	20000	5,7	3828,12	23828.1
Adsorption chiller	5000	1,8	1208,88	6208.88
ORC-VCC	36694,6732	-	-	36694,7
ORC	26694,6732	-	-	26694,6
VCC	10000	-	-	10000

In both tables, the ORC-VCC costs are demonstrated separately for the ORC and for the VCC and as a system, in order to demonstrate the costs of each subsystem clearly. In Table 31, the SIC refers to the cost of the core system (without the cost for the gas-hot water heat exchanger. However, the final cost which is demonstrated is the total cost, including the heat exchanger.

From Table 31, it can be seen that the ORC-VCC system is the most expensive, due to the high cost of the ORC. The ECC system is the next most expensive system. Even though it consists of relatively simple components, like heat exchangers or pump, the fact that it is not a commercialized chiller justifies the higher cost. In connection with that, the adsorption chiller has a lower cost than the ECC, even though the adsorber bed is more complex than the components of the ECC. That is because of its commercialization, which can decrease the cost. All these are based on the fact that the assumed price for the adsorption chiller is based on a commercial chiller. The absorption chiller has a relatively low investment cost, mostly due to the fact that is a commercialized chiller, something that decreases its cost.

Same thing goes for the VCC, which is the most commercialized chiller and thus its price is the lowest among the other.

Finally, in order to evaluate the investment of the chillers, the substitution of a VCC is examined. A VCC which has R134a as working fluid is considered, since that is the most common fluid used for refrigeration. When operating under the same conditions as the investigated chillers, the VCC achieves a COP of 5.5. Each chiller is considered to substitute cooling power produced by the VCC with the power it can produce from the waste heat recovery. The income from such an investment per year is the savings of electricity, which would be needed to produce the specific amount of cooling and the maintenance costs of the VCC. The following summarizes the cost savings in each case of chiller:

Table 33 : VCC cost savings for each case

	Q(kW)	Operational power (kW)	Cost savings (€/a)
ECC	592,34	107,4	72143
Absorption chiller	1207	218,98	147006
Adsorption chiller	1121,2	203,3	136556
ORC-VCC	1144,6	207,6	139406

Table 33 shows the cost savings for the case of cost of electricity of 0.115 $\frac{€}{\text{Kwh}}$, which is the industrial price of electricity for the case of Greece for 2016. This price is 0.125 $\frac{€}{\text{Kwh}}$ for the whole euro area [109].

In this thesis, a sensitivity analysis based on several parameters was conducted. The base case's data were considered to be: an interest rate of 8 %, the electricity price of Greece (0.115 $\frac{€}{\text{Kwh}}$) and 5840 hours of operation per year (16 hours per day). The first parameter for the analysis was the price of electricity, examining prices from 0.1 to 0.16 $\frac{€}{\text{Kwh}}$. Those are the minimum and maximum prices observed in the EU area [109]. The operating hours per year were used as a variable as well. For this, the hours ranged from 2000 to 8000 hours of operation per year. The latter value practically stands for continuous operation of the systems. Three of the four systems are able to work for that amount of hours. However, the absorption chiller needs daily shut-down for the maintenance of the mixture. So, for the case of the absorption chiller, operation up to 7000 per year was estimated. The final parameter was the interest rate, for which values from 0 to 10 % where examined.

Table 34 : Data for the economic analysis

Interest rate(%)	0-10 (8)
Evaluation period (years)	20 years
Price of electricity (€/kWh)	0,1-0,16 (0.115)
Hours of operation	2000-8000 (5840)
Loan(%)	0
Subsidy(%)	0
Tax(%)	0

Table 34 summarizes the inputs used in the economical analysis. For the variables that are used in a range, the value in the parenthesis shows the base case value for the variable. The expenses of each investment are equal to the operational costs of it. In this case, it is considered that the investment cost was paid without a loan or a subsidy. Also, since this investment is part of an industrial process and its product is consumed by the process itself and there are no sales of energy or cooling etc., no tax was considered. So, since the incomes and the expenses are known, the three basic economic measures can be calculated. Those are [110]:

1. Net present value (NPV)

The net present value is defined as:

$$NPV = -K + \sum_{i=1}^{N} \frac{NCF_i}{(1+k)^i} \qquad 4.4$$

The following comments on the variables of the NPV should be done:

The Net Cash Flow (NCF) of each year is calculated from the incomes of the investment minus the operating and maintenance costs and the interests and taxes which must be paid. In this case, no interests or taxes were considered. The investment evaluation period was considered to be 20 years, since the service life of all the systems is at least 20 years. The interest rate k represents the return rate of the invested capitals which is targeted by the investor. This value is defined by several factors and it is not necessarily the same for every investor or in every country. For this reason, interest rates from 0 to 10 % where examined.

The NPV result can be interpreted in the following way:

- NPV>0 means that the investment is beneficial
- NPV=0 means that it is uncertain whether the investment is beneficial or not
- NPV<0 means that the investment is not beneficial

2. Internal Rate of Return (IRR)

The IRR is defined as the interest rate which would result in a zero NPV:

$$-K + \sum_{i=1}^{N} \frac{NCF_i}{(1+IRR)^i} = 0 \qquad 4.5$$

The IRR result can be interpreted in the following way, with k_{min} representing the minimum accepted interest rate:

- $IRR \geq k_{min}$ means that the investment is beneficial
- $IRR < k_{min}$ means that the investment is not beneficial

Furthermore, when two investments are compared, the one that has the higher IRR is considered more profitable.

3. Payback period

The payback period is defined as the number of years at which the investment cost is fully reimbursed and the investors are starting to earn money from it. The payback period is calculated as a decimal number.

4.6 Results

The results of the economic analysis are presented below.

Table 35 : Economic analysis' results for the base case

	NPV (€)	IRR (%)	PBT (years)
ECC	78740	11,02%	7,95
Absorption chiller	835408	40,06%	2,49
Adsorption chiller	663308	22,75%	4,32
ORC-VCC	233338	12,23%	7,36

From the above table, it can be seen that the absorption chiller has the best values for the economic measures, followed by the adsorption chiller. On the other hand, the ORC-VCC systems have worse values, since their IRR and PBP suggest an investment not clearly profitable.

Diagrams which show the variation of the three economic measures with the parameters were plotted.

First the results for the different operating hours are presented:

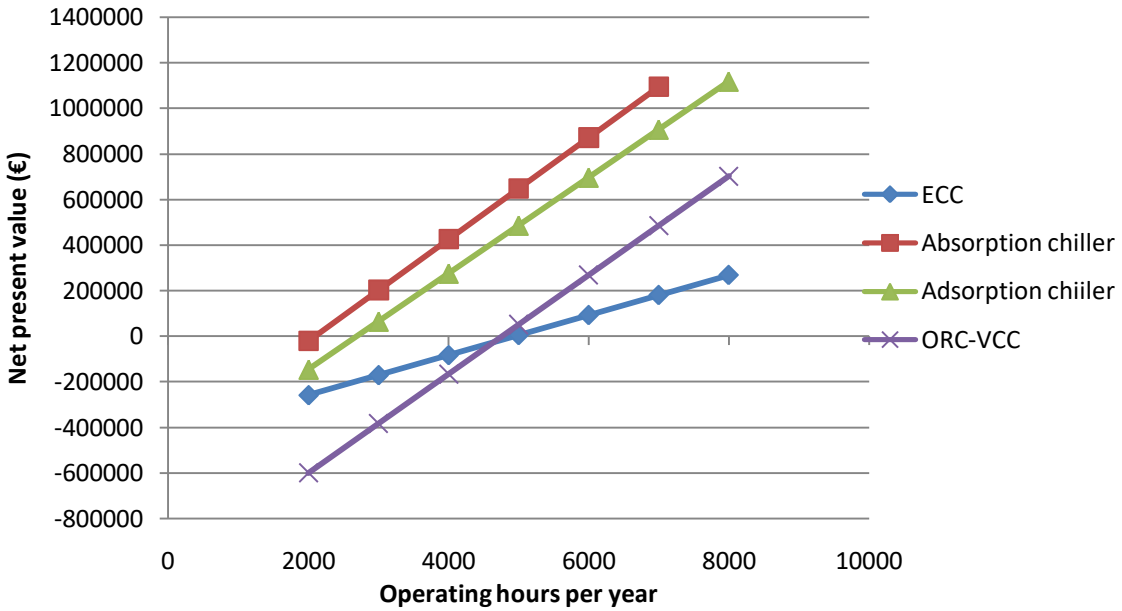

Figure 87 : NVP variation with the operating hours per year (For electricity cost 0.115 $\frac{€}{\text{Kwh}}$, Interest rate 8 %)

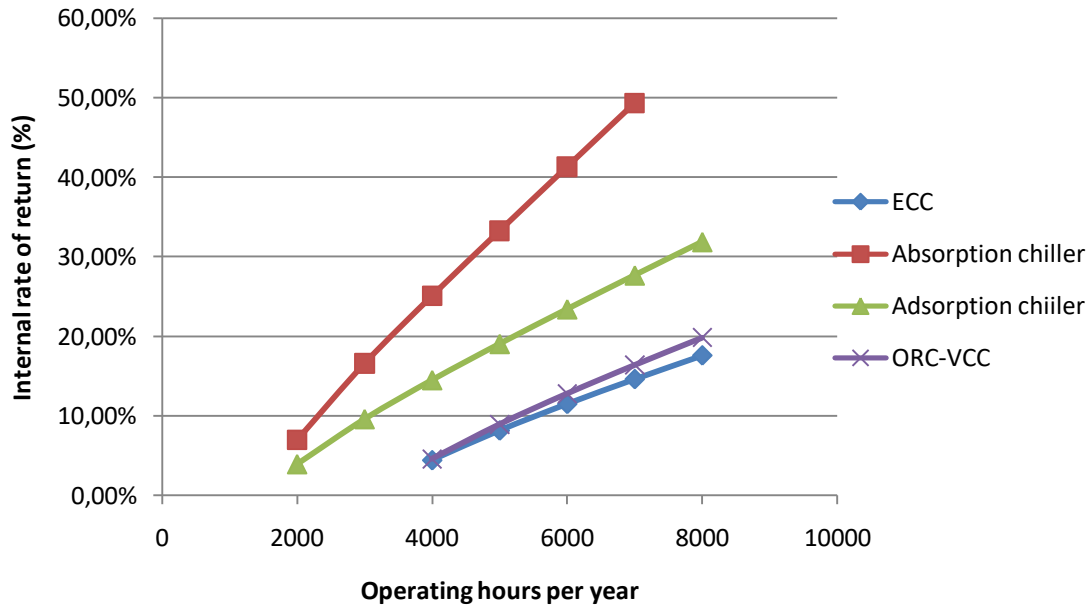

Figure 88 : IRR variation with the operating hours per year (For electricity cost 0.115 $\frac{€}{\text{Kwh}}$, Interest rate 8 %)

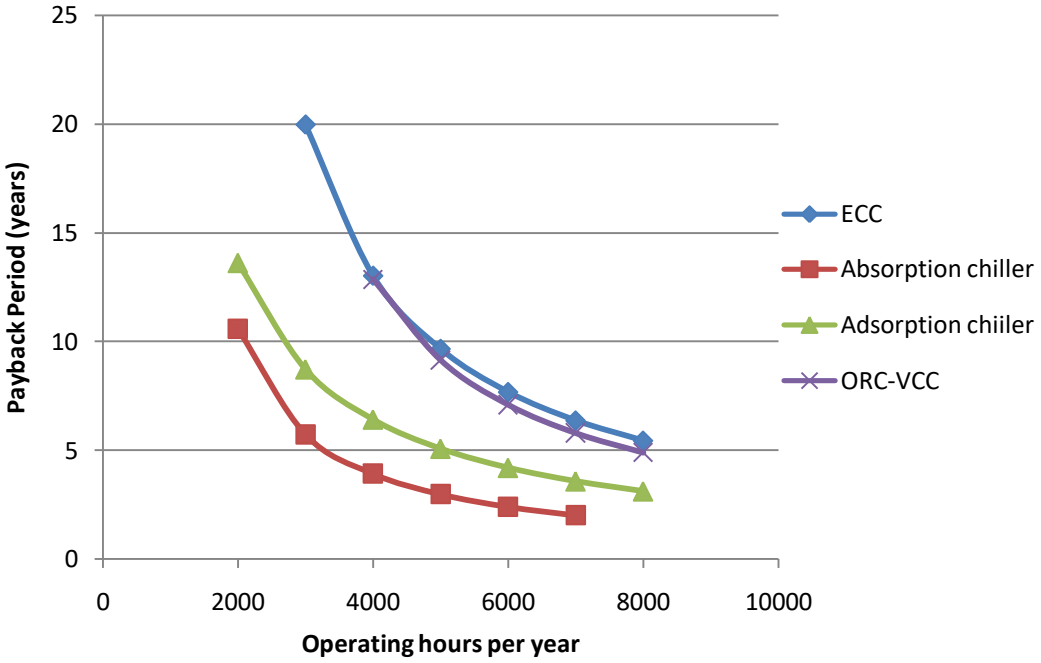

Figure 89 : PBP variation with the operating hours per year (For electricity cost 0.115 $\frac{€}{\text{Kwh}}$, Interest rate 8 %)

From Figure 87, it can be concluded that for 2000 hours of use per year, neither of the investments is beneficial and up to 4000 hours, the ECC and ORC-VCC systems' investment is rejected. However, 2000 hours is a small number for industrial refrigeration. For 5000 and more hours, the investments are more beneficial, with the measures reaching their maximum values at the highest number of hours as it was expected. In general, the absorption chiller is the investment with the highest economic measures, followed by the adsorption chiller. Their IRR and payback period reach 49 and 31.9 % and 2.02 and 3.12 years respectively. They both are beneficial from 3000 hours. The ORC-VCC is starting to become an interesting investment after 6000 hours, since then its IRR is higher than 10 %. The ECC system has a similar performance. However, both systems have a minimum PBP of 4.9 and 5,45 years (for 8000 hours), which is still a relatively high number, especially when comparing with the absorption and adsorption chiller's PBP. In any case, from this sensitivity analysis, it seems that these systems are profitable for many operating hours, something that suggest industrial cooling instead of smaller residential or air conditioning applications.

Next, the results for different electricity price are presented:

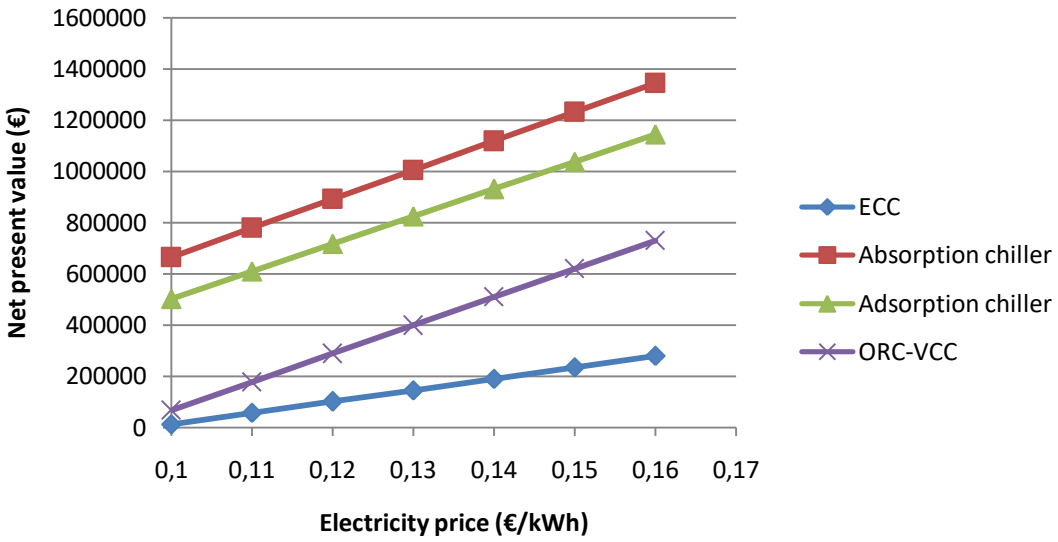

Figure 90 : NVP variation with the electricity price (For 5840 hours of operation per year, Interest rate 8 %)

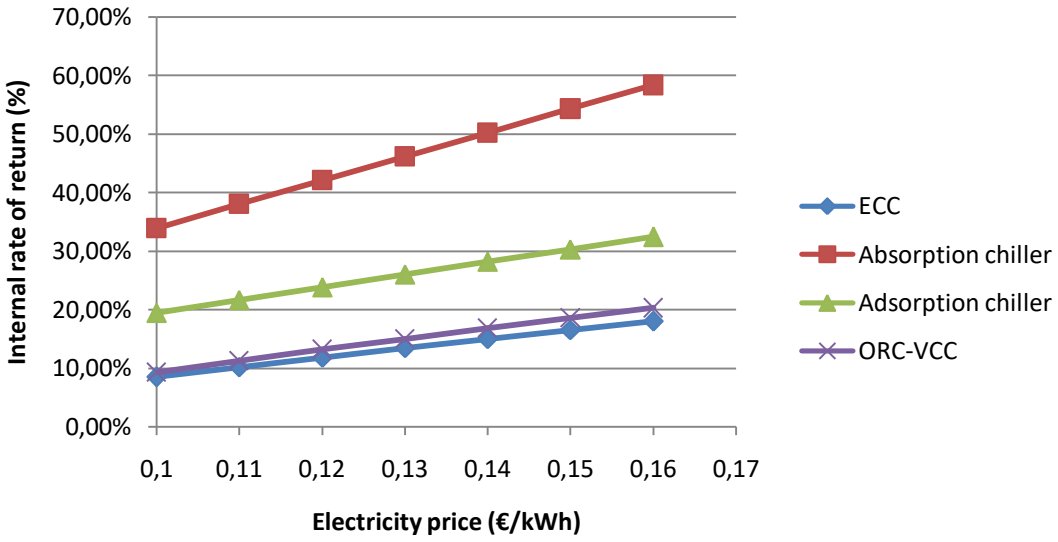

Figure 91 : IRR variation with the electricity price (For 5840 hours of operation per year, Interest rate 8 %)

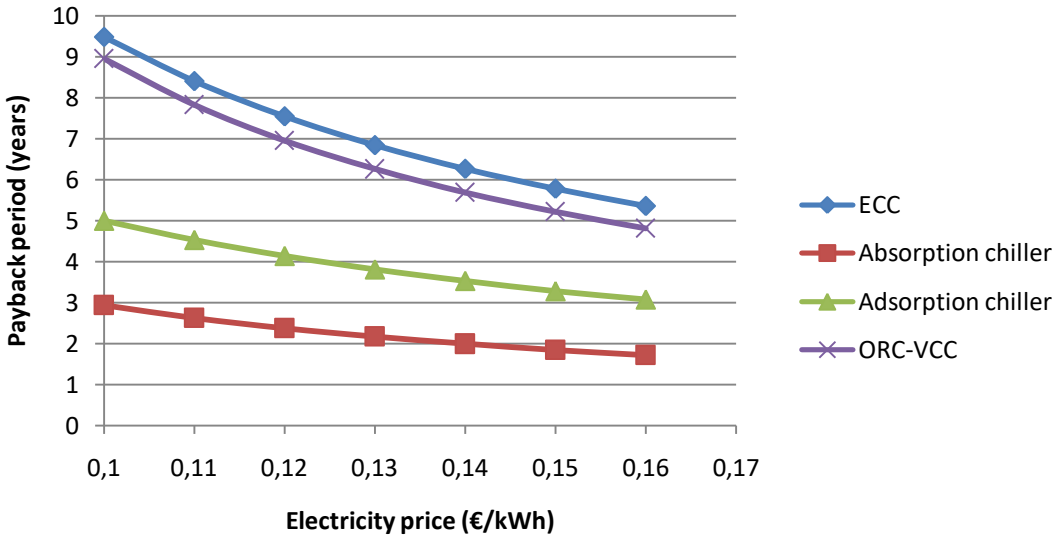

Figure 92 : PBP variation with the electricity price (For 5840 hours of operation per year, Interest rate 8 %)

From the diagrams, a great variation of the measures is observed as the electricity price changes. Since the case is considered to have 5840 operating hours, a value for which the absorption and adsorption chiller were already a beneficial investment, the measures for those chillers in this case are high, with the IRR starting from 34 and 20 % and PBP from 2 and 5 years respectively. Those are expected values and suggest that both chillers' investment is interesting. For the ORC-VCC, the IRR ranges from 9.2 to 20 % and the PBP from 9 to 4.81 years. For the ECC the IRR ranges from 8.5 to 18 % and the PBP from 9.5 to 5.3 years. For both chillers, the investment is more beneficial as the price of electricity increases; however, in the cases of low price, the PBP is high.

Finally, the variation of the NPV with the interest rate is displayed, since the other two measures don't change with the interest rate. In general, it seems that with the rise in the electricity price, the four curves have a tendency to converge to a similar PBP value.

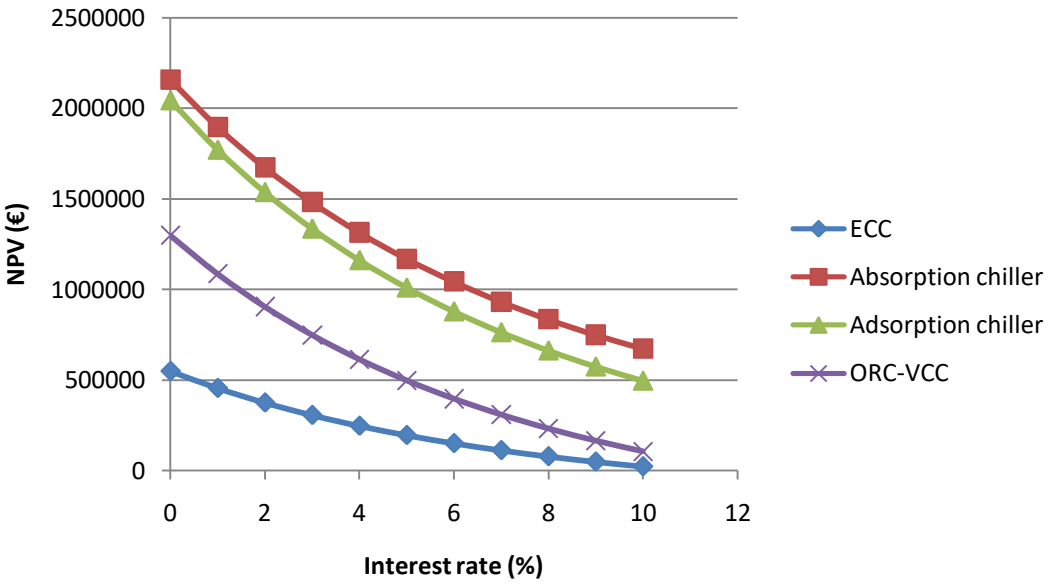

Figure 93 : NVP variation with the interest rate (For electricity cost 0.115 $\frac{€}{Kwh}$, 5840 hours of operation per year)

The variation presented in Figure 93 is expected, as rise in the interest rate reduces the NPV

In general, the following conclusions can be derived:

- The absorption chiller is generally an interesting investment, except from extreme cases (such as very low number of operating hours). That is an expected result, since that chiller is the cheapest among the others and has the highest efficiency. That means that for almost any case, that investment should be considered as an interesting option.
- The adsorption chiller is also an interesting investment, even though not as good as the previous. Its PBP and IRR values are satisfying in many cases. Since its cost is not that high and its efficiency not extremely low, that result is expected as well.
- The ORC-VCC system is the third most beneficial system, since in many of its cases, whether the investment would be accepted would depend on the investor and they are not definitely profitable cases. Even though the system has a high efficiency, its cost reduces the investment's potential.
- The ECC has the worst efficiency and a relatively high cost among the chillers. As it was expected, its investment is the worst among those investigated. In that case as well, some cases are not accepted; for the other cases, the investor's criteria would be the decisive factor.

5. Conclusions

In this thesis, an investigation of the use of four thermal cooling systems for waste heat recovery was performed. The heat source was considered to be gases at specific mass flow rate, inlet and outlet temperature. The gases transferred their heat to a pressurized water circuit and from there, the heat was transferred to the working fluid via a second heat exchanger. For each system, the efficiency for cooling production was calculated, based on three measures, the COP, cooling power and exergetic efficiency. These measures were calculated in a range of hot water temperatures and the respective diagrams were plotted. These calculations took place for three specific chilled water outlet temperatures.

Then, the results of each case were compared with each other, in order to find out which system could achieve the highest efficiency and at which temperature. Finally, the investment, operational and maintenance costs were calculated for each case and a possible investment for substituting an electric-powered vapor compression chiller were evaluated, using the NPV, IRR and PBP measures.

From the study, it can be concluded that the absorption chiller is the system that can achieve the highest efficiency. In both cases of chilled water outlet temperature (7, 10 ℃), the absorption chiller could achieve the highest efficiency among the examined systems. Its hot water inlet temperature operational range was small and the highest efficiency was achieved at about 119 ℃ for each case. However, in the third case of chilled water outlet temperature (4 ℃), the absorption chiller cannot operate, since it uses water as the refrigerant and in such low temperatures the freezing point of water impedes the operation. From the economical point of view, the absorption chiller was found to have the lowest cost among the systems, as it is a commercial chiller. However, it requires high maintenance and cannot operate for more than 7000 hours per year. As it was found from the economic analysis, its economic measures reveal a profitable investment, with PBP less than three years and IRR at about 40 % for the base case and generally values for different electricity price or operating hours. So in general, this chiller is a very interesting choice for waste heat recovery.

The adsorption chillers that were investigated (ECO-MAX, Nak) were found to achieve relatively high efficiency, which however was depending on the chilled water outlet value. For example, for the ECO-MAX chiller, in the 10 ℃ case, the chiller's COP was the third highest among the chillers, while for 7 ℃, the Nak chiller achieved 0.66, which was higher than the ORC-VCC efficiency. In any case, the adsorption chiller has a relatively high efficiency, while its best attribute is the fact that it can operate in very low hot water temperatures, even up to 50 ℃. Moreover, for the case that was economically evaluated, the adsorption chiller had a COP of 0.704, which is relatively high. Its cost was found to be a bit lower than that of the ECC and much higher than the cost of the absorption chiller. Finally, the investment of that chiller was found to have a PBP of 4.32 years and IRR of 23 %, which suggest an interesting investment.

The ORC-VCC chiller can achieve a relatively high efficiency. It can operate in a big range of hot water temperatures, even though its efficiency reaches the maximum value for the maximum temperature. Moreover, in the case of 4°C, since the previous systems cannot operate, the ORC-VCC has the highest efficiency. As for the working fluids, it was found that among the examined fluids, with the specific modeling of the cycle, those with medium critical temperature show a better efficiency, with butane achieving the highest values. Finally, the cost for the system was found to be the highest among the systems, due to its complexity. That made the ORC-VCC's investment not that profitable, with its PBP and IRR being 7.3 and 12 %, while the PBP doesn't drop below 5 years even for the most favorable cases (many operating hours, high electricity price).

Finally, the ECC system had the lowest performance among the systems for every case of chilled water temperature, being much lower than that of the other systems. This system can also operate in a big range of temperatures and reaches its highest efficiency at the highest water temperature. Among the tested working fluids for the ECC, those with medium and medium to low critical temperatures achieve better efficiency, with butane achieving the highest. Finally, the cost of the system was found to be relatively high, mainly because it is not a commercially produced chiller. So, since the system has both low efficiency and high specific cost, it was expected that a possible investment wouldn't be that profitable. Its PBP and IRR were found to be 8 years and 11 % and much like in the ORC-VCC case, the PBP didn't fall below 5 years for any tested value of operating hours and electricity price.

The following issues could be further studied, in order to make this study more complete

- Detailed modeling of the adsorption chiller in a way similar to the other systems, in order to apply the same assumptions and have a more fair comparison.
- Study of the possibility of combined heat and cooling production. As it can be seen from the Sankey diagrams, big amounts of heat are rejected in each system, which could be used for heating. However, that case would require higher condenser temperature, in order to have a high enough water temperature, and thus the COP would be reduced.
- Study of the possibility of combined cooling and electricity production.

Appendix

Here, tables with the properties of the working fluid and the entering water streams are demonstrated for each case of chilled water outlet temperature, for the ORC-VCC, ECC and absorption chiller.

Table 36 : Results for ORC-VCC for chilled water outlet temperature of 10℃

	T(°C)	P(bar)	h(kj/kg)	s(kj/kgK)
1	36,69	30	290,06	1,2921
2	139,69	30	757,26	2,5285
3	64,7	3,7849	690,06	2,5789
4	35	3,7849	284,24	1,2883
1vc	10	1,2425	600,79	2,4409
2vc	47,26	3,7849	656,15	2,4758
3vc	35	3,7849	284,24	1,2883
4vc	5	1,2425	284,24	1,3031

	Tinlet(°C)	Toutlet(°C)	Mass Flow (kg/s)	P(bar)
Hot water	180	80,68	3,753	12
Chilled water	15	10	54,6174	2
Cooling water	15	31,31	39,9831	1,2

Qin (KW)	1592,6	
Qcond (KW)	2728,1	
Qevap (KW)	1144,6	
Working fluid mass flow (kg/s)	ORC	VCC
	3,4088	3,6157

Table 37 : Results for ECC for chilled water outlet temperature of 10°C

	T(°C)	P(bar)	h(kj/kg)	s(kj/kg/K)
0	10	1,2425	600,79	2,4409
1	139,69	30	757,26	2,5285
6	70,63	3,7849	701,81	
7	35	3,7849	284,24	1,2883
8	5	1,2425	284,24	1,3031
9	36,69	30	290,06	1,2921
w	0,5489			
Pmixing (bar)	0,9227			

	Tinlet(°C)	Toutlet(°C)	Mass flow (kg/s)	P(bar)
Hot water	180	80,735	3,753	12
Chilled water	15	10	28,2657	2
Cooling water	15	32,56	30,0178	1,2
Working fluid			5,28	

Qin (kW)	1592,6
Qcond (kW)	2204,8
Qevap (kW)	592,34

Table 38 : Results for the absorption chiller for chilled water outlet temperature of 10℃

	T(°C)	P(kPa)	h(kj/kg)	s(kj/kg/K)	X
1	40	0,8726	106,7	0,2384	58,22
2	40	7,3849	106,7	0,2384	58,22
3	68,2	7,3849	164,8	0,4125	58,22
4	102,4	7,3849	292,8	0,5304	69,7
5	64,98	7,3849	223,3	0,3418	69,7
6	64,98	0,8726	223,3	0,3418	69,7
7	80,27	7,3849	2650,3	8,4862	0
8	35	7,3849	146,6	0,5051	0
9	5	0,8726	146,6	0,5279	0
10	10	0,8726	2519,5	9,0584	0

	T(°C)	P(bar)	Mass flow (kg/s)
11	118,68	3,9	53,7169
12	111,68	3,9	53,7169
13	15	1,2	23,46
14	30,54	1,2	23,46
15	15	1,2	19,58
16	30,54	1,2	19,58
17	15	2	57,59
18	10	2	57,59

Qcond (kW)	1273,5		
Qevap (kW)	1207		
Qin(kW)	1592,6		
Mass flow (kg/s)	Strong	Weak	Refrigerant
	2,5635	3,0722	0,5087

Table 39 : Results for the ORC-VCC for chilled water outlet temperature of 7°C

	T(°C)	P(bar)	h(kj/kg)	s(kj/kg/K)
1	36,69	30	290,06	1,2921
2	139,69	30	757,26	2,5285
3	64,69	3,7849	690,06	2,5789
4	35	3,7849	284,24	1,2883
1vc	7	1,1127	596,43	2,4405
2vc	47,74	3,7849	657,09	2,4787
3vc	35	3,7849	284,24	1,2883
4vc	2	1,1127	284,24	1,3062

	Tinlet(°C)	Toutlet(°C)	Mass flow (kg/s)	Pressure
Hot water	180	80,68	3,753	12
Chilled water	12	7	49,1043	2
Cooling water	15	31,4022	38,0968	1,2

Qinput (kW)	1592,6
Qcond (kW)	2613,7
Qevap (kW)	1030,1

Working fluid mass flow	ORC	VCC
	3,4088	3,2997

Table 40 : Results for the ECC for chilled water outlet temperature of 7 °C

	T(°C)	P(bar)	h(kj/kg)	s(kj/kg/K)
0	7	1,1127	596,43	2,4405
1	139,69	30	757,26	2,5285
6	72,37	3,7849	705,28	
7	35	3,7849	284,24	1,2883
8	2	1,1127	284,24	1,3062
9	36,69	30	290,06	1,2921

w	0,4776
Pmixing (bar)	0,929

	Tinlet(°C)	Toutlet(°C)	Mass flow (kg/s)	P(bar)
Hot water	180	80,735	3,753	12
Chilled water	12	7	24,2258	2
Cooling water	15	32,6649	28,7028	1,2
Working fluid			5,0367	

Qinput (kW)	1592,6
Qcond (kW)	2120,6
Qevap (kW)	508,226

Table 41 : Results for the absorption chiller for chilled water outlet temperature of 7°C

	T(°C)	P(kPa)	h(kj/kg)	s(kj/kg/K)	X
1	40	0,706	115,6	0,23	59,9747
2	40	7,3849	115,6	0,23	59,9747
3	70,98	7,3849	175,4	0,409	59,9747
4	108,6	7,3849	292,8	0,5304	69,77
5	67,4751	7,3849	223,3	0,3418	69,77
6	67,4751	0,706	223,3	0,3418	69,77
7	84,15	7,3849	2657,7	8,507	0
8	35	7,3849	146,6	0,5051	0
9	2	0,706	146,6	0,533	0
10	7	0,706	2514	9,1365	0

	T(°C)	P(bar)	Mass flow (kg/s)
11	118,68	3,9	53,7169
12	111,68	3,9	53,7169
13	15	1,2	23,39
14	30,54	1,2	23,39
15	15	1,2	19,208
16	30,54	1,2	19,208
17	12	2	56,1361
18	7	2	56,1361

Qcond (kW)	1249,1
Qevap (kW)	1177,7
Qin(kW)	64,69

Mass flow (kg/s)	Strong	Weak	Refrigerant
	2,5635	3,0722	0,5087
	3,0454	3,5429	0,4975

Table 42 : Results for the ORC-VCC for chilled water outlet temperature of 4°C

	T(°C)	P(bar)	h(kj/kg)	s(kj/kg/K)
1	36,69	30	290,06	1,2921
2	139,69	30	757,26	2,5285
3	64,69	3,7849	690,06	2,5789
4	35	3,7849	284,24	1,2883
1vc	4	0,9938	592,08	2,4404
2vc	48,2964	3,7849	658,14	2,482
3vc	35	3,7849	284,24	1,2883
4vc	-1	0,9938	284,24	1,3096

	Tinlet(°C)	Toutlet(°C)	Mass flow (kg/s)	P(bar)
Hot water	180	80,68	3,753	12
Chilled water	9	4	44,3969	2
Cooling water	15	31,4022	36,6757	1,2

Qinput (kW)	1592,6
Qcond (kW)	2516,2
Qevap (kW)	932,653

Working fluid mass flow (kg/s)	ORC	VCC
	3,4088	3,0297

Table 43 : Results for the ECC for chilled water outlet temperature of 4°C

	T(°C)	P(bar)	h(kj/kg)	s(kj/kg/K)
0	4	0,9938	592,08	2,4404
1	139,69	30	757,26	2,5285
6	74,88	3,7849	710,3	
7	35	3,7849	284,24	1,2883
8	-1	0,9938	284,24	1,3096
9	36,69	30	290,06	1,2921

w	0,3972
Pmixing (bar)	0,9401

	Tinlet(°C)	Toutlet(°C)	Mass flow (kg/s)	P(bar)
Hot water	180	80,735	3,753	12
Chilled water	9	4	19,8406	2
Cooling water	15	32,8766	27,1402	1,2
Working fluid			4,7627	

Qinput (kW)	1592,6
Qcond (kW)	2029,2
Qevap (kW)	416,796

References

1. *United States Environmental Protection Agency : Greenhouse Gas Emissions*. Available from: https://www.epa.gov/ghgemissions/global-greenhouse-gas-emissions-data.
2. *Kyoto Protocol*. Available from: http://www.kyotoprotocol.com/.
3. *U.S. Department of Energy Industrial Technologies Program : Waste heat recovery: Technology and Opportunities in U.S. Industry*. 2008.
4. Choudhury, B., et al., *An overview of developments in adsorption refrigeration systems towards a sustainable way of cooling.* Applied Energy, 2013. **104**: p. 554-567.
5. Quoilin, S., et al., *Techno-economic survey of Organic Rankine Cycle (ORC) systems.* Renewable and Sustainable Energy Reviews, 2013. **22**: p. 168-186.
6. Brückner, S., et al., *Industrial waste heat recovery technologies: An economic analysis of heat transformation technologies.* Applied Energy, 2015. **151**: p. 157-167.
7. Brueckner, S., et al., *Methods to estimate the industrial waste heat potential of regions – A categorization and literature review.* Renewable and Sustainable Energy Reviews, 2014. **38**: p. 164-171.
8. Lu, H., L. Price, and Q. Zhang, *Capturing the invisible resource: Analysis of waste heat potential in Chinese industry.* Applied Energy, 2016. **161**: p. 497-511.
9. Miró, L., S. Brückner, and L.F. Cabeza, *Mapping and discussing Industrial Waste Heat (IWH) potentials for different countries.* Renewable and Sustainable Energy Reviews, 2015. **51**: p. 847-855.
10. *European Commision : Heating and cooling*. 2017 04/06/2017 4/6/2017]; Available from: https://ec.europa.eu/energy/en/topics/energy-efficiency/heating-and-cooling.
11. *THE MONTREAL PROTOCOL ON SUBSTANCES THAT DEPLETE THE OZONE LAYER.*
12. Bao, J. and L. Zhao, *A review of working fluid and expander selections for organic Rankine cycle.* Renewable and Sustainable Energy Reviews, 2013. **24**: p. 325-342.
13. Vélez, F., *Selecting working fluids in an organic Rankine cycle for power generation from low temperature heat sources.* DYNA, 2014. **81**: p. 173-180.
14. Braimakis, K., et al., *Low grade waste heat recovery with subcritical and supercritical Organic Rankine Cycle based on natural refrigerants and their binary mixtures.* Energy, 2015. **88**: p. 80-92.
15. Li, H., et al., *Hydrocarbon working fluids for a Rankine cycle powered vapor compression refrigeration system using low-grade thermal energy.* Energy and Buildings, 2013. **65**: p. 167-172.
16. Yılmaz, A., *Transcritical organic Rankine vapor compression refrigeration system for intercity bus air-conditioning using engine exhaust heat.* Energy, 2015. **82**: p. 1047-1056.
17. Karellas, S. and K. Braimakis, *Energy–exergy analysis and economic investigation of a cogeneration and trigeneration ORC–VCC hybrid system utilizing biomass fuel and solar power.* Energy Conversion and Management, 2016. **107**: p. 103-113.
18. Wang, H., et al., *Performance of a combined organic Rankine cycle and vapor compression cycle for heat activated cooling.* Energy, 2011. **36**(1): p. 447-458.
19. Molés, F., et al., *Thermodynamic analysis of a combined organic Rankine cycle and vapor compression cycle system activated with low temperature heat sources using low GWP fluids.* Applied Thermal Engineering, 2015. **87**: p. 444-453.

20. Nasir, M.T. and K.C. Kim, *Working fluids selection and parametric optimization of an Organic Rankine Cycle coupled Vapor Compression Cycle (ORC-VCC) for air conditioning using low grade heat.* Energy and Buildings, 2016. **129**: p. 378-395.
21. Wang, H., R. Peterson, and T. Herron, *Design study of configurations on system COP for a combined ORC (organic Rankine cycle) and VCC (vapor compression cycle).* Energy, 2011. **36**(8): p. 4809-4820.
22. Cola, F., A. Romagnoli, and J. Hey, *An evaluation of the technologies for heat recovery to meet onsite cooling demands.* Energy Conversion and Management, 2016. **121**: p. 174-185.
23. Aneke, M., et al., *Thermodynamic analysis of alternative refrigeration cycles driven from waste heat in a food processing application.* International Journal of Refrigeration, 2012. **35**(5): p. 1349-1358.
24. Chen, J., H. Havtun, and B. Palm, *Investigation of ejectors in refrigeration system: Optimum performance evaluation and ejector area ratios perspectives.* Applied Thermal Engineering, 2014. **64**(1–2): p. 182-191.
25. Chen, J., et al., *A review on versatile ejector applications in refrigeration systems.* Renewable and Sustainable Energy Reviews, 2015. **49**: p. 67-90.
26. Zhu, Y. and P. Jiang, *Hybrid vapor compression refrigeration system with an integrated ejector cooling cycle.* International Journal of Refrigeration, 2012. **35**(1): p. 68-78.
27. Zeyghami, M., D.Y. Goswami, and E. Stefanakos, *A review of solar thermo-mechanical refrigeration and cooling methods.* Renewable and Sustainable Energy Reviews, 2015. **51**: p. 1428-1445.
28. Milazzo, A., A. Rocchetti, and I.W. Eames, *Theoretical and Experimental Activity on Ejector Refrigeration.* Energy Procedia, 2014. **45**: p. 1245-1254.
29. Thongtip, T., N. Ruangtrakoon, and S. Aphornratana, *Development of a Steam Jet Refrigeration Cycle for the Actual Application Driven by Low Grade Thermal Energy.* Energy Procedia, 2014. **52**: p. 110-119.
30. Yapıcı, R. and C.C. Yetişen, *Experimental study on ejector refrigeration system powered by low grade heat.* Energy Conversion and Management, 2007. **48**(5): p. 1560-1568.
31. Saleh, B., *Performance analysis and working fluid selection for ejector refrigeration cycle.* Applied Thermal Engineering, 2016. **107**: p. 114-124.
32. Alexis, G.K. and J.S. Katsanis, *Performance characteristics of a methanol ejector refrigeration unit.* Energy Conversion and Management, 2004. **45**(17): p. 2729-2744.
33. Meyer, A.J., T.M. Harms, and R.T. Dobson, *Steam jet ejector cooling powered by waste or solar heat.* Renewable Energy, 2009. **34**(1): p. 297-306.
34. Sadeghi, M., S.M.S. Mahmoudi, and R. Khoshbakhti Saray, *Exergoeconomic analysis and multi-objective optimization of an ejector refrigeration cycle powered by an internal combustion (HCCI) engine.* Energy Conversion and Management, 2015. **96**: p. 403-417.
35. Zegenhagen, M.T. and F. Ziegler, *Feasibility analysis of an exhaust gas waste heat driven jet-ejector cooling system for charge air cooling of turbocharged gasoline engines.* Applied Energy, 2015. **160**: p. 221-230.
36. Wang, J., Y. Dai, and Z. Sun, *A theoretical study on a novel combined power and ejector refrigeration cycle.* International Journal of Refrigeration, 2009. **32**(6): p. 1186-1194.
37. Zheng, B. and Y.W. Weng, *A combined power and ejector refrigeration cycle for low temperature heat sources.* Solar Energy, 2010. **84**(5): p. 784-791.
38. ASHRAE, *2010 ASHRAE HANDBOOK REFRIGERATION*. 2010, Atlanta.
39. ASHRAE, *2009 ASHRAE HANDBOOK-FUNDAMENTALS*. 2009, Atlanta.

40. Herold, K.E., R. Radermacher, and S.A. Klein, *ABSORPTION CHILLERS AND HEAT PUMPS*. 2016: CRC Press.
41. Srikhirin, P., S. Aphornratana, and S. Chungpaibulpatana, *A review of absorption refrigeration technologies.* Renewable and Sustainable Energy Reviews, 2001. **5**(4): p. 343-372.
42. Popli, S., P. Rodgers, and V. Eveloy, *Trigeneration scheme for energy efficiency enhancement in a natural gas processing plant through turbine exhaust gas waste heat utilization.* Applied Energy, 2012. **93**: p. 624-636.
43. Kalogirou, S.A., *Chapter six - Solar Space Heating and Cooling*, in *Solar Energy Engineering*. 2009, Academic Press: Boston. p. 315-389.
44. Bellos, E., *EXPLOITATION AND OPTIMIZATION OF SOLAR SYSTEMS IN BUILDINGS*, in *School of Mechanical Engineering*. 2016, National Technical University of Athens.
45. Mortazavi, A., et al., *Enhancement of APCI cycle efficiency with absorption chillers.* Energy, 2010. **35**(9): p. 3877-3882.
46. Rodgers, P., et al., *Enhancement of LNG plant propane cycle through waste heat powered absorption cooling.* Applied Thermal Engineering, 2012. **48**: p. 41-53.
47. Popli, S., P. Rodgers, and V. Eveloy, *Gas turbine efficiency enhancement using waste heat powered absorption chillers in the oil and gas industry.* Applied Thermal Engineering, 2013. **50**(1): p. 918-931.
48. Kalinowski, P., et al., *Application of waste heat powered absorption refrigeration system to the LNG recovery process.* International Journal of Refrigeration, 2009. **32**(4): p. 687-694.
49. Hedström, S., *Thermal energy recovery of low grade waste heat in hydrogenation process*, in *Faculty of Health, Science and Technology*. 2014, Karlstad University.
50. Wang, L.W., R.Z. Wang, and R.G. Oliveira, *A review on adsorption working pairs for refrigeration.* Renewable and Sustainable Energy Reviews, 2009. **13**(3): p. 518-534.
51. Ruzhu Wang, Liwei Wang, and J. Wu, *Adsorption Refrigeration Technology : Theory and Application*. 2014: John Wiley & Sons Singapore Pte. Ltd.
52. GBU.
53. Qu, T.F., R.Z. Wang, and W. Wang, *Study on heat and mass recovery in adsorption refrigeration cycles.* Applied Thermal Engineering, 2001. **21**(4): p. 439-452.
54. Wang, K. and E.A. Vineyard, *New Opportunities for Solar Adsorption Refrigeration.* 2011.
55. Deng, J., R.Z. Wang, and G.Y. Han, *A review of thermally activated cooling technologies for combined cooling, heating and power systems.* Progress in Energy and Combustion Science, 2011. **37**(2): p. 172-203.
56. Wang, R.Z., *Performance improvement of adsorption cooling by heat and mass recovery operation.* International Journal of Refrigeration, 2001. **24**(7): p. 602-611.
57. *ECO-MAX adsorption chillers*. 2009.
58. Zhai, H., et al., *Energy and exergy analyses on a novel hybrid solar heating, cooling and power generation system for remote areas.* Applied Energy, 2009. **86**(9): p. 1395-1404.
59. Saha, B.B., A. Akisawa, and T. Kashiwagi, *Solar/waste heat driven two-stage adsorption chiller: the prototype.* Renewable Energy, 2001. **23**(1): p. 93-101.
60. Khan, M.Z.I., et al., *Study on solar/waste heat driven multi-bed adsorption chiller with mass recovery.* Renewable Energy, 2007. **32**(3): p. 365-381.
61. Saha, B.B., et al., *Waste heat driven dual-mode, multi-stage, multi-bed regenerative adsorption system.* International Journal of Refrigeration, 2003. **26**(7): p. 749-757.
62. Liu, Y.L., R.Z. Wang, and Z.Z. Xia, *Experimental performance of a silica gel–water adsorption chiller.* Applied Thermal Engineering, 2005. **25**(2–3): p. 359-375.

63. Myat, A., et al., *Experimental investigation on the optimal performance of Zeolite–water adsorption chiller.* Applied Energy, 2013. **102**: p. 582-590.
64. Grisel, R.J.H., S.F. Smeding, and R.d. Boer, *Waste heat driven silica gel/water adsorption cooling in trigeneration.* Applied Thermal Engineering, 2010. **30**(8–9): p. 1039-1046.
65. Kong, X.Q., et al., *Experimental investigation of a micro-combined cooling, heating and power system driven by a gas engine.* International Journal of Refrigeration, 2005. **28**(7): p. 977-987.
66. Chorowski, M. and P. Pyrka, *Modelling and experimental investigation of an adsorption chiller using low-temperature heat from cogeneration.* Energy, 2015. **92, Part 2**: p. 221-229.
67. Wang, R.Z. and R.G. Oliveira, *Adsorption refrigeration—An efficient way to make good use of waste heat and solar energy.* Progress in Energy and Combustion Science, 2006. **32**(4): p. 424-458.
68. Hamdy, M., et al., *An overview on adsorption cooling systems powered by waste heat from internal combustion engine.* Renewable and Sustainable Energy Reviews, 2015. **51**: p. 1223-1234.
69. Sah, R.P., B. Choudhury, and R.K. Das, *A review on low grade heat powered adsorption cooling systems for ice production.* Renewable and Sustainable Energy Reviews, 2016. **62**: p. 109-120.
70. ESTCP, *Demonstration of a Solar Thermal Combined Heating, Cooling and Hot Water System Utilizing an Adsorption Chiller for DoD Installations*. 2014.
71. SorTech. *SorTech Website*. Available from: http://www.sortech.de/en/products/our-products/ezea/.
72. InvenSor. *InvenSor Website*. 2017; Available from: http://www.invensor.com/en/technology/adsorption-technology.htm.
73. Bayrakçi, H.C. and A.E. Özgür, *Energy and exergy analysis of vapor compression refrigeration system using pure hydrocarbon refrigerants.* International Journal of Energy Research, 2009. **33**(12): p. 1070-1075.
74. Braimakis, K. and S. Karellas, *Integrated thermoeconomic optimization of standard and regenerative ORC for different heat source types and capacities.* Energy, 2017. **121**: p. 570-598.
75. Li, Y.-R., et al., *Performance analysis of a novel power/refrigerating combined-system driven by the low-grade waste heat using different refrigerants.* Energy, 2014. **73**: p. 543-553.
76. Kim, K.H. and H. Perez-Blanco, *Performance analysis of a combined organic Rankine cycle and vapor compression cycle for power and refrigeration cogeneration.* Applied Thermal Engineering, 2015. **91**: p. 964-974.
77. *British Refrigeration Association, Institute of Refrigeration : Guide to Good Commercial Refrigeration Practice, Part 2 : System Design and Component Selection*.
78. *Chiller Training Manual*.
79. LG, *LG HVAC SOLUTION WATER COOLED SCREW CHILLER*. 2015.
80. *BROAD X Absorption Chiller Model Selection & Design Manual*. 2008.
81. Chen, J., H. Havtun, and B. Palm, *Screening of working fluids for the ejector refrigeration system.* International journal of refrigeration, 2014. **47**: p. 1-14.
82. Besagni, G., et al., *A study of working fluids for heat driven ejector refrigeration using lumped parameter models.* International Journal of Refrigeration, 2015. **58**: p. 154-171.
83. Chen, J., H. Havtun, and B. Palm, *Parametric analysis of ejector working characteristics in the refrigeration system.* Applied Thermal Engineering, 2014. **69**(1–2): p. 130-142.

84. Yu, J., et al., *Applying mechanical subcooling to ejector refrigeration cycle for improving the coefficient of performance.* Energy Conversion and Management, 2007. **48**(4): p. 1193-1199.
85. El-Dessouky, H., et al., *Evaluation of steam jet ejectors.* Chemical Engineering and Processing: Process Intensification, 2002. **41**(6): p. 551-561.
86. Khalil, A., M. Fatouh, and E. Elgendy, *Ejector design and theoretical study of R134a ejector refrigeration cycle.* International Journal of Refrigeration, 2011. **34**(7): p. 1684-1698.
87. Huang, B.J., et al., *A 1-D analysis of ejector performance.* International Journal of Refrigeration, 1999. **22**(5): p. 354-364.
88. Rashidi, M.M., A. Aghagoli, and R. Raoofi, *Thermodynamic analysis of the ejector refrigeration cycle using the artificial neural network.* Energy, 2017. **129**: p. 201-215.
89. Chua, H.T., et al., *Improved thermodynamic property fields of LiBr–H2O solution.* International Journal of Refrigeration, 2000. **23**(6): p. 412-429.
90. Bellos, E., C. Tzivanidis, and K.A. Antonopoulos, *Exergetic and energetic comparison of LiCl-H2O and LiBr-H2O working pairs in a solar absorption cooling system.* Energy Conversion and Management, 2016. **123**: p. 453-461.
91. Bellos, E., C. Tzivanidis, and K.A. Antonopoulos, *Exergetic, energetic and financial evaluation of a solar driven absorption cooling system with various collector types.* Applied Thermal Engineering, 2016. **102**: p. 749-759.
92. Gogoi, T.K. and D. Konwar, *Exergy analysis of a H2O–LiCl absorption refrigeration system with operating temperatures estimated through inverse analysis.* Energy Conversion and Management, 2016. **110**: p. 436-447.
93. Kaita, Y., *Thermodynamic properties of lithium bromide–water solutions at high temperatures.* International Journal of Refrigeration, 2001. **24**(5): p. 374-390.
94. Eldakamawy, M.H., M.V. Sorin, and M. Brouillette, *Energy and exergy investigation of ejector refrigeration systems using retrograde refrigerants.* International Journal of Refrigeration, 2017. **78**: p. 176-192.
95. Chen, J., H. Havtun, and B. Palm, *Conventional and advanced exergy analysis of an ejector refrigeration system.* Applied Energy, 2015. **144**: p. 139-151.
96. Lemmens, S. *A perspective on costs and cost estimation techniques for organic Rankine cycle systems*. in *Proceedings of the 3rd International Seminar on ORC Power Systems (ASME ORC 2015), Brussels, Belgium*. 2015.
97. Labus, J., *Modelling of small capacity absorption chillers driven by solar thermal energy or waste heat*. 2011, Universitat Rovira i Virgili.
98. Southon, M., *Performance and cost evaluation to inform the design and implementation of Organic Rankine Cycles in New Zealand*. 2015, University of Canterbury.
99. Murugavel, V. and R. Saravanan. *LIFE CYCLE COST ANALYSIS OF WASTE HEAT OPERATED ABSORPTION COOLING SYSTEMS FOR BUILDING HVAC APPLICATIONS*. in *Tenth International Conference Enhanced Building Operations*. 2010. Kuwait,.
100. Jacob, U., *Best Practice Brochure*. 2015.
101. *Authorized Federal Supply Schedule Price List General Services Administration - Federal Supply Service.* 2017.
102. ASHRAE, *2011 ASHRAE HANDBOOK HVAC Applications.* 2011.
103. Sherif, S.A., et al., *A FEASIBILITY STUDY OF STEAM-JET REFRIGERATION.* INTERNATIONAL JOURNAL OF ENERGY RESEARCH, 1998: p. 1323-1336.
104. Milazzo, A. and F. Mazzelli, *Future perspectives in ejector refrigeration.* Applied Thermal Engineering, 2017. **121**: p. 344-350.
105. Nguyen, V.M., S.B. Riffat, and P.S. Doherty, *Development of a solar-powered passive ejector cooling system.* Applied Thermal Engineering, 2001. **21**(2): p. 157-168.

106. Lazzarin, R.M., *Solar cooling: PV or thermal? A thermodynamic and economical analysis.* International Journal of Refrigeration, 2014. **39**: p. 38-47.
107. Weeda, M., et al., *Combined cold heat and power generation; Techno-economic assessment of integrated fuel cell and sorption heat pump systems.* ECN Clean Fossil Fuels, ECN Project, 2002(7.2915).
108. Turton, R., et al., *Analysis, synthesis and design of chemical processes*. 2008: Pearson Education.
109. Eurostat. *Energy price statistics*. 2016 20/6/2017]; Available from: http://ec.europa.eu/eurostat/statistics-explained/index.php/Energy_price_statistics.
110. Short, W., D.J. Packey, and T. Holt, *A manual for the economic evaluation of energy efficiency and renewable energy technologies*. 2005: University Press of the Pacific Hawaii.